Petrosal and Inner Ear of the Thylacine, Thylacinus cynocephalus (Harris, 1808) (Mammalia, Marsupialia, Dasyuromorphia)

Authors: Wible, John R., and Bertrand, Ornella C.

Source: Annals of Carnegie Museum, 91(1) : 93-134

Published By: Carnegie Museum of Natural History

URL: https://doi.org/10.2992/007.091.0105

ANNALS OF CARNEGIE MUSEUM

VOL. 91, NUMBER 1, PP. 93–134 5 MAY 2025

PETROSAL AND INNER EAR OF THE THYLACINE, *THYLACINUS CYNOCEPHALUS* (HARRIS, 1808) (MAMMALIA, MARSUPIALIA, DASYUROMORPHIA)

JOHN R. WIBLE
Curator, Section of Mammals, Carnegie Museum of Natural History
5800 Baum Boulevard, Pittsburgh, Pennsylvania 15206
wiblej@carnegiemnh.org

ORNELLA C. BERTRAND
[Research Associate, Section of Mammals, Carnegie Museum of Natural History]
Institut Català de Paleontologia Miquel Crusafont, Universitat Autònoma de Barcelona, Edifici ICTA-ICP, Cerdanyola del Vallès, Barcelona, Spain
ornella.bertrand@icp.cat

ABSTRACT

The petrosal and inner ear are described for the thylacine, *Thylacinus cynocephalus* (Harris, 1808), based on µCT datasets. Comparisons are made with a sample of six extant marsupials, also from µCT datasets: the didelphid *Monodelphis* sp. (short-tailed opossum), the notoryctid *Notoryctes caurinus* Thomas, 1920 (northern marsupial mole or kakarratul), the peramelid *Isoodon macrourus* (Gould, 1842) (northern brown bandicoot), the myrmecobiid *Myrmecobius fasciatus* Waterhouse, 1836 (numbat), and the dasyurids *Dasyurus hallucatus* Gould, 1842 (northern quoll) and *Sminthopsis macroura* Gould, 1842 (stripe-faced dunnart). Dural sinuses and veins are reconstructed based on sulci, canals, and foramina as well as the few studies in the literature on cranial veins in marsupials. The most striking observations with the thylacine concern the pattern of venous drainage. Nearly all of its dural sinuses in the middle and caudal cranial fossae are enclosed in canals, whereas in the remaining taxa most of the sinuses run in open sulci. The thylacine has a novel canal through the substance of the pars canalicularis of the petrosal for the sigmoid sinus. It also has a novel canal that runs successively through the substance of the parietal, interparietal, and supraoccipital and then between the petrosal and exoccipital to join the sigmoid sinus that is called here the parieto-occipital diploic vein. In the two thylacines studied, this venous channel is paired in one but is only on the right side in the other. The exoccipital has an unusual canal that runs from the jugular foramen to the condyloid canal and connects the sigmoid sinus and inferior petrosal sinus; this arrangement is also present in *Notoryctes caurinus*. Another striking feature concerns the area of petrosal occupied by the inner ear, which appears to differ with body size: in the smaller taxa (*Monodelphis* sp. and *Sminthopsis macroura*), the inner ear occupies much of the petrosal volume; in the medium-sized taxa (*Isoodon macrourus*, *Myrmecobius fasciatus*, and *Dasyurus hallucatus*), there is considerably more petrosal than the area occupied by the inner ear; and lastly, in the largest (*Thylacinus cynocephalus*), the petrosal is roughly twice the area of the inner ear. Much of the "extra" petrosal in the thylacine is in the robust paroccipital process and in the endocranial floor of the impression of the cerebellar hemisphere. The inner ear of *T. cynocephalus* has an overall similar morphology to other marsupials. One notable difference is the lack of a secondary common crus in *T. cynocephalus*, as in its close relatives *My. fasciatus* and *S. macroura*, while it is present in *D. hallucatus* and other published dasyuromorphians. As previously reported, this feature appears to be relatively variable among marsupials.

KEY WORDS: bony labyrinth, dural sinuses, *Dasyurus*, *Isoodon*, *Monodelphis*, *Myrmecobius*, *Notoryctes*, sigmoid sinus, *Sminthopsis*.

INTRODUCTION

The mammalian petrosal encloses the inner ear, provides a scaffold for the hard- and soft-tissue structures of the middle ear, and gives passage to several cranial nerves and their branches along with major cranial arteries and veins. Because these anatomical structures vary across Mammalia, the petrosal is an important source of characters for morphological phylogenetic analyses. Within marsupials and their fossil relatives, there is a large literature on the petrosal and inner ear (e.g., Archer 1976; Wible 1990; Sanchez-Villagra and Wible 2002; Ladevèze 2004, 2007; Ladevèze and Muizon 2007; Sánchez-Villagra and Schmelzle 2007; Schmelzle et al. 2007; Alloing-Séguier et al. 2013; Pfaff et al. 2017), including as pointed out by a reviewer of an early draft of this paper (R.M.D. Beck) a number of unpublished theses (e.g., Aplin 1990; Ladevèze 2005; Maga 2008; Dickson 2012; Czerny 2017). Much of the literature on the marsupial petrosal predates the now widespread use of µCT scan data. It is the goal of this report to add to the literature on the marsupial petrosal and inner ear, using µCT scan data on the extinct thylacine (Tasmanian tiger or wolf), the dasyuromorphian *Thylacinus cynocephalus* (Harris, 1808).

Studies predating the availability of µCT scans have addressed the ear region of the thylacine. The most substantive is Archer's (1976) comparative monograph on the basicranium of marsupicarnivores. Archer described the petrosal and neighboring bones, including when present the middle ear ossicles and ectotympanic, in a dozen extant didelphimorphians, dasyuromorphians, and notoryctemorphians, the thylacine, and three South American fossil metatherians. For the thylacine, he studied eight specimens, including an isolated petrosal and a sagittally-sectioned cranium; they ranged from a juvenile with the M2 erupting to an adult with all teeth worn. The thylacine basicranium was illustrated with twelve unlabeled stereophotographs, including two of the isolated petrosal, and two additional photographs with labels (Archer 1976: plates 1A–B, 2–3, 19A–B). This was a ground-breaking comparative effort with detailed descriptions. However, it was not always possible to locate structures in Archer's

unlabeled figures. Moreover, the petrosal is partially hidden by its bony neighbors, which makes description and illustration challenging.

Several more recent morphological contributions deserve mention here. Wroe (1997) reported on aspects of the dasyuromorphian basicranium related to the bulla and associated foramina and spaces, including *T. cynocephalus*. Ladevèze (2004: fig. 4D) included an illustration of the petrosal of *T. cynocephalus* in ventral view and comparisons to other marsupials. Murray and Megirian (2006) studied the composition of the tympanic floor in fossil thylacinids along with *T. cynocephalus*. Compared to Oligo-Miocene thylacinids, *T. cynocephalus* has a less enclosed tympanic floor, which these authors concluded is a derived condition within the family. In contrast, Archer (1976) argued the condition in *T. cynocephalus* was primitive and derived from a didelphid morphology. In an unpublished thesis, Dickson (2012; figs. 1, 8) included images of the inner ear of *T. cynocephalus* based on CT scan data. Newton et al. (2018) provided access to CT scans of thylacine pouch young; although not studied here, these data provide a wealth of information for cranial and skeletal ontogenesis. Warburton et al. (2019) published a well-illustrated comprehensive skeletal atlas of the thylacine. The craniodental descriptions were based primarily on one adult specimen and represent a useful introduction to the cranial anatomy, but contain few details of the basicranium. In their large comparative treatment of marsupials, Beck et al. (2022: fig. 40) addressed numerous cranial features of the thylacine and illustrated the skull. Lastly, MacPhee et al. (2023) is a broad comparative treatise on the pericarotid venous network (which includes the transverse canal foramen vein and internal carotid artery) in representatives of the seven marsupial orders and selected placentals. The thylacine is included based on a μCT scanned specimen and a coronally hemisected cranium. Although the pericarotid venous network is peripheral to the current report, MacPhee et al. (2023: figs. 30–31) included reconstructions of the major dural sinuses and selected coronal sections through the basicranium from the μCT scans.

Thylacinus cynocephalus is scored for basicranial characters in several recent phylogenetic analyses (e.g., Wroe et al. 2000; Kealy and Beck 2017; Muizon et al. 2018; Rovinsky et al. 2019; Muizon and Ladevèze 2020; Churchill et al. 2024). The most recent broadscale analysis across Marsupialia is Beck et al. (2022), which combined molecular data with 180 craniodental characters, including 35 from the ear region, for 97 marsupial terminals representing every currently recognized extant genus. They scored *T. cynocephalus* based on 22 specimens, including adults, subadults, and juveniles, along with several fossil thylacinids.

The Section of Mammals, Carnegie Museum of Natural History, has a single specimen of *T. cynocephalus*, CM 20975, the μCT scans of which are the focus of this report. Although the thylacine petrosal and inner ear have been the subject of prior studies as noted above, it is fitting that we glean more from the available museum specimens. As stated by Linnard and Sleightholme (2023:287) "For a species whose extinction was hastened by anthropogenic interventions, we have a moral obligation to preserve as much factual detail as possible about the Thylacine."

MATERIALS AND METHODS

The primary specimen studied is *Thylacinus cynocephalus*, CM 20975, a skull (Fig. 1) and nearly complete postcranial skeleton of a subadult thylacine, with the last lower molar erupting and the last upper molar not yet formed or missing. Unfortunately, beyond its provenance from Tasmania, additional data on this specimen are not available. It is unclear when Carnegie Museum acquired the specimen; it was accessioned in 1942 as one of 212 specimens "found during the recent reorganization of the storeroom and osteological collection." The braincase has ten small drill holes for wires that held loose bones together, primarily the left exoccipital (Fig. 1). The wires were removed and replaced by string prior to μCT scanning by the senior author. The basicranium was scanned at the Center for Quantitative Imaging, The Pennsylvania State University, with the 300 kV microfocus directional tube of the GE v|tome|x L300 X-ray CT Scanner. The 360° specimen rotation produced 2,024 equally spaced images; voxel size is 0.03 mm.

A second thylacine was studied, an adult female *T. cynocephalus*, AMNH 35866, received September 13, 1919, from the New York Zoological Society. The cranium minus the tip of the rostrum was scanned at the Duke Shared Materials Instrumentation Facility (SMiF), Duke University, with the Nikon Metrology XT H 225 ST. Funding was provided by National Science Foundation BCS 1825129 to D.M. Boyer and A.R. Harrington. The scan resulted in 1,870 tiff files (MorphoSource ark:/87602/m4/M76782); voxel size is 0.089392 mm. The files were downloaded from MorphSource.org, Duke University.

Additional μCT datasets were consulted for the following:

Monodelphis domestica (Wagner, 1842), AMNH 261241, adult male, collected 14 July 1985 in Porvenir, Luis Calvo, Chiquisaca, Bolivia. The cranium was scanned on the General Electric phoenix v|tome|x s240 at the American Museum of Natural History (AMNH) Microscopy and Imaging Facility (MIF). Eric Delson and the AMNH Department of Mammalogy provided access to these data, the collection of which was funded by AMNH and NYCEP. The files were downloaded from www.MorphoSource.org, Duke University. The CT image series included 1,586 tiff files (MorphoSource ark:/87602/m4/M23879); voxel size is 0.024336 mm. The cranial osteology of this specimen was described and illustrated in Wible (2022).

Monodelphis sp., DU BAA 0181, adult of unknown sex, received September 3, 1993, from Kathleen K. Smith's Lab, Department of Biological Anthropology and Anatomy, Duke University. The cranium was scanned at the

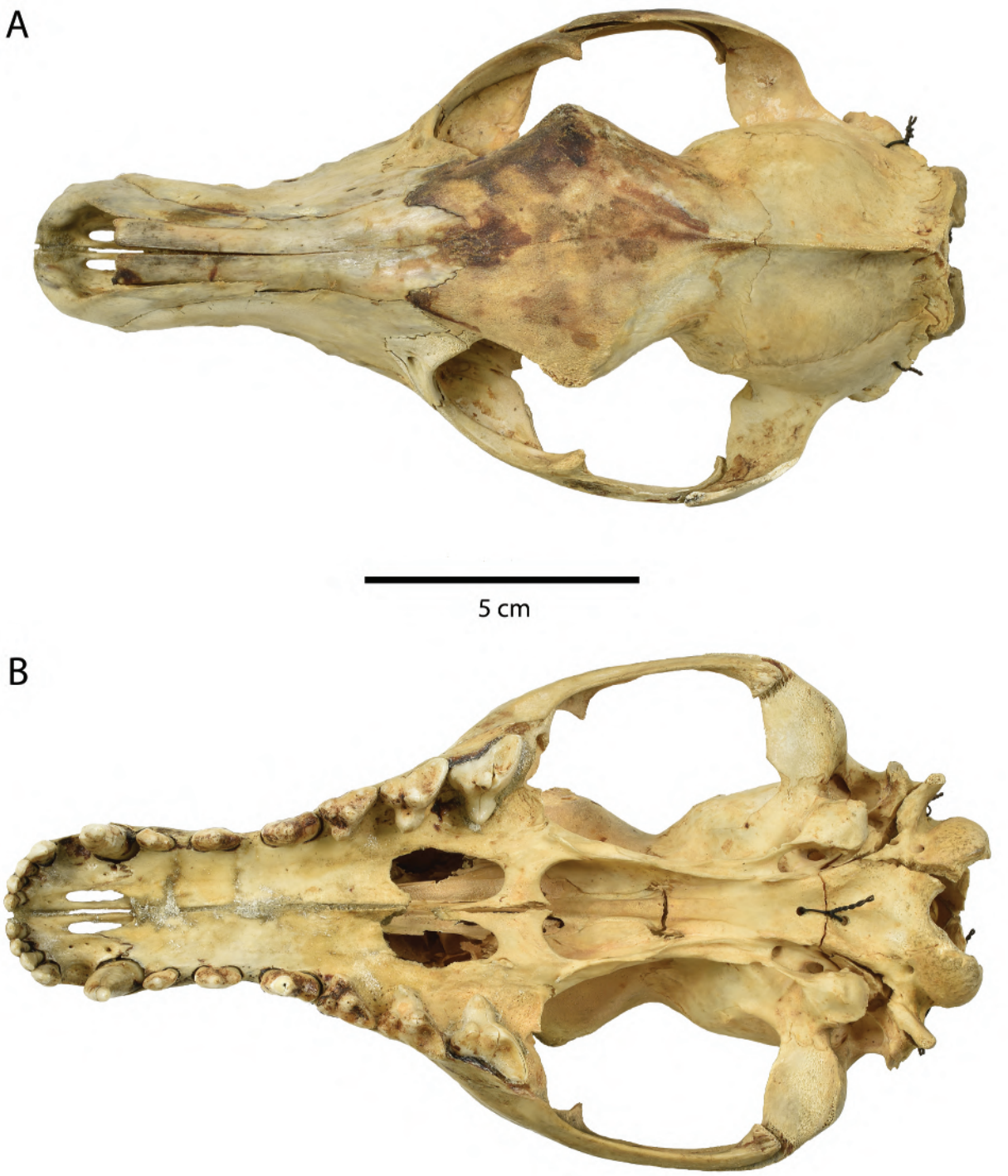

Fig. 1.—*Thylacinus cynocephalus*, CM 20975, cranium. **A,** dorsal and **B,** ventral views. Note wires holding loose bones together.

Duke Shared Materials Instrumentation Facility (SMiF), Duke University, with the Nikon Metrology XT H 225 ST. Funding was provided by National Science Foundation BCS 1552848 to D.M. Boyer and DBI 1458192 to G.F. Gunnell. The files were downloaded from MorphoSource.org, Duke University. The CT image series included 1,761 tiff files (MorphoSource doi:10.17602/M2/M58082); voxel size is 0.023166 mm.

Notoryctes caurinus Thomas, 1920, SAM M3139, adult of unknown sex, collected 1931 in Western Australia. The skull was scanned at the Medical Device Research Institute, Flinders University with Nikon Metrology XT H 225 ST. The files were downloaded from MorphoSource.org, Duke University. The CT image series included 1,813 tiff files (MorphoSource ark:/87602/m4/557574); voxel size is 0.013000 mm.

Isoodon macrourus (Gould, 1842), AMNH 160364, adult female, collected February 18, 1960, from Innisfail, Queensland. The skull was scanned at the Duke Shared Materials Instrumentation Facility (SMiF), Duke University, with the Nikon Metrology XT H 225 ST. Funding was provided by National Science Foundation 1825129 to D.M. Boyer and A.R. Harrington. The files were downloaded from MorphoSource.org, Duke University. The CT image series included 1,801 tiff files (MorphoSource doi:10.17602/M2/M99588); voxel size is 0.039881 mm.

Myrmecobius fasciatus Waterhouse, 1836, AMNH 155328, adult of unknown sex, received September 11, 1950, in exchange from Western Australian Museum. The skull was scanned at The University of Texas High-Resolution X-ray Computed Tomography Facility (University of Texas at Austin) with the Varian Medical Systems (BioImaging Research, Inc) ACTIS CT scanner with FeinFocus X-ray source. The files were downloaded from MorphoSource.org, Duke University. The CT image series included 782 tiff files (MorphoSource ark:/87602/m4/M167371); X and Y spacing is 0.035160 mm and Z spacing 0.076430.

Dasyurus hallucatus Gould, 1842, AMNH 196840, adult male collected June 17, 1965, from Inglis Gap, Western Australia. The skull was scanned at the Duke Shared Materials Instrumentation Facility (SMiF), Duke University, with the Nikon Metrology XT H 225 ST. Funding was provided by National Science Foundation BCS 1825129 to D.M. Boyer and A.R. Harrington. The files were downloaded from MorphoSource.org, Duke University. The CT image series included 1,801 tiff files (MorphoSource doi:10.17602/M2/M106395); voxel size is 0.047736 mm.

Sminthopsis macroura (Gould, 1845), AMNH 108934, adult male collected June 1, 1938, from Malbon, Queensland. The skull was scanned at the Duke Shared Materials Instrumentation Facility (SMiF), Duke University, with the Nikon Metrology XT H 225 ST. Funding was provided by National Science Foundation BCS 1825129 to D.M. Boyer and A.R. Harrington. The files were downloaded from MorphoSource.org, Duke University. The CT image series included 1,741 tiff files (MorphoSource doi:10.17602/M2/M84585); voxel size is 0.014372 mm.

Table 1 includes pertinent cranial measurements of the studied sample.

The elements of the middle ear, inner ear, and major venous channels were segmented manually slice by slice from the µCT datasets using the segmentation tools and measured in Avizo (Thermo Fischer Scientific, Waltham, Massachusetts).

Terminology follows prior works by the authors (e.g., Wible 2003, 2008, 2022; Wible and Bertrand 2024). Where appropriate, terms are used from the Nomina Anatomica Veterinaria (2017). During our investigations, we encountered osteological correlates for a novel venous system in the two thylacines, CM 20975 and AMNH 35866, involving channels through the parietal, interparietal, supraoccipital, exoccipital, and petrosal. A small portion of the canal system is present in the didelphimorphian *Mo. domestica*, which Wible (2022) called the interparietal diploic vein. We introduce this system here because it touches the petrosal, but we intend to more thoroughly study this system in a comparative manner in a subsequent paper (Wible and Bertrand in preparation). For the terminology of the bony labyrinth, we follow Orliac and O'Leary (2016).

Some quantitative data are generated for the inner ear of the different specimens. We estimated the cochlear coil and numbers of cochlear turns using the method of Geisler and Luo (1996). At the base of the cochlea above the fenestra cochleae, a line was drawn from the intersection between the primary and secondary bony laminae, that then passed through the center of the cochlea. Half a turn was counted each time the line was crossed. Then an angle was added for the remainder of the cochlear canal. The number of turns corresponds to the total angle divided by 360°. The secondary bony lamina coil was calculated in a similar manner which corresponds to the extent of the secondary bony lamina. Angles between each semicircular canal were measured following Ekdale (2009), and the height and width of each canal was measured using Ekdale's (2013: fig. 3e) method. The radius of curvature was calculated with the following equation: [0.5*((h+w)/2)] (Spoor and Zonneveld 1998), where h is the height of the canal and w is the width (see Ekdale 2013: fig. 3d).

Institutional Abbreviations.—AMNH, Department of Mammalogy, American Museum of Natural History, New York, New York, USA; **CM,** Section of Mammals, Carnegie Museum of Natural History, Pittsburgh, Pennsylvania, USA; **DU BAA,** Department of Biological Anthropology and Anatomy, Duke University, Durham, North Carolina, USA; **J,** Queensland Museum, Brisbane, Australia; **SAM,** Mammalogy, South Australian Museum, Adelaide, Australia; **UMZC,** University Museum of Zoology, Cambridge University, Cambridge, United Kingdom; **USNM,** Division of Mammals, National Museum of Natural History, Smithsonian Institution, Washington, D.C., USA.

TABLE 1. Cranial measurements from μCT scans of the studied sample in mm. Some measurements are missing for *T. cynocephalus*, AMNH 35866, as the tip of the snout is not included in the scans. Abbrevations: **BBP,** breadth of bony palate across first molar; **LR,** length of rostrum anterior to infraorbital foramen; **ONL,** occipitonasal length; **PCL,** premaxillary-condylar length; **PL,** palatal length; **POB,** minimum postorbital breadth; **POL,** preorbital length; **PPL,** postpalatal length; **ZB,** greatest zygomatic breadth.

	Thylacinus cynocephalus CM 20975	*Thylacinus cynocephalus* AMNH 35866	*Monodelphis domestica* AMNH 261241	*Monodelphis* sp. DU BAA 0181	*Notoryctes caurinus* SAM M3139	*Isoodon macrourus* AMNH 160364	*Myrmecobius fasciatus* AMNH 155328	*Dasyurus hallucatus* AMNH 196840	*Sminthopsis macroura* AMNH 108934
ONL	143.5		36.1	40.0	22.4	69.9	57.0	61.9	24.1
PCL	159.4		36.4	39.4	19.9	71.3	58.5	65.5	25.1
LR	70.6		11.6	12.9	7.5	26.2	22.1	21.9	8.2
POL	56.7		13.9	13.6	10.9	36.7	24.9	26.1	8.6
PL	86.0		20.0	21.3	10.2	40.9	39.7	35.2	12.4
PPL	74.3	95.3	16.7	18.5	9.9	27.4	20.2	31.9	13.0
POB	29.6	42.7	6.5	5.9	9.5	11.2	17.4	8.4	6.0
ZB	87.5	114.4	20.1	22.1	14.3	30.6	31.5	39.8	14.4
BBP	39.1	51.8	10.8	12.5	8.4	18.3	11.1	17.0	6.9

DESCRIPTIONS

Osteology

The descriptions primarily focus on the subadult *T. cynocephalus*, CM 20975, with comments on AMNH 35866. Although the paired petrosal and inner ear are the main subjects, we begin with salient points on the neighboring bones, which include the paired squamosal, alisphenoid, exoccipital, and parietal, and the unpaired basisphenoid, basioccipital, and supraoccipital. This should also include the paired bones of the auditory apparatus, the ectotympanic, malleus, incus, and stapes. However, none of these auditory elements are preserved in AMNH 35866 and only the stapes is preserved in CM 20975. For the first three bones, we refer the reader to the literature. Archer (1976) provided descriptions of the ectotympanic, malleus, and incus, but only the first is figured; all four bones are illustrated in Doran (1878: plate 64, figs. 17, 43). Below, we treat the exterior and interior bony neighbors before addressing the petrosal and inner ear. The left side is figured, and differences between the sides are noted.

Basisphenoid ("bs").—The unpaired basisphenoid is a rectangular midline element (Fig. 2A) that is fused laterally to its paired wings, the alisphenoids ("as" in Fig. 2A). However, what appears to be a short sutural remnant demarcating the two is visible on the posterolateral margin of the basisphenoid on the endocranial surface ("ssu" in Fig. 3). The basisphenoid contacts the basioccipital posteriorly ("bo" in Fig. 2A) and has a small, posterolaterally-directed spinous process ("sp" in Fig. 2A) that nearly contacts the anteromedial tip of the petrosal ("pe" in Fig. 2A). With the petrosal, this spinous process forms the medial aspect of the slit-like foramen for the greater petrosal nerve (Wible 2003; "fgpn" in Fig. 2B), which is closed laterally by the alisphenoid. This foramen is fully closed in AMNH 35866. The ventral surface of the basisphenoid is flat except posteriorly where there is a slight midline concavity flanked by thick elevations that posteriorly continue and are more substantial on the basioccipital ("mt" in Fig. 2B), representing attachments for neck muscles (rectus capitis ventralis = rectus capitis anticus in *Didelphis virginiana* (Kerr, 1792), according to Coues 1872). Anterior to this thickening is a thin, ventrally projecting crest on the lateral margin of the basisphenoid, the lateral process of Warburton et al. (2019; "lpbs" in Figs. 2B, 4A, 5). The medial surface of the lateral process has four or five small nutrient foramina, one of which is visible in Figure 5A ("f"). Lateral and then anterior to the lateral process is the narrow sulcus for the nerve of the pterygoid canal ("snpc" in Fig. 2B). Anterior to the nerve sulcus on the lateral margin

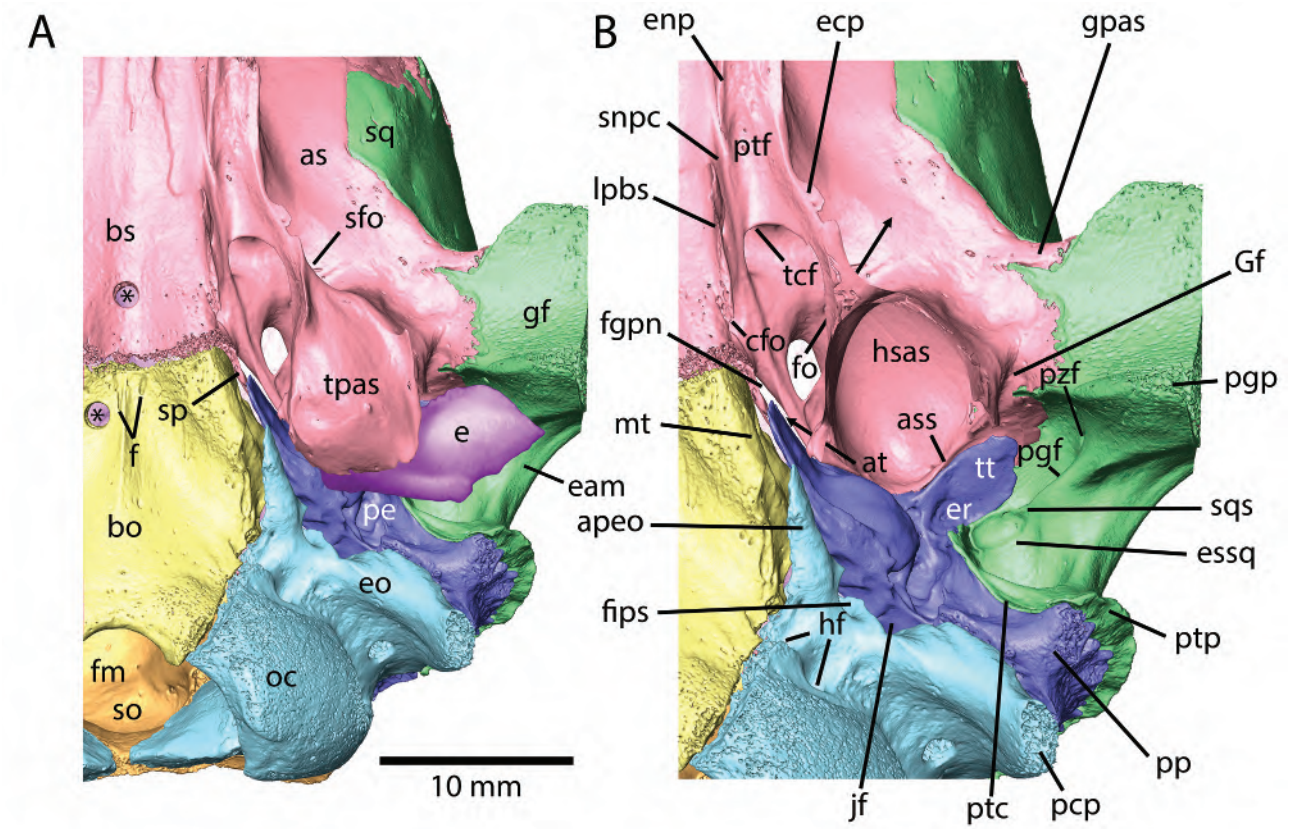

Fig. 2.—*Thylacinus cynocephalus*, CM 20975, isosurface of left basicranium derived from µCT scans in ventral views. **A,** full basicranium; **B,** close up of middle ear with ectotympanic and ventral half of the tympanic process of the alisphenoid removed. Anterior to top of page. Asterisks are in drill holes; lateral aspect of glenoid fossa and postglenoid process are missing from the scans; anterior process of exoccipital is shifted laterally and would lie in a facet on the basioccipital. The ectotympanic is not preserved in CM 20975 but is added in A based on Warburton et al. (2019: fig. 2). Abbreviations: **apeo,** anterior process of exoccipital; **as,** alisphenoid; **ass,** alisphenoid septum; **at,** arrow indicates passage of auditory tube; **bo,** basioccipital; **bs,** basisphenoid; **cfo,** carotid foramen; **e**, ectotympanic; **eam,** external acoustic meatus; **ecp,** ectopterygoid process; **enp,** entopterygoid process; **eo,** exoccipital; **er,** epitympanic recess; **essq,** posterior epitympanic sinus of squamosal; **f,** foramen; **fgpn,** foramen for greater petrosal nerve; **fips,** foramen for inferior petrosal sinus; **fm,** foramen magnum; **fo,** foramen ovale with arrow showing course of mandibular nerve to secondary foramen ovale; **gf,** glenoid fossa; **Gf,** Glaserian fissure; **gpas,** glenoid process of alisphenoid; **hf,** hypoglossal foramina; **hsas,** hypotympanic sinus of alisphenoid; **jf,** jugular foramen; **lpbs,** lateral process of basisphenoid; **mt,** muscular tubercle; **oc,** occipital condyle; **pcp,** paracondylar process of exoccipital; **pe,** petrosal; **pgf,** postglenoid foramen; **pgp,** postglenoid process; **pp,** paroccipital process of petrosal; **ptc,** posttympanic crest of squamosal; **ptf,** pterygoid fossa; **ptp,** posttympanic process of squamosal; **pzf,** postzygomatic foramen; **sfo,** secondary foramen ovale; **snpc,** sulcus for nerve of pterygoid canal; **so,** supraoccipital; **sp,** spinous process of basisphenoid; **sq,** squamosal; **sqs,** squamosal septum; **tcf,** transverse canal foramen; **tpas,** tympanic process of alisphenoid; **tt,** tegmen tympani..

of the basisphenoid is the low posterior base of the entopterygoid process ("enp" in Fig. 2B), which anteriorly supports the pterygoid bone. The side of the basisphenoid dorsolateral to the lateral process has two foramina that are largely hidden in direct ventral view. Posteriorly is the slightly larger carotid foramen ("cfo" in Fig. 2B; entocarotid foramen of Archer 1976 and Murray and Megirian 2006) and anterodorsolaterally the transverse canal foramen ("tcf" in Fig. 2B). As reported by MacPhee et al. (2023) for *Thylacinus*, these foramina open into the same intramural space (Fig. 5) and then into paired large oval openings in the endocranial floor (Fig. 3). Posterolateral to these endocranial openings are paired shallow sulci for the inferior petrosal sinus ("sips" in Fig. 3) and anterolaterally are paired sulci for the contents of the sphenorbital fissure ("sof" in Fig. 3). MacPhee et al. (2023: figs. 30F, 31A–B) illustrated a hypophyseal fossa for *Thylacinus* on an endocast reconstruction and also labelled the hypophyseal fossa and infundibular sulcus on coronal sections from a µCT dataset. Comparable structures are not present CM 20975 and AMNH 38566, and a distinct hypophyseal fossa is not visible (Fig. 3).

Alisphenoid ("as").—Posteriorly, the paired alisphenoid has a broad contact with the petrosal (Fig. 2), laterally, it is overlapped by the squamosal ("sq" in Figs. 2A, 4A), and anterolaterally, it overlaps the frontal. Immediately lateral to the basisphenoid, from posterior to anterior, the

alisphenoid has the foramen ovale for the mandibular nerve ("fo" in Fig. 2B), a shelf leading to the carotid and transverse canal foramina in the basisphenoid, and a narrow longitudinal gutter, the pterygoid fossa ("ptf" in Fig. 2B), in the position of the internal pterygoid muscle attachment in *Didelphis marsupialis* Linnaeus, 1758 (Hiiemae and Jenkins 1969; Turnbull 1970). The lateral margin of the pterygoid fossa is formed by a low crest, the ectopterygoid process ("ecp" in Fig. 2B) that increases in height posterolaterally and contacts the enlarged tympanic process of the alisphenoid ("tpas" in Fig. 2A). Opposite the foramen ovale, this crest has an opening that is twice the size of the foramen ovale, the secondary foramen ovale of Archer (1976; "sfo" in Figs. 2A, 4A), that transmits the mandibular nerve, as in a variety of other marsupials (Wroe 1997). Archer (1976:320) referred to this connecting bridge as a "bony strut from alisphenoid tympanic wing forming foramen ovale canal." Here, we identify this strut and the connecting crest anterior to it as the ectopterygoid process, a structure that is wholly absent in the didelphid *Monodelphis* (Wible 2003, 2022). The globular tympanic process has sharp, ventrally-directed medial and lateral crests, the former continuous with the ectopterygoid process (both are visible in the anterior view in Fig. 5B on either side of the leader line indicating the tympanic process). In addition to covering the anterior part of the petrosal, the tympanic process also covers the medial part of the ectotympanic ("e"in Fig. 2A; Archer 1976; Warburton et al. 2019).

The tympanic process (tympanic wing of alisphenoid of Archer 1976) is attached to its alisphenoid base anteriorly, medially, and laterally; its posterior edge is free, allowing for communication between the space it contains and the middle ear cavity. This gap continues onto the posteromedial aspect of the tympanic process, where it accommodates the auditory tube ("at" in Fig. 2B), which connects the middle ear and nasopharynx. The ventral part of the tympanic process is removed in Figure 2B, exposing the deeply concave hypotympanic sinus of the alisphenoid ("hsas" in Fig. 2B), an accessory air space of the middle ear that does not contain any principal elements such as the auditory ossicles (Klaauw 1931). The hypotympanic sinus is longer than wide and its roof is formed by the epitympanic wing of the alisphenoid (sensu MacPhee 1981). Its posterior edge is downturned and forms a low septum ("ass" in Fig. 2B) that abuts the petrosal. Lateral to the tympanic process, the alisphenoid epitympanic wing has a steep wall extending posterodorsally into the middle ear that is overlain by a tongue-shaped process of the petrosal, the tegmen tympani ("tt" in Fig. 2B). A narrow groove ("Gf" in Fig. 2B) runs along this surface just lateral to the tympanic process; this is the Glaserian fissure, which transmits the chorda tympani nerve. The alisphenoid's contribution to the foramen for the greater petrosal nerve was mentioned above (Fig. 2B). Warburton et al. (2019:14) noted "Just lateral to this foramen is the groove for the auditory tube, which is lined medially by the petrosal, and dorsally and laterally by the alisphenoid." CM 20975 and AMNH 35866 do not have a recognizable groove for the auditory tube.

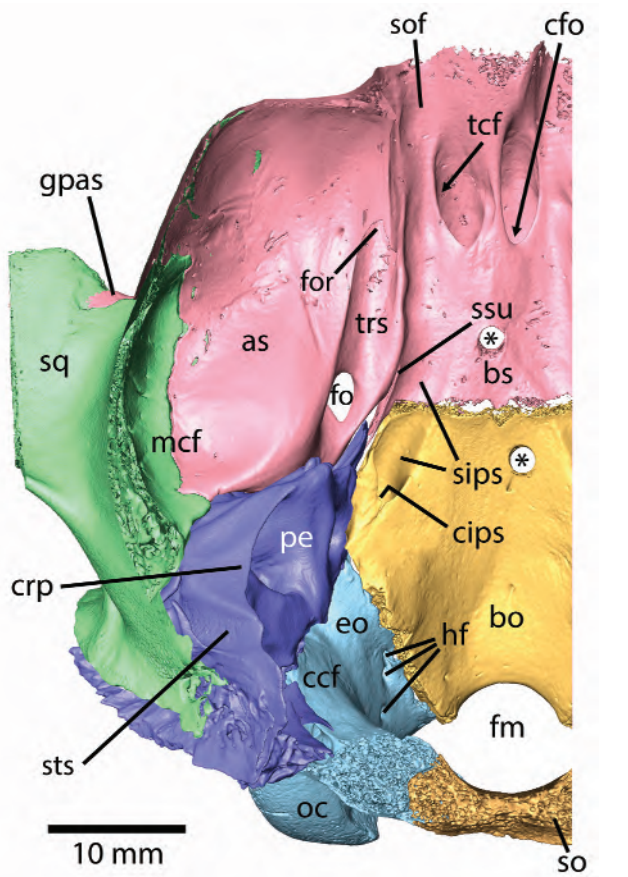

Fig. 3.—*Thylacinus cynocephalus*, CM 20975, isosurface of left endocranial floor derived from μCT scans in dorsal view. The dorsal aspects of the alisphenoid, squamosal, exoccipital, and supraoccipital have all been removed in the same plane but the petrosal has been left intact. The canal for the inferior petrosal sinus in the basioccipital is missing from the left side due to damage, but is reconstructed here based on the right side. Anterior to top of page. Asterisks are in drill holes. Abbreviations: **as,** alisphenoid; **bo,** basioccipital; **bs,** basisphenoid; **ccf,** caudal cranial fossa; **cfo,** carotid foramen; **cips,** canal for inferior petrosal sinus; **crp,** crista petrosa; **eo,** exoccipital; **fm,** foramen magnum; **fo,** foramen ovale; **for,** foramen rotundum; **gpas,** glenoid process of alisphenoid; **hf,** hypoglossal foramina; **mcf,** middle cranial fossa; **oc,** occipital condyle; **pe,** petrosal; **sips,** sulcus for inferior petrosal sinus; **so,** supraoccipital; **sof,** sphenorbital fissure; **sq,** squamosal; **ssu,** remnant of sphenoid suture; **sts,** sulcus for transverse sinus; **tcf,** transverse canal foramen; **trs,** trigeminal sulcus.

The alisphenoid is a major component of the floor of the middle cranial fossa (Fig. 3). Immediately lateral to the basisphenoid is a longitudinal gutter for the trigeminal nerve ("trs" in Fig. 3) connecting the foramen ovale and foramen rotundum ("for" in Fig. 3). The other notable feature is how far dorsally the roof of the hypotympanic sinus ("hsas" in Fig. 5) projects into the middle cranial fossa floor.

Squamosal ("sq").—In the lateral braincase wall, the paired squamosal overlaps the parietal dorsally ("p" in Fig. 4A), the frontal anterodorsally ("fr" in Fig. 4A), and the alisphenoid anteroventrally. Its only other bony contact is with the petrosal, which the posterior third of the squamosal nearly completely covers (Fig. 4A). Two ventrally-directed processes occur along the ventral margin of the squamosal's posterior third: the larger postglenoid process ("pgp" in Fig. 4A), and behind it the posttympanic process ("ptp" in Fig. 4A). The latter is appressed to the paroccipital process of the petrosal ("pp" in Fig. 4A; mastoid process of Archer 1976), and a crest extends posterodorsally from these two processes, contributing to the nuchal crest ("nc" in Fig. 4A). Between the postglenoid and posttympanic processes is a deep concavity in lateral view that marks the passage of the external acoustic meatus ("eam" in Fig. 2B). Posterodorsal to the midpoint of this concavity is the posteriorly-directed suprameatal foramen ("sumf" in Fig. 4A; subsquamosal foramen of Cope 1880).

In ventral view, the interval on the squamosal between the postglenoid and posttympanic processes is dominated anteriorly by the postglenoid foramen (=dorsal postglenoid foramen of Archer 1976; "pgf" in Fig. 2B) and posteriorly by the posterior epitympanic sinus of Wroe et al. (1998; see below) ("essq" in Fig. 2B). The postglenoid foramen is not visible in ventral view; it is an anteriorly-directed foramen obscured by a broad crest running posteromedially from the rear of the postglenoid process (Fig. 2). Whereas the postglenoid foramen is entirely within the squamosal on the left side and bilaterally in AMNH 35866, it is between the squamosal and petrosal on the right of CM 20975 (see Petrosal below). The roof of the space that the postglenoid foramen opens into is an epitympanic wing of the squamosal (sensu MacPhee 1981; postglenoid concavity of Archer 1976). Archer (1976) noted that the in situ ectotympanic delimits dorsal and ventral postglenoid foramina in *Thylacinus*: the former in the squamosal and the latter near the Glaserian fissure between the squamosal, alisphenoid, and ectotympanic (Archer 1976: plate 1B). Warburton et al. (2019:14) stated "Anterior to the ectotympanic, the postglenoid foramen is subdivided into two foramina by a posteriorly-directed process on the alisphenoid." This process on the alisphenoid is not noted on their figures, and CM 20975 and AMNH 38566 have no comparable structure. Anterior to the postglenoid foramen are two tiny postzygomatic foramina in CM 20975; the anterior of the two is partially visible in direct ventral view ("pzf" in Fig. 2B).

Following Klaauw (1931), an epitympanic sinus is an accessory air space of the middle ear either in the squamosal or petrosal that does not contain any principal elements such as auditory ossicles and is derived from the epitympanic recess, the space over the articulation between the malleus and incus ("er" in Fig. 2B). Wroe et al. (1998) differentiated anterior and posterior epitympanic sinuses in the squamosal in some diprotodontians, the anterior in the zygomatic process and the posterior proximal to the epitympanic recess. CM 20975 has a roughly circular posterior epitympanic sinus in the squamosal that is less than half the size of the hypotympanic sinus of the alisphenoid (Fig. 2B). Its anterior border is formed by a low septum ("sqs" in Fig. 2B) that also forms the posterolateral border of the epitympanic recess, which otherwise is within the petrosal. The medial edge of this septum forms the lateral wall of the fossa incudis, a separate space behind the epitympanic recess for the crus breve of the incus (not visible in Fig. 2; see Petrosal below). In both CM 20975 and AMNH 38566, a second lower septum weakly delimits a small oval depression within the anteriormost part of the posterior epitympanic sinus (the "essq" leader line is on this septum in Fig. 2B). The function of this subdivision of the sinus is unknown. The posteromedial wall of the posterior epitympanic sinus is formed by the posttympanic crest (sensu Wible et al. 2004; "ptc" in Figs. 2B, 4A), which continues posterolaterally and ends at the posttympanic process. The posttympanic crest is appressed to the crista parotica of the petrosal (see Petrosal below). With the ectotympanic bone in place, most of the posterior epitympanic sinus of the squamosal is hidden from ventral view (Archer 1976: plate 1B; Warburton et al. 2019: fig. 2.2).

In endocranial view (Fig. 5), the squamosal is a large element in the posterior wall of the middle cranial fossa and has no exposure in the caudal cranial fossa. The squamosal contributes to or solely forms canals for veins draining from the transverse sinus, including those in the postglenoid, postzygomatic, and suprameatal foramina (MacPhee et al. 2023).

Occipital Complex.—The subadult thylacine, CM 20975, has four bones in the occipital complex described separately below: a ventral midline element (basioccipital), paired lateral elements (exoccipitals), and a dorsal midline element (supraoccipital). In contrast, in the adult, AMNH 38566, these four fuse to form a single occipital bone.

Basioccipital ("bo").—In ventral and dorsal views, the unpaired basioccipital (Figs. 2A, 3) contacts the basisphenoid anteriorly, the petrosal anterolaterally, and the exoccipital posterolaterally. The occipital condyle is primarily on the exoccipital ("oc" in Fig. 2A), but a small articular area crosses the suture onto the basioccipital. The basioccipital's ventral surface has a low midline crest on its anterior half, and a pronounced muscular tubercle ("mt" in Fig. 2B) for neck muscle attachment (rectus capitis ventralis = rectus capitis anticus in *Didelphis virginiana,* according to Coues 1872) opposite the basioccipital's contact with the petrosal. The muscular tubercle continues anteriorly onto the basisphenoid and posteriorly onto the exoccipital, and the combined structure is more prominent in the adult AMNH 38566. Archer (1976) described a nutrient foramen piercing the midline crest anteriorly present in all specimens, which he named the median basioccipital foramen; he noted young specimens had additional foramina adjacent to this one. AMNH 38566 has the median

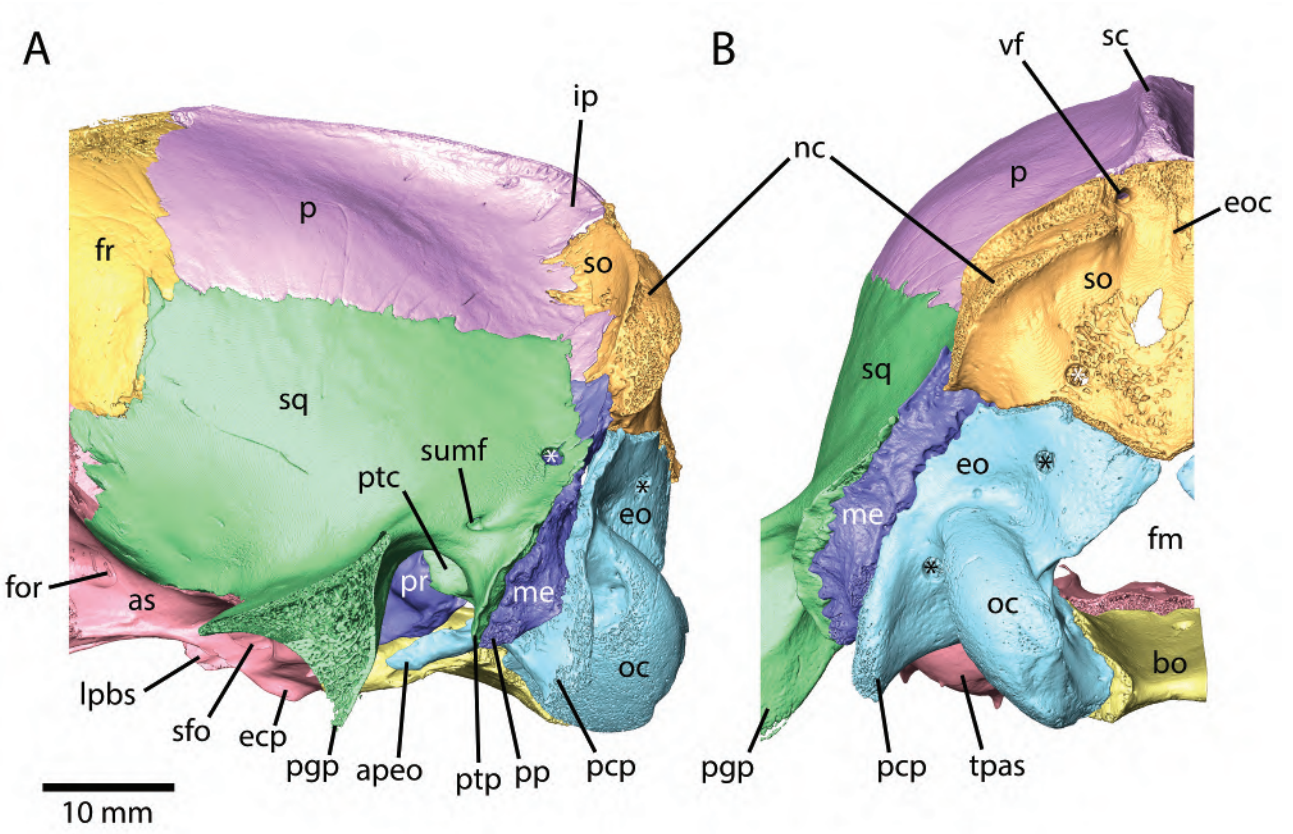

Fig. 4.—*Thylacinus cynocephalus*, CM 20975, isosurface of left posterior cranium derived from µCT scans. **A,** lateral view (anterior to left); **B,** posterior view (lateral to left). Asterisks are in drill holes; lateral aspect of glenoid fossa and postglenoid process are missing from the scans; anterior process of exoccipital is shifted laterally and would lie in a facet on the basioccipital. Abbreviations: **apeo,** anterior process of exoccipital; **as,** alisphenoid; **bo,** basioccipital; **ecp,** ectopterygoid process; **eo,** exoccipital; **eoc**, external occipital crest; **fm,** foramen magnum; **for,** foramen rotundum; **fr,** frontal; **ip,** interparietal; **lpbs,** lateral process of basisphenoid; **me,** mastoid exposure of petrosal; **nc,** nuchal crest; **oc,** occipital condyle; **p,** parietal; **pcp,** paracondylar process of exoccipital; **pgp,** postglenoid process; **pp,** paroccipital process of petrosal; **pr,** promontorium of petrosal; **ptc,** posttympanic crest of squamosal; **ptp,** posttympanic process of squamosal; **sc,** sagittal crest; **sfo,** secondary foramen ovale; **so,** supraoccipital; **sq,** squamosal; **sumf,** suprameatal foramen; **tpas,** tympanic process of alisphenoid; **vf,** venous foramen.

foramen, whereas CM 20975 has two foramina asymmetrically arranged ("f" in Fig. 2A). The most noteworthy structure on the basioccipital's endocranial surface is the wide and deep sulcus for the inferior petrosal sinus ("sips" in Fig. 3) in the interval opposite the contact with the petrosal. The sulcus continues anteriorly onto the basisphenoid and posteriorly into a canal within the basioccipital ("cips" in Fig. 3). Archer (1976) and Murray and Megirian (2006) called this the internal jugular canal, but it transmits the inferior (ventral) petrosal sinus in didelphids (Dom et al. 1970; Wible 2003).

Exoccipital ("eo").—In ventral view, the paired exoccipital (Fig. 2A; paroccipital of Archer 1976) is triangular, with its anteromedial side contacting the basioccipital, its anterolateral side the petrosal, and its posterior side forming the rear aspect of the basicranium. Prominent structures occur at the three angles. At the rostral angle is a novel structure, an anteriorly-directed spine-like process wedged between the basioccipital and petrosal that we call the anterior process of the exoccipital ("apeo" in Fig. 2B). At the posteromedial angle is the occipital condyle, and at the posterolateral angle the prominent paracondylar process ("pcp" in Figs. 2B, 4; paroccipital process of Archer 1976 and Murray and Megirian 2006). The latter is vertical, mediolaterally compressed, and abuts though is much longer than the paroccipital process of the petrosal ("pp" in Figs. 2B, 4A).

In posterior view, the exoccipitals contact the mastoid exposure of the petrosal laterally and the supraoccipital dorsally ("me" and "so," respectively in Fig. 4B). The exoccipitals form the dorsal border of the foramen magnum, excluding the supraoccipital. The occipital condyle is cylindrical, much longer dorsoventrally than mediolaterally wide. In the endocranial surface (Fig. 5), the exoccipital contacts the basioccipital ventromedially, the petrosal anteriorly, and the supraoccipital dorsally.

Several neurovascular foramina lie within the exoccipital or between it and the petrosal. On the ventral surface

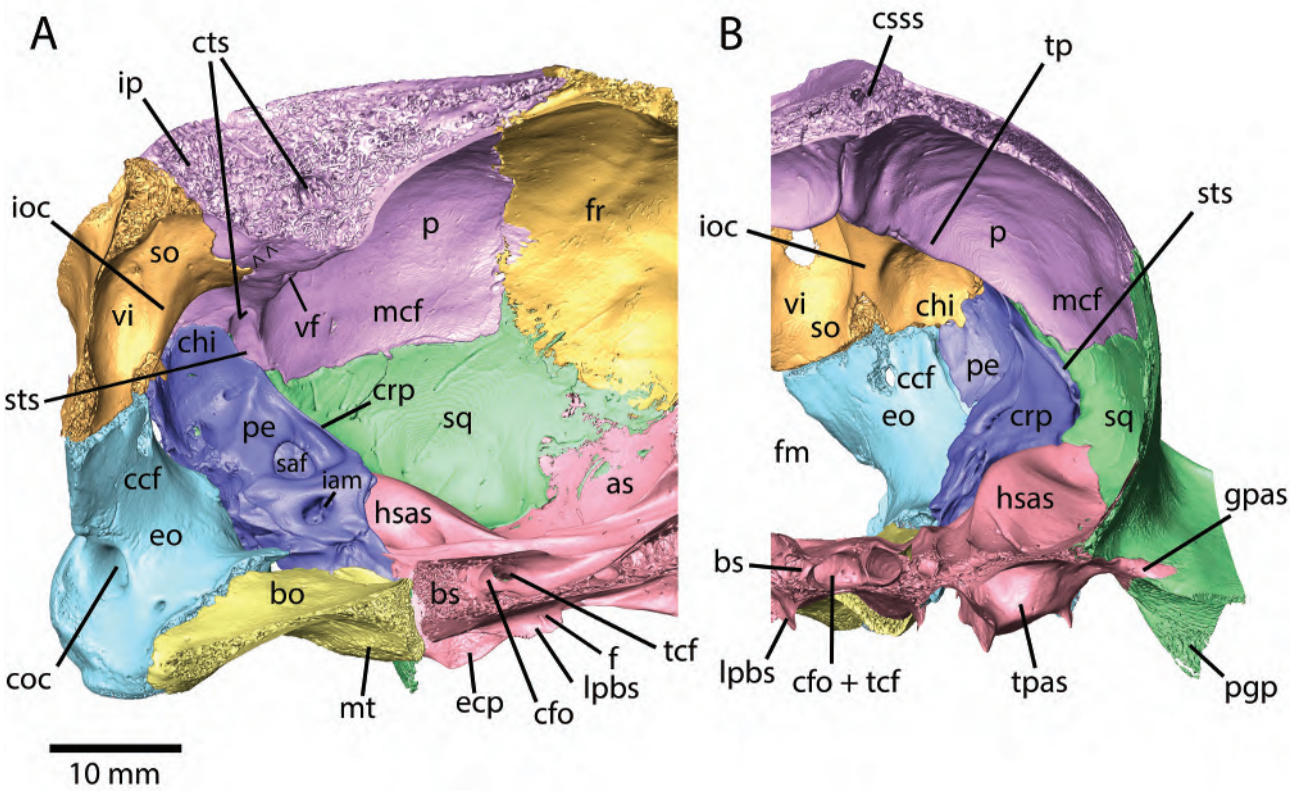

Fig. 5.—*Thylacinus cynocephalus*, CM 20975, isosurface of left posterior cranium derived from µCT scans. **A,** medial view (anterior to right); **B,** anterior view (lateral to right). In A, parasagittal cut is to the left of the midline; "^" indicates sutural remnant between parietal and interparietal; in B, transverse cut is posterior to frontoparietal suture. Lateral aspect of glenoid fossa and postglenoid process are missing from the scans. Abbreviations: **as,** alisphenoid; **bo,** basioccipital; **bs,** basisphenoid; **ccf,** caudal cranial fossa; **cfo,** carotid foramen; **chi,** cerebellar hemisphere impression; **coc,** condyloid canal; **crp,** crista petrosa; **csss,** canal for superior sagittal sinus; **cts,** canal for transverse sinus; **ecp,** ectopterygoid process; **eo,** exoccipital; **f,** foramen; **fm,** foramen magnum; **fr,** frontal; **gpas,** glenoid process of alisphenoid; **hsas,** roof of hypotympanic sinus; **iam,** internal acoustic meatus; **ioc,** internal occipital crest; **ip,** interparietal; **lpbs,** lateral process of basisphenoid; **mcf,** middle cranial fossa; **mt,** muscular tubercle; **p,** parietal; **pe,** petrosal; **pgp,** postglenoid process; **saf,** subarcuate fossa; **so,** supraoccipital; **sq,** squamosal; **sts,** sulcus for transverse sinus; **tcf,** transverse canal foramen; **tp,** tentorial process of parietal; **tpas,** tympanic process of alisphenoid; **vf,** venous foramen; **vi,** vermiform impression.

anterior to the occipital condyle are two anteriorly-directed foramina ("hf" in Fig. 2B). The posterolateral one is larger and entirely within the exoccipital; the anteromedial one has a small contribution from the basioccipital to its anteromedial margin. On the endocranial surface posterior to the suture with the basioccipital are three small openings in the exoccipital ("hf" in Fig. 3), with the anterior two closer together. All three connect to the same space within the exoccipital, which in turn connects to the two foramina on the ventral surface. On the ventral surface, Archer (1976) reported two or three foramina in *T. cynocephalus* and identified the lateralmost and largest as the venous condylar foramen and the other(s) as hypoglossal foramina. As we are unsure of the contents of these openings in CM 20975, we provisionally identify the two openings on the ventral surface and three endocranial openings as hypoglossal foramina. Two larger foramina lie in the abutment between the exoccipital and petrosal; the two are only partially separated by a projection from the exoccipital. The posterolateral opening is the jugular foramen ("jf" in Fig. 2B; posterior lacerate foramen of Archer 1976 and Murray and Megirian 2006), which in light of the course of the sigmoid sinus (see below) only transmits cranial nerves IX, X, and XI. The anteromedial opening is the foramen for the inferior petrosal sinus ("fips" in Fig. 2B; internal jugular canal of Archer 1976 and Murray and Megirian 2006), which lies at the posterior end of the canal for the inferior petrosal sinus in the basioccipital mentioned above.

Two large venous canals run through the exoccipital and unite just anterior to their common posterior exit at the condyloid canal ("coc" in Fig. 5A; craniospinal foramen of MacPhee et al. 2023) in the rim of the foramen magnum. A longitudinal canal begins just posterior to the foramen for the inferior petrosal sinus and represents an additional conduit for venous blood in that vessel. The second canal, which we interpret for the sigmoid sinus (see below) extends vertically and then turns anterolaterally to end in a

space in the contact between the exoccipital and petrosal. Two more canals diverge from this one: a lateral canal for the continuation of the sigmoid sinus through the petrosal and a vertical canal that runs between the exoccipital and petrosal (see below). The latter continues in canals through the supraoccipital, interparietal, and parietal to meet the canal for the transverse sinus (see below). We have not encountered a similar structure in other mammals, and in light of the bones contributing to its passageway, we call it the parieto-occipital diploic vein.

Supraoccipital ("so").—On the occiput, the unpaired supraoccipital abuts the exoccipitals ventrally and the mastoid exposure of the petrosals ventrolaterally (Fig. 4B), and on the braincase roof is overlain by the parietals anterodorsolaterally and the interparietal anterodorsomedially ("p" and "ip," respectively in Fig. 4A). The dorsal margin of the supraoccipital is the main constituent of the nuchal crest ("nc" in Fig. 4). A narrow medial portion of the nuchal crest is not robust and is formed by supraoccipital and interparietal, whereas the wider lateral portion is very robust and formed exclusively by the supraoccipital (Fig. 4). Extending ventrally on the occiput midline from the nuchal crest is a short external occipital crest ("eoc" in Fig. 4B). To the left of the crest is a venous foramen that joins the canals in the supraoccipital, interparietal, and parietal described above.

On the endocranial surface, the supraoccipital forms the posterior wall of the caudal cranial fossa housing the cerebellum. It has a large central concave surface for the vermis ("vi" in Fig. 5) and laterally, paired smaller concavities for the cerebellar hemispheres ("chi" in Fig. 5B). The petrosal and parietal also contribute to the latter concavity, more than doubling the size of this space that is on the supraoccipital.

Parietal ("p") + Interparietal ("ip").—Warburton et al. (2019) reported an interparietal for the thylacine, although they did not specify whether it was separate from or fused with the parietal. They labelled the bone in photographs of the crania of two specimens (Warburton et al. 2019: figs. 2.1, 4.2) but sutures are not evident. Beck et al. (2022) reported a large interparietal delimited by sutures in juvenile *T. cynocephalus* (e.g., SAM M1958) and noted the bone is fused to the parietals and supraoccipital in older specimens. In CM 20975, the dorsal (extracranial) surface of the braincase lacks a midline suture between the right and left parietals (Fig. 4B) as well as a suture delimiting a separate interparietal, but retains a suture between the parietal/interparietal and the supraoccipital (Fig. 4A). The ventral (endocranial) surface has a midline suture between the parietals (Fig. 5B) as well as sutural remnants ("^" in Fig. 5A) delimiting a small triangular interparietal abutting the supraoccipital on the midline.

The parietal overlaps the frontal anteriorly and the supraoccipital posteriorly, and underlies the squamosal laterally (Figs. 4A, 5A). On the extracranial surface, the parietal has a narrow contact with the petrosal posteroventrally (Fig. 4A), but endocranially, the two bones have a broad contact in the caudal cranial fossa (Fig. 5A). The interparietal overlaps the supraoccipital (Figs. 4A, 5A). A sagittal crest ("sc" in Fig. 4B) runs the length of the parietals and interparietal; on the latter the sagittal crest divides posteriorly forming the nuchal crest.

As apparent from the parasagittally sectioned cranium (Fig. 5A), the parietal is a remarkably thick bone. It is thickest along the midline and perpendicular to that where the endocranial surface of the parietal forms a smooth crest delimiting the middle and caudal cranial fossae. We identify this crest as a tentorial process of the parietal ("tp" in Fig. 5B), which resembles what Klintworth (1968) described as a posteromedian tentorial ossification in the wallaby *Macropus brownii*. The thick portions of the parietal (and interparietal) in CM 20975 contain canals for venous sinuses. The superior sagittal sinus runs in a canal in the parietal along the midline in the middle cranial fossa ("csss" in Fig. 5B). At the level of the tentorial process, the canal for the superior sagittal sinus divides into canals for the left and right transverse sinuses ("cts" in Fig. 5A). Near the dorsal border of the petrosal, the canal for the transverse sinus opens into a short ventrally-directed sulcus for the transverse sinus on the parietal (Fig. 5A) that in life ran in the membranous tentorium cerebelli; this sulcus disappears into a canal between the squamosal and petrosal. Lastly, on the left side (bilaterally in AMNH 35866) there is a posterior venous channel, the parieto-occipital diploic vein, comparable in size to the canal for the transverse sinus from which it branches that runs posteriorly and then ventrally in a canal through the diploë of the parietal and interparietal; it sends a small branch through the supraoccipital to the unpaired foramen on the occiput ("vf" in Fig. 4B). The main channel enters a canal between the exoccipital and petrosal at the ventral end of which it joins the sigmoid sinus before turning posteriorly in a canal in the exoccipital towards the condyloid canal.

Petrosal ("pe").—As we have done elsewhere (Wible and Bertrand 2024), we divide the petrosal into two parts, the pars cochlearis (for the cochlea and utricle) and the pars canalicularis (for the sacculus and semicircular canals). The pars cochlearis includes the promontorium and anterior extensions in ventral view and the internal acoustic meatus and anterior extensions in dorsal view; the remainder of the bone is the pars canalicularis.

Tympanic surface.—In the direct ventral view of the left petrosal (Figs. 2, 6A), many significant structures of the middle ear are not visible. Consequently, we provide another view with the isolated left petrosal rotated medially that exposes most hidden structures (Fig. 6B). The main part of the pars cochlearis is the promontorium ("pr" in Fig. 6), which is oval, longer anteroposteriorly than mediolaterally wide. Two openings occur in the posterior and posterolateral aspect of the promontorium. The former is the aperture of the cochlear fossula ("acf" in Fig. 6B),

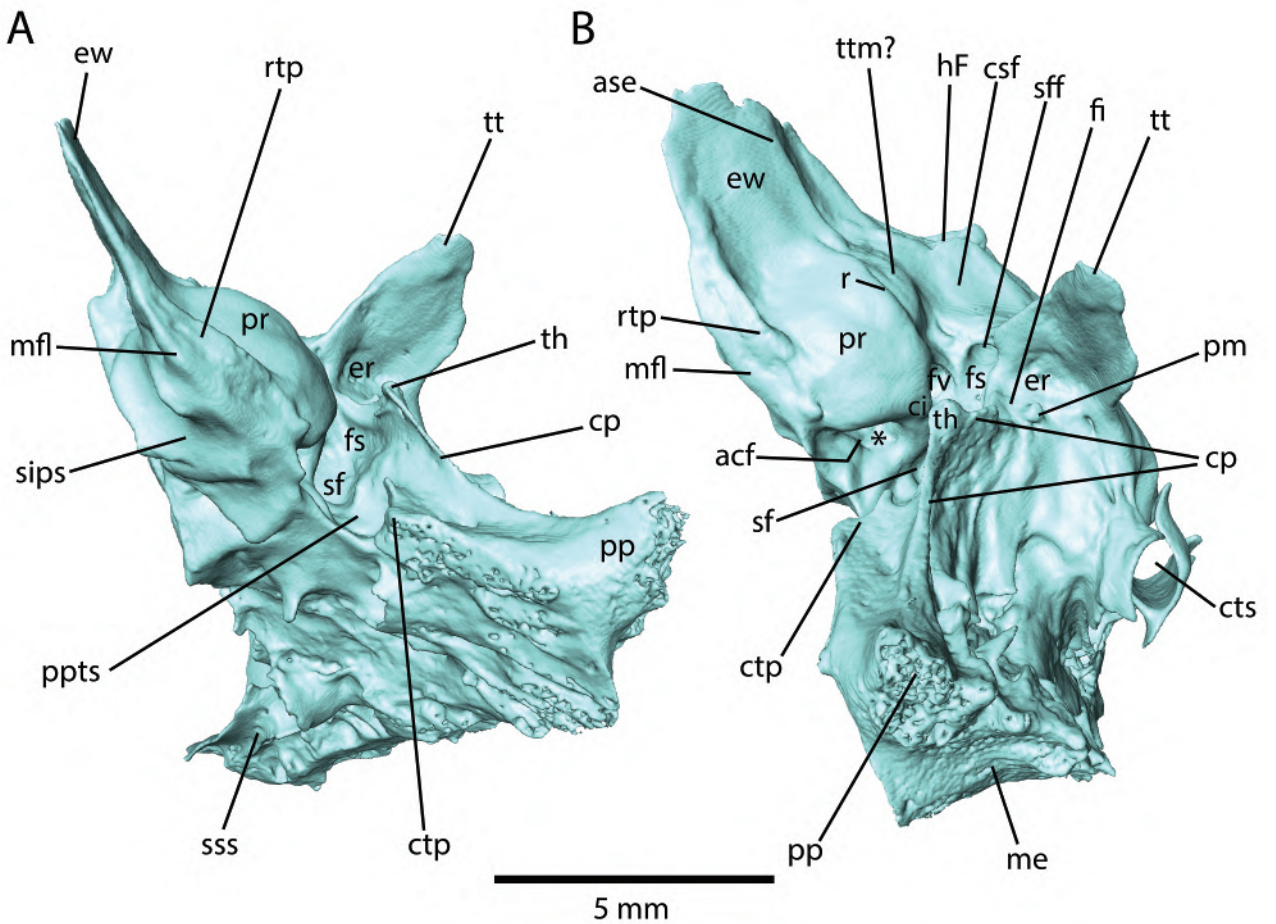

Fig. 6.—*Thylacinus cynocephalus*, CM 20975, isosurface of left petrosal derived from µCT scans. **A,** ventral view; **B,** oblique ventral view. Anterior to top of page. Asterisk in B is in the cochlear fossula. Abbreviations: **acf,** aperture of cochlear fossula; **ase,** anterior septum; **ci,** crista interfenestralis; **cp,** crista parotica; **csf,** cavum supracochleare floor; **ctp,** caudal tympanic process; **cts,** canal for transverse sinus; **er,** epitympanic recess; **ew,** epitympanic wing; **fi,** fossa incudis; **fs,** facial sulcus; **fv,** fenestra vestibuli; **hF,** hiatus Fallopii; **me,** mastoid exposure; **mfl,** medial flange; **pm,** postmeatal process; **pp,** paroccipital process; **ppts,** postpromontorial tympanic sinus; **pr,** promontorium; **r,** ridge; **rtp,** rostral tympanic process; **sf,** stapedius fossa; **sff,** secondary facial foramen; **sips,** sulcus for inferior petrosal sinus; **sss,** sulcus for sigmoid sinus; **th,** tympanohyal; **tt,** tegmen tympani; **ttm?,** attachment for tensor tympani muscle?

which is oval, wider than tall; the true round window, the fenestra cochleae (fenestra rotunda of Archer 1976 and Murray and Megirian 2006), is recessed, round, and smaller than the aperture of the cochlear fossula. There is a distinct depression, the cochlear fossula, in the roof of the aperture ("*" in Fig. 6B). The other opening, the oval window, the fenestra vestibuli (fenestra ovalis of Archer 1976 and Murray and Megirian 2006; "fv" in Fig. 6B), is smaller and has a stapedial ratio (of Segall 1970; length/width) of 1.15. It is recessed in a shallow vestibular fossula. Separating the oval window and aperture of the cochlear fossula is a narrow crista interfenestralis ("ci" in Fig. 6B).

Running the length of the promontorium is a low, rounded ridge ("r" in Fig. 6B). The promontorial surface medial to the ridge is smooth, while lateral to it is a small, half-moon shaped area with a rougher texture ("ttm?" in Fig. 6B). The adult, AMNH 35866, also has this ridge and a shallow concavity lateral to it (also visible in the isolated adult petrosal, J11446, in Archer 1976: plate 19A). We suggest that this shallow concavity represents the origin of the tensor tympani muscle, which has no other obvious attachment site on the petrosal. This origin may have extended onto a small adjacent depression on the alisphenoid posterior to the foramen ovale, outside the middle ear.

The pars cochlearis includes a broad, thin shelf, the epitympanic wing (sensu MacPhee 1981; "ew" in Fig. 6), that extends anteriorly from and is subequal in length to the promontorium. In light of its relationship to the tympanic process of the alisphenoid and auditory tube, most of the epitympanic wing is outside the tympanic cavity (Fig. 2). A low anterior septum ("ase" in Fig. 6B) subdivides the epitympanic wing into a broad medial part and narrow lateral part. The lateral part is concave and partially underlain

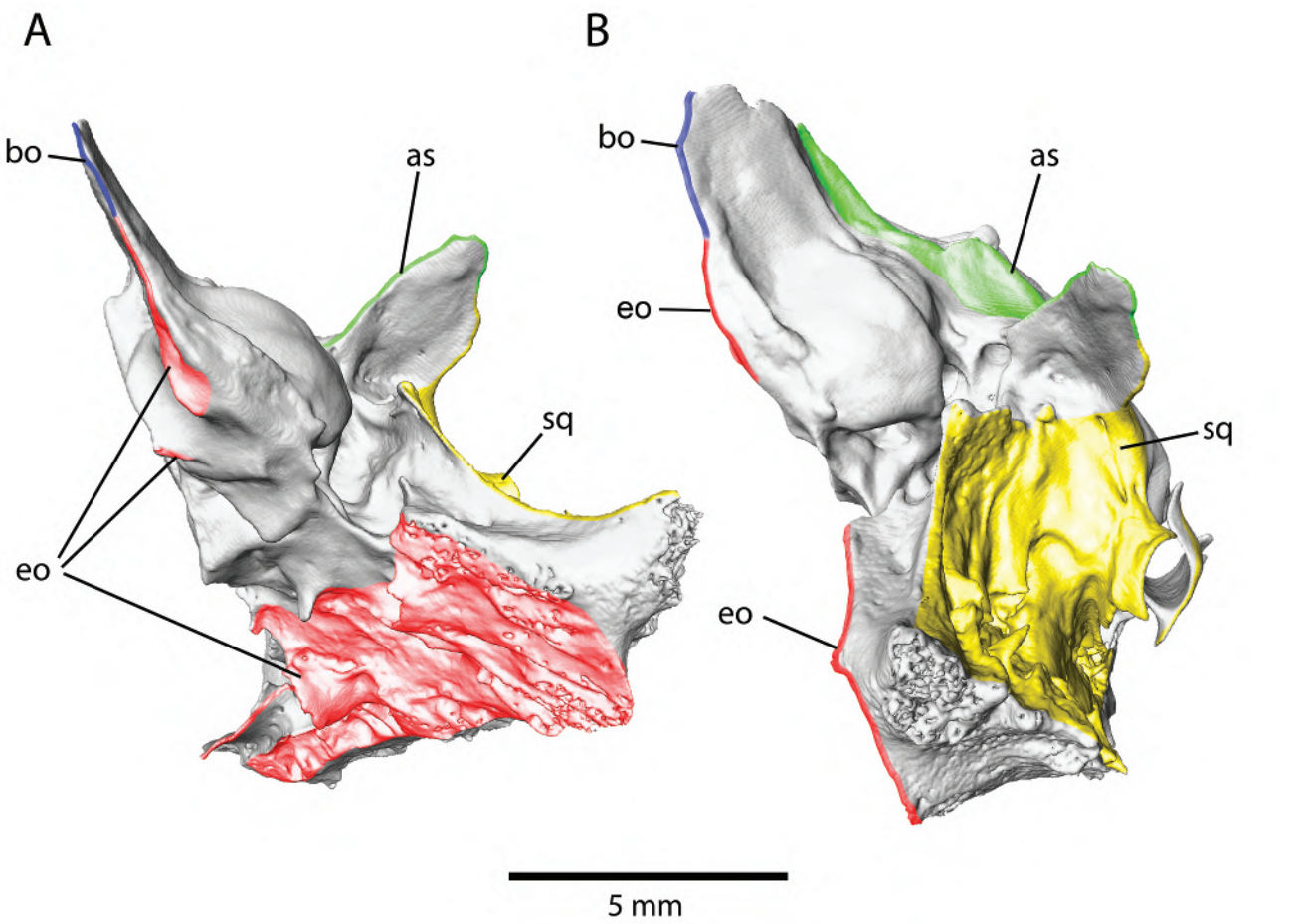

Fig. 7.—*Thylacinus cynocephalus*, CM 20975, isosurface of left petrosal derived from µCT scans. **A,** ventral view; **B,** oblique ventral view. Anterior to top of page. Colored areas indicate contact with neighboring bones: green = alisphenoid; blue = basioccipital; red = exoccipital; yellow = squamosal. Abbreviations: **as,** surface for alisphenoid; **bo,** surface for basioccipital; **eo,** surface for exoccipital; **sq,** surface for squamosal.

by the alisphenoid (Fig. 7B). A narrow shelf, the medial flange, continuous with the epitympanic wing extends medially from the promontorium ("mfl" in Fig. 6). Projecting perpendicularly from the medial flange is a low rostral tympanic process (sensu MacPhee 1981; "rtp" in Fig. 6), which decreases in height anteriorly and extends halfway along the epitympanic wing.

The pars canalicularis lies lateral and posterolateral to the pars cochlearis. The lateral section is dominated by the laminar, triangular, anteroventrally-projecting tegmen tympani ("tt" in Figs. 2B, 6), which underlies the alisphenoid and squamosal (Fig. 7). At the base of the tegmen tympani is a shallow, oval depression, wider than long, the epitympanic recess ("er" in Figs. 2B, 6B), which forms the roof over the malleoincudal articulation. In the posteromedial corner of the epitympanic recess is a small depression, the fossa incudis ("fi" in Fig. 6B), which accommodated the crus breve of the incus. With the squamosal in place, the low posterior wall of the epitympanic recess and lateral wall of the fossa incudis are formed by the squamosal septum ("sqs" in Fig. 2B); the low medial wall of the fossa incudis is formed by the anterior continuation of the crista parotica ("cp" in Fig. 6B). With the squamosal removed, the isolated petrosal has a small, rounded prominence lateral to the fossa incudis that we identify as the postmeatal process (see Wible 1990; "pm" in Figs. 6B, 8A); it is covered by squamosal (Fig. 7B). Between the epitympanic recess and the promontorium is the sulcus for the facial nerve ("fs" in Fig. 6B) and anterior to it, the secondary facial foramen ("sff" in Fig. 6B). The bone anterior to the secondary facial foramen is gently concave and underlain by the alisphenoid (Fig. 7B); it forms the floor of the cavum supracochleare ("csf" in Fig. 6B), a space in the petrosal that holds the geniculate ganglion of the facial nerve. At the anterior aspect of this floor is a small, slit-like aperture, the hiatus Fallopii ("hF" in Fig. 6B), which opens endocranially; it transmits the greater petrosal nerve from the cavum supracochleare. Sánchez-Villagra and Wible (2002) reported a prootic canal near the secondary facial foramen in one of nine specimens of *T. cynocephalus*

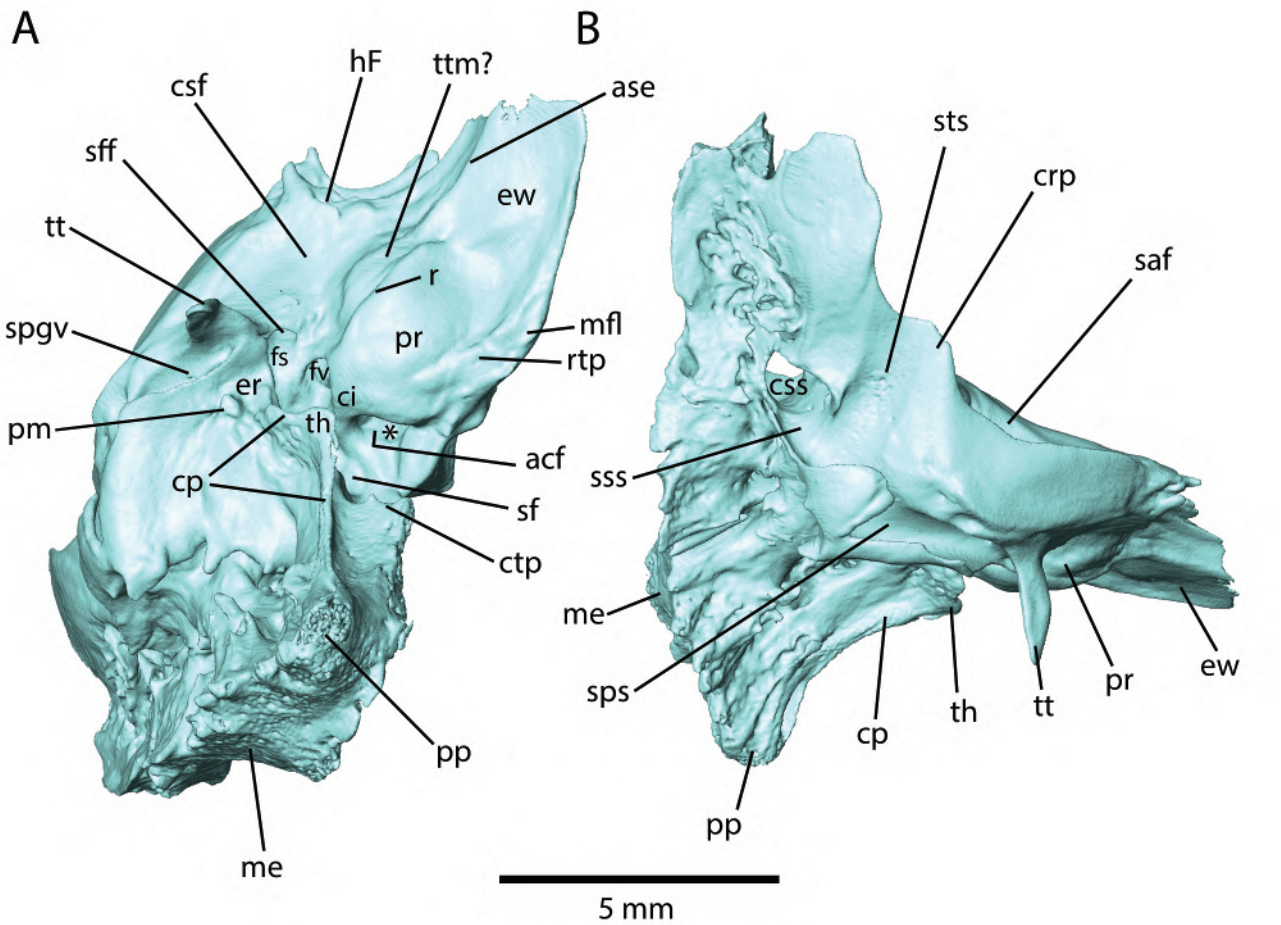

Fig. 8.—*Thylacinus cynocephalus*, CM 20975, isosurface of right petrosal derived from μCT scans. **A,** oblique ventral view (anterior to top of page); **B,** lateral view (anterior to right). Asterisk in A is in the cochlear fossula. Abbreviations: **acf,** aperture of cochlear fossula; **ase,** anterior septum; **ci,** crista interfenestralis; **cp,** crista parotica; **crp,** crista petrosa; **csf,** cavum supracochleare floor; **css,** canal for sigmoid sinus; **ctp,** caudal tympanic process; **er,** epitympanic recess; **ew,** epitympanic wing; **fs,** facial sulcus; **fv,** fenestra vestibuli; **hF,** hiatus Fallopii; **me,** mastoid exposure; **mfl,** medial flange; **pm,** postmeatal process; **pp,** paroccipital process; **pr,** promontorium; **r,** ridge; **rtp,** rostral tympanic process; **saf,** subarcuate fossa; **sf,** stapedius fossa; **sff,** secondary facial foramen; **spgv**, sulcus for the postglenoid vein; **sps,** sulcus for prootic sinus; **sss,** sulcus for sigmoid sinus; **sts,** sulcus for transverse sinus; **th,** tympanohyal; **tt,** tegmen tympani; **ttm?,** attachment for tensor tympani muscle?

(USNM 115365). A reviewer of an early draft of this paper (R.M.D. Beck) noted he has seen a tympanic aperture in a subadult (UMZC A6.7/7) and on the right side only in a juvenile (SAM M1958). Neither the subadult or adult studied here have a prootic canal.

Archer (1976:237) described several structures neighboring the facial sulcus that we do not find in our specimens. "Several small bony processes appear to consistently develop in association with postero-dorsal region of sulcus for facial nerve. One of these is small knob-like ectotympanic process of periotic. Immediately dorsal to this is a small bony vertical flange which may have provided attachment for ligament to auditory ossicles. On posterior side of sulcus for facial nerve and posterior to this flange, is another, larger knob-like process which may also have provided attachment for ligaments." Archer's use of the name ectotympanic process of periotic suggests contact between these two bones. However, in his description of the ectotympanic, he did not mention contact with the petrosal. Archer (1976:237) did end this description with "Conceivable that one of these bony processes represents fused tympanohyal," which suggests he was unsure of the anatomy here. A reviewer of an early draft (R.M.D. Beck) suggested that Archer's "ectotympanic process" is our postmeatal process and the "small bony vertical flange" is our crista parotica.

The tegmen tympani of the right petrosal is half the width of that on the left (cf. Figs. 6 and 8). While the left tegmen tympani contacts both the alisphenoid and squamosal (Fig. 7), the right one contacts only the alisphenoid (Fig. 8). The right epitympanic recess is also narrower than that on the left (cf. Figs. 6B and 8A), seemingly because of

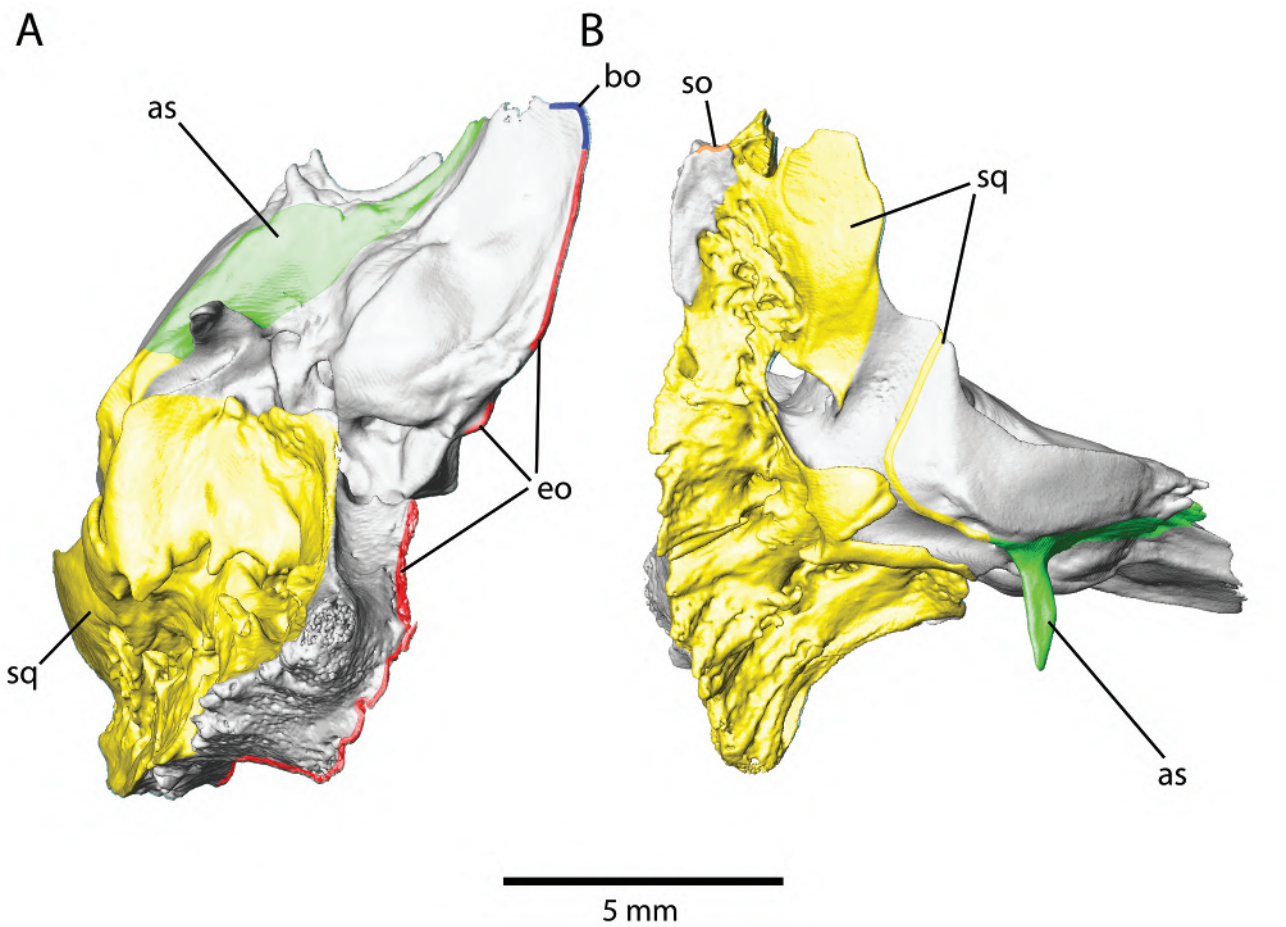

Fig. 9.—*Thylacinus cynocephalus*, CM 20975, isosurface of right petrosal derived from μCT scans. **A,** oblique ventral view (anterior to top of page); **B,** lateral view (anterior to right). Colored areas indicate contact with neighboring bones: green = alisphenoid; blue = basioccipital; red = exoccipital; yellow = squamosal; orange = supraoccipital. Abbreviations: **as,** surface for alisphenoid; **bo,** surface for basioccipital; **eo,** surface for exoccipital; **so,** surface for supraoccipital; **sq,** surface for squamosal.

the encroachment of a well-developed vascular sulcus in the petrosal for the prootic sinus ("sps" in Fig. 8A). On the left side, as bilaterally in AMNH 35866, the postglenoid vein at its exit is entirely within the squamosal, but on the right the sulcus in the petrosal lateral to the epitympanic recess forms the roof of the postglenoid foramen.

The posterolateral section of the pars canalicularis is a wedge of bone between the exoccipital medially and squamosal laterally (Fig. 7) that is narrower but longer than the promontorium (Fig. 6). The medial and lateral edges of the wedge are subparallel but diverge slightly anteriorly. Both edges have crests with the surface between them concave. The lateral crest, the crista parotica, is longer, sharper, and more pronounced. Anteriorly, the crista parotica bears a thickened area that is slightly medially inflected that we interpret as the tympanohyal ("th" in Fig. 6). Although not indicated in bone, the exit of the facial nerve from the middle ear lies posterior to the tympanohyal. Anterior to the tympanohyal, the crista parotica decreases in height to form the low medial wall of the epitympanic recess described above. The medial crest on the wedge falls far short of the promontorium, leaving a wide gap, the post-promontorial tympanic sinus ("ppts" in Fig. 6A). The anterior face of the wedge forms the posterior wall of the sinus and represents the caudal tympanic process (sensu MacPhee 1981; "ctp" in Fig. 6). In the lateral aspect of the sinus is an oval depression, longer than wide, the stapedius fossa ("sf" in Fig. 6), for the attachment of the stapedius muscle. Finally, at the rear of the wedge is the prominent, anteroventrally-directed paroccipital process of the petrosal ("pp" in Figs. 2B, 4A, 6; mastoid process of Archer 1976 and Murray and Megirian 2006), which is sandwiched between the posttympanic process of the squamosal and the paracondylar process of the exoccipital. Regarding the extent of its ventral projection, the paroccipital process is shorter than the paracondylar, and subequal to the posttympanic (Fig. 4A).

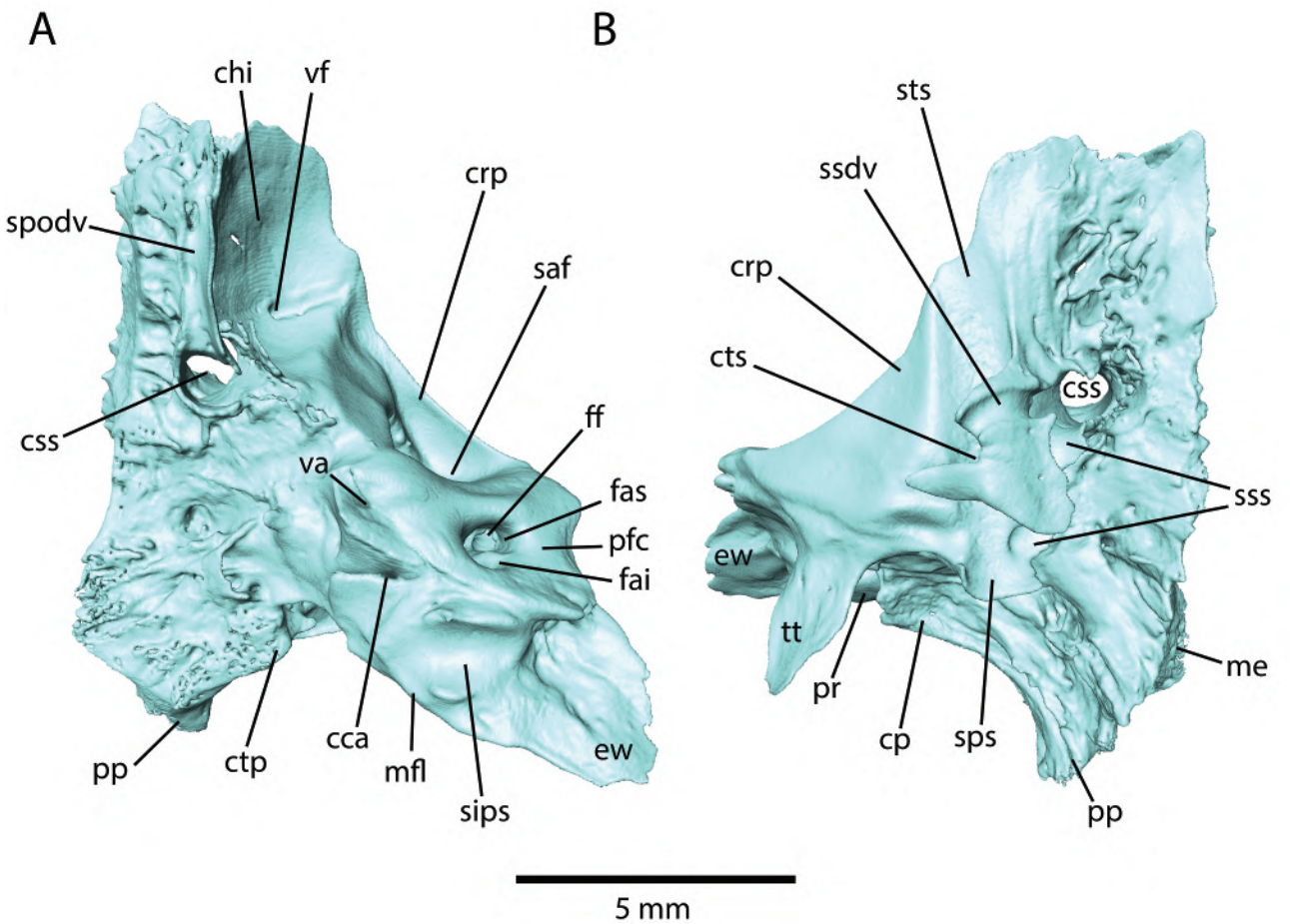

Fig. 10.—*Thylacinus cynocephalus*, CM 20975, isosurface of left petrosal derived from μCT scans. **A,** medial view; **B,** lateral view. Dorsal to top of page. Abbreviations: **cca,** cochlear canaliculus; **chi,** cerebellar hemisphere impression; **cp,** crista parotica; **crp,** crista petrosa; **ctp,** caudal tympanic process; **css**, canal for sigmoid sinus; **cts,** canal for transverse sinus; **ew,** epitympanic wing; **fai,** foramen acusticum inferius; **fas,** foramen acusticum superius; **ff,** facial foramen; **me,** mastoid exposure; **mfl,** medial flange; **pfc,** prefacial commissure; **pp,** paroccipital process; **pr,** promontorium; **saf,** subarcuate fossa; **sips,** sulcus for inferior petrosal sinus; **sps,** sulcus for prootic sinus; **ssdv,** sulcus for squamosal diploic vein; **spodv,** sulcus for parieto-occipital diploic vein; **sss,** sulcus for sigmoid sinus; **sts,** sulcus for transverse sinus; **tt,** tegmen tympani; **va,** vestibular aqueduct; **vf,** venous foramen.

Lateral surface.—In direct lateral view (Fig. 4A), only a small patch of petrosal contributes to the external braincase wall and nuchal crest in the interval between the squamosal, parietal, supraoccipital, and exoccipital. Although the mastoid exposure ("me" in Fig. 4A) is visible in lateral view, it is technically on the occiput (Fig. 4B). The isolated left petrosal in lateral view (Fig. 10B) is almost entirely comprised of the pars canalicularis; most of the pars cochlearis is hidden by the tegmen tympani, with only parts of the epitympanic wing and promontorium visible. The pars canalicularis is nearly completely covered laterally by bone, primarily the squamosal, with a small area of alisphenoid (Fig. 11B). The main part that is not covered is the tall, thin crista petrosa ("crp" in Figs. 5B, 10B) to which the tentorium cerebelli attached. Part of the area covered by the squamosal encloses several major veins and venous sinuses within canals between the petrosal and squamosal (Fig. 12B). The surface of the pars canalicularis has well-developed sulci for these vessels: the transverse sinus ("sts" in Fig. 10B), sigmoid sinus ("sss" in Fig. 10B), superior petrosal sinus ("sps" in Fig. 10B), and squamosal diploic vein ("ssdv" in Fig. 10B), as well as a canal through the petrosal connecting the lateral and medial surfaces for the sigmoid sinus ("css" in Figs. 10). Because this canal on the left side is in line with a drill hole through the rear of the squamosal (white asterisk in squamosal in Fig. 4A) and originally had a wire through it, we initially interpreted the canal as artificial. However, the canal on the left side is real as one is also present on the right petrosal (Fig. 8B) along with a nearby separate drill hole (hidden in Fig. 8). Additionally, the canal is present bilaterally in AMNH 35866 and is visible in the isolated left petrosal J 11446 figured in Archer (1976: plate 19A).

The prevalent therian pattern for venous drainage (e.g.,

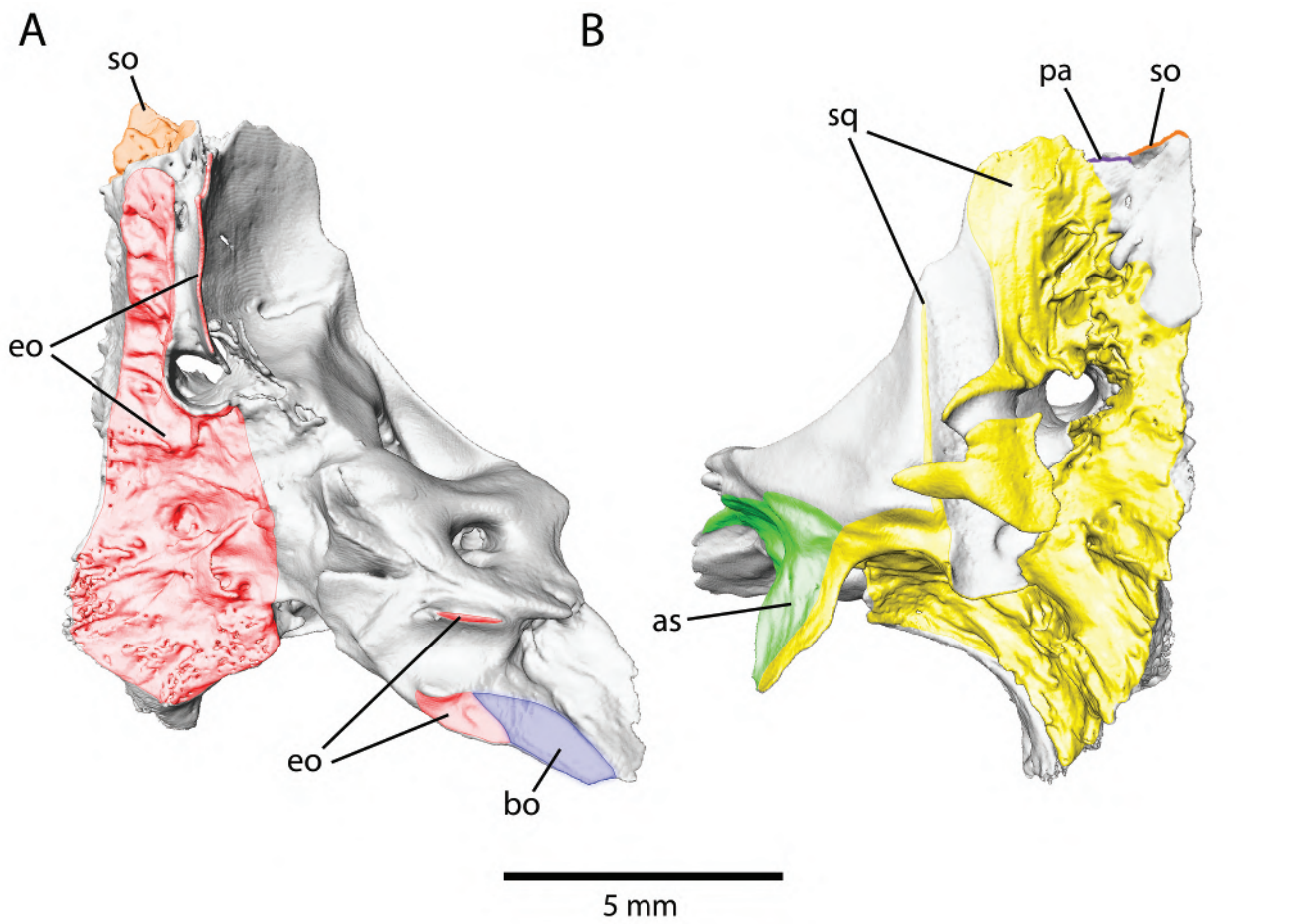

Fig. 11.— *Thylacinus cynocephalus*, CM 20975, isosurface of left petrosal derived from μCT scans. **A**, medial view; **B**, lateral view. Dorsal to top of page. Colored areas indicate contact with neighboring bones: green = alisphenoid; blue = basioccipital; red = exoccipital; purple = parietal; yellow = squamosal; orange = supraoccipital. Abbreviations: **as**, surface for alisphenoid; **bo**, surface for basioccipital; **eo**, surface for exoccipital; **pa**, surface for parietal; **so**, surface for supraoccipital; **sq**, surface for squamosal..

Reinhard et al. 1962; Dom et al. 1970) has the midline superior sagittal sinus dividing into left and right transverse sinuses running in the tentorium cerebelli. At the dorsal aspect of the petrosal, the transverse sinus divides into anterior and posterior channels. The posterior channel is the sigmoid sinus, but a variety of names have been used for the anterior channel, including temporal sinus (Reinhard et al. 1962), retroarticular foramen emissary vein (Dom et al. 1970), postglenoid vein (Archer 1976), and capsuloparietal and sphenoparietal emissary veins (Gelderan 1924). We follow Wible et al. (2021) here and use prootic sinus, which exits the cranium at the postglenoid foramen as the postglenoid vein. This venous pattern is also present in CM 20975 and AMNH 35866, but it differs in significant ways from the prevalent therian pattern that impact the petrosal morphology. First, whereas these vessels typically run in sulci on the endocranial surface, they are largely enclosed in bony canals in the thylacine; there is only a small section of the transverse sinus on the parietal that is open ("sts" in Fig. 5A). Second, whereas the origin of the prootic sinus and sigmoid sinus from the transverse sinus is typically dorsal to the petrosal, this origin is near the ventral margin of the left petrosal of CM 20975 (Fig. 12B). This ventral origin alters the pathways of all three vessels: the transverse sinus has a long course on the petrosal ("sts" in Fig. 10B; "ts" in Fig. 12B); the prootic sinus has an anterior course to the postglenoid foramen ("ps" in Fig. 12B); and the sigmoid sinus initially has a dorsal course ("sss" in Fig. 10B; "ss" in Fig. 12B) and then passes medially through the canal in the petrosal ("css" in Fig. 10; "ss" in Fig. 12). Another oddity is the channel draining the squamosal that runs in a sulcus on the outside of the canal for the transverse sinus ("ssdv" in Fig. 10B; "sdv" in Fig. 12B), which we term the squamosal diploic vein.

The bony structures related to these venous channels differ on the right petrosal of CM 20975 (Fig. 8B). While part of the course of the transverse sinus is enclosed in a canal in the left petrosal ("cts" in Figs. 6B, 10B), the course

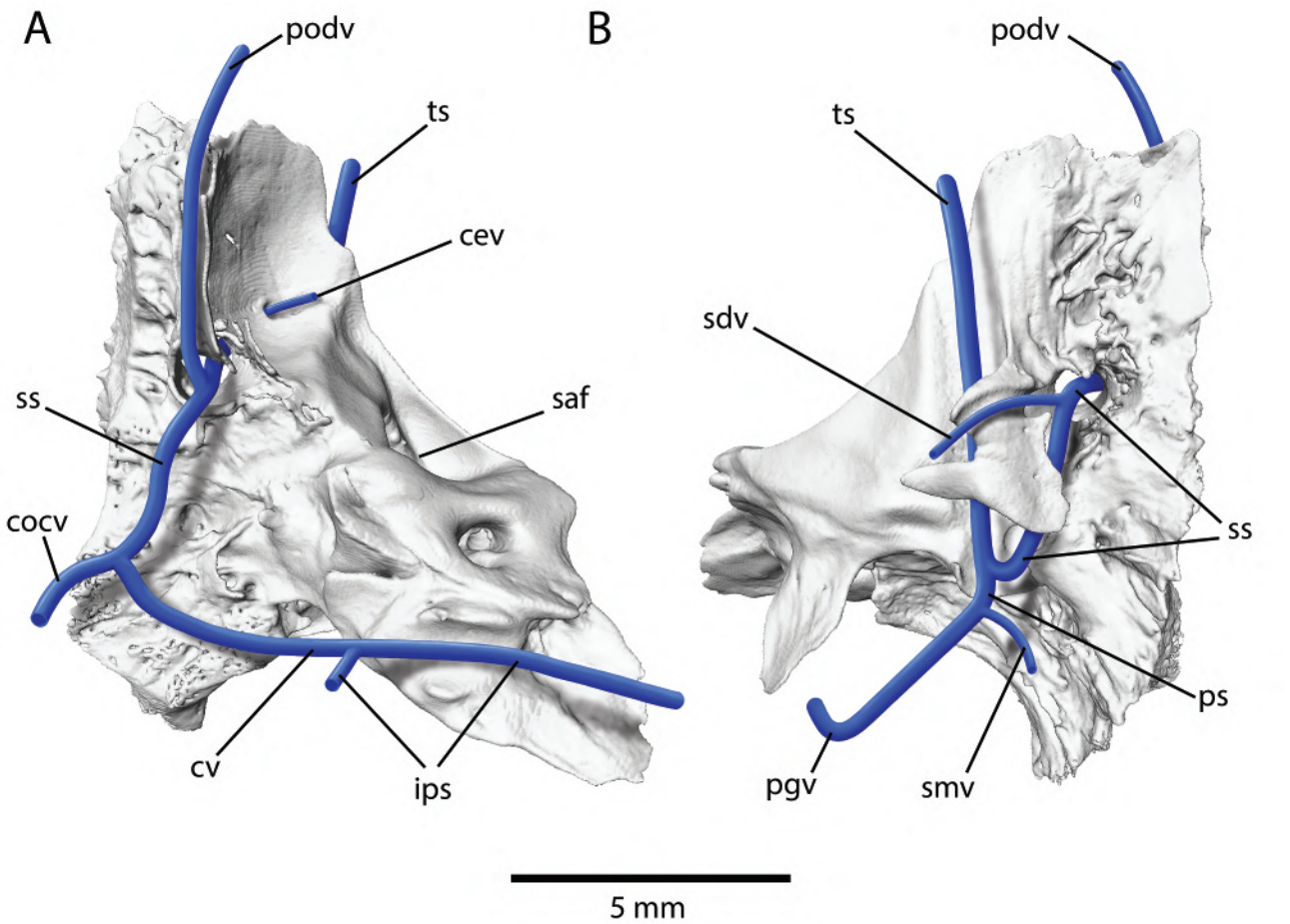

Fig. 12.—*Thylacinus cynocephalus*, CM 20975, isosurface of left petrosal derived from µCT scans, with veins reconstructed based on sulci and canals. **A,** medial view; **B,** lateral view. Dorsal to top of page. Abbreviations: **cev,** cerebellar vein; **cocv,** condyloid canal vein; **cv,** connecting vein (inferior petrosal sinus and sigmoid sinus; **ips,** inferior petrosal sinus; **podv,** parieto-occipital diploic vein; **pgv,** postglenoid vein; **ps,** prootic sinus; **saf,** subarcuate fossa; **sdv,** squamosal diploic vein; **smv,** suprameatal vein; **ss,** sigmoid sinus; **ts,** transverse sinus.

on the right petrosal is open on that bone ("sts" in Fig. 8B). The origin of the sigmoid sinus and prootic sinus from the transverse sinus on the right side is not as far ventral as it is on the left. The prootic sinus has only a short sulcus on the left petrosal (Figs. 10B, 12B) and the bulk of its course is entirely in the squamosal. However, on the right there is a long sulcus for the prootic sinus that is partially enclosed by petrosal (Fig. 8B); the isolated left petrosal J 11446 figured by Archer (1976: plate 19A) shows the same pattern. Lastly, the sulcus for the squamosal diploic vein and parieto-occipital diploic vein present on the left petrosal (Fig. 10B) are absent on the right side (Fig. 8B).

Medial surface.—The direct medial view provides access to most of the endocranial surface (Fig. 5A). The petrosal is composed of three regions that are roughly similar in area. Ventromedially is the internal acoustic meatus ("iam" in Fig. 5A), which transmitted the seventh and eighth cranial nerves; dorsolateral to that is the subarcuate fossa ("saf" in Fig. 5A), which accommodated the petrosal lobule of the cerebellum; and posterodorsal to that is a large concavity ("chi" in Fig. 5A), the petrosal's contribution to the housing for the cerebellar hemisphere, which is completed by the supraoccipital and parietal (Fig. 5). The first, the internal acoustic meatus, is on the pars cochlearis, whereas the other two are on the pars canalicularis. All three lie in the caudal cranial fossa ("ccf" in Fig. 5A).

The internal acoustic meatus is shallow, much wider than deep (Fig. 5A). It includes the foramen acusticum superius ("fas" in Fig. 10A) and the foramen acusticum inferius ("fai" in Fig. 10A), which are only partially separated by an incomplete transverse septum. The foramen acusticum superius includes the facial foramen laterally ("ff" in Fig. 10A) and the smaller cribriform dorsal vestibular area posteriorly. Most of the foramen acusticum inferius is occupied by the spiral cribriform tract, but posteromedially is the foramen singulare and posterolaterally the ventral vestibular area. Anterior to the foramen acusticum

superius is the prefacial commissure ("pfc" in Fig. 10A), which is similar in width to the internal acoustic meatus. Extending anteroventrally from the meatus is the broad dorsal surface of the epitympanic wing, partially covered by the basioccipital and exoccipital (Fig. 11A). The medial side of the pars cochlearis above the medial flange has a short but wide sulcus for the inferior petrosal sinus ("sips" in Fig. 10A), which meets a sulcus on the exoccipital to complete a canal. This sulcus opens on the ventral surface at the foramen for the inferior petrosal sinus between the petrosal and exoccipital ("fips" in Fig. 2B). It also leads to a canal entirely within the exoccipital that carries a vein connecting the inferior petrosal sinus and sigmoid sinus ("cv" in Fig. 12A). Posterodorsal to the sulcus for the inferior petrosal sinus is the small opening for the cochlear canaliculus ("cca" in Fig. 10A), which carried the perilymphatic duct.

As noted above, the remainder of the petrosal in medial view is the pars canalicularis, which is roughly twice the size of the pars cochlearis (Fig. 10A). The anterior part of the pars canalicularis is occupied by the subarcuate fossa, which housed the petrosal lobule. The fossa is globular, as wide as deep. The opening into the subarcuate fossa, which includes the gyrus for the anterior semicircular canal, is only slightly larger than the internal acoustic meatus (Fig. 5A), and constricted compared to the globular space housing the petrosal lobule. Medial to the subarcuate fossa is the slit-like vestibular aqueduct ("va" in Fig. 10A), which transmitted the endolymphatic duct. Lateral to the subarcuate fossa is the tall, thin crista petrosa mentioned above (Figs. 5A, 10A); its anterolateral face is exposed in the rear of the middle cranial fossa ("mcf" in Fig. 5B). A sulcus for the superior petrosal sinus, which occurs between the crista petrosa and subarcuate fossa in some marsupials (Archer 1976), is lacking in both CM 20975 and AMNH 35866.

The posterior part of the pars canalicularis is the tallest part of the petrosal, stretching from the paroccipital process ventrally to its contact with the supraoccipital dorsally (Figs. 10A, 11A). Most of surface is covered by exoccipital (Fig. 11A) but there is a large concavity that is exposed in the caudal cranial fossa, contributing with the parietal and supraoccipital to the large impression for the cerebellar hemisphere ("chi" in Fig. 5). In the ventrolateral margin of this impression, on the left petrosal only, is a small foramen with a sulcus leading anteriorly from it ("vf" in Fig. 10A). We traced this back to the sulcus for the sigmoid sinus on the lateral surface and suggest it is a cerebellar vein ("cev" in Fig. 12B).

Slightly dorsal to the midpoint of the posterior part of the pars canalicularis is the opening for the canal for the sigmoid sinus (Fig. 10A). Leading into this opening from above is a sulcus for the parieto-occipital diploic vein ("spodv" in Fig. 10A; "podv" in Fig. 12A), which is enclosed in a canal between the petrosal and exoccipital. In AMNH 35866, this canal is not fully enclosed between the two bones, and the vein is exposed in the caudal cranial fossa.

Stapes.—The stapes has been described for *T. cynocephalus* by Doran (1878) and Archer (1976), with the former having the only illustrations of the bone (plate 64, figs. 17, 43). In CM 20975, the stapes is preserved on both sides with no significant differences between the two; the left is in situ in the fenestra vestibuli and the right fell into the inner ear space. The stapes has one relatively straight crus ("c" in Figs. 13A, C) with a slightly expanded head ("h" in Figs. 13A, C) that is offset anteriorly from the crus. On the posterior aspect of the crus is a low muscular process ("mp" in Figs. 13A, C) for the attachment of the stapedius muscle, also reported by Archer (1967). In contrast, Doran (1878) neither reported or illustrated a muscular process. The crus is centrally placed on the footplate ("fp" in Fig. 13), which has a stapedial ratio (of Segall 1970: length to width) of 1.26; that for the oval window reported above is 1.15. The medial surface of the stapes, which faces the inner ear, is deeply concave (Fig. 13C).

Inner Ear

As noted above, in an unplublished thesis, Dickson (2012: figs. 1, 8) included illustrations of the inner ear of *T. cynocelphalus* based on CT scan data in views much like those presented here (Figs. 14B–C, D, F). He did not include descriptions, but the morphology in his illustrations is essentially the same as reported here with one exception: the vestibular aqueduct is not shown.

Cochlear canal.— In life, the membranous cochlea is housed in a bony structure known as the cochlear canal ("co" in Figs. 14, 15B, D). The right and left inner ears of CM 20975 do not exhibit any noticeable morphological differences; therefore, we describe and illustrate the right one only. The right inner ear displays 1.90 cochlear turns with a rotation of 683.9°. The cochlear canal has primary (inner) and secondary (outer) bony lamina that partially divide the scala tympani from the scala vestibuli (Meng and Fox 1995). The scala tympani has a connection to the fenestra cochleae, while the scala vestibuli is linked to the fenestra vestibuli (Ekdale 2016). The secondary bony lamina is generally present within therians, but cases exist in which this morphological feature is absent (Meng and Fox 1995; Ekdale 2009). The secondary bony lamina in CM 20975 starts just dorsolateral to the fenestra cochleae and extends into the cochlear canal ("sbl" in Figs. 14A, B, F, 15B, D) for about 21.5% of the entire cochlear coil, representing a rotation of 147°. In addition, the secondary bony lamina does not extend beyond the basal turn. The primary bony lamina extends all the way to the apex of the cochlear canal ("pbl" in Figs. 14C–D). The cochlea fossula ("cf"), which leads to the aperture of the fenestra cochleae ("afc"), was reconstructed and is more expanded with a bulge (Fig. 14D), while the one leading to the fenestra vestibuli is less pronounced ("fv" and "ffv" in Fig. 14E). The fenestra cochleae is oriented posterolaterally, while the fenestra vestibuli is oriented laterally ("afc" and "fv" in

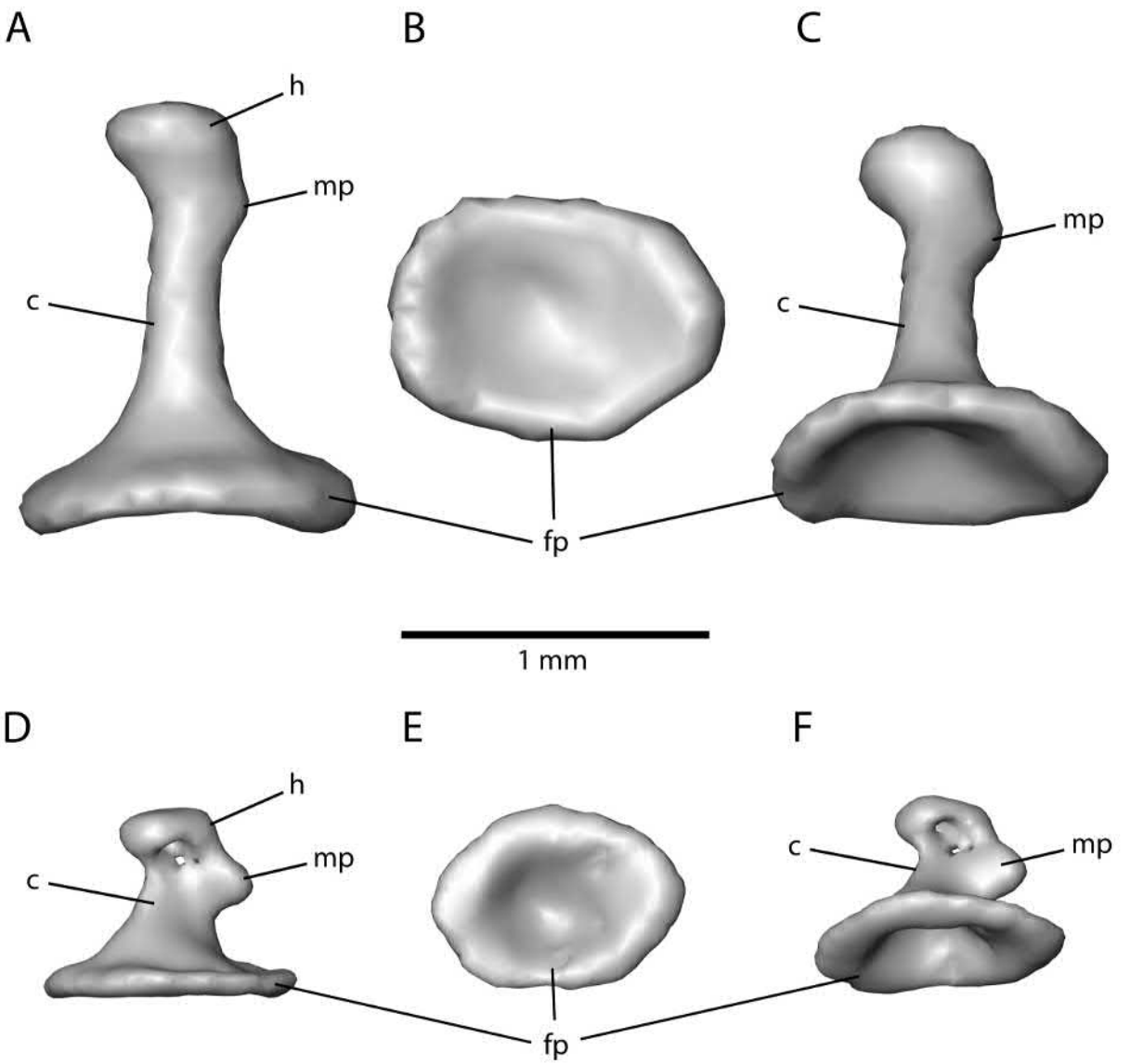

Fig. 13.—Isosurfaces of right stapes derived from µCT scans. **A–C,** *Thylacinus cynocephalus*, CM 20975; **D–F,** *Notoryctes caurinus*, SAM M3139. Anterior to left. **A, D,** ventral view; **B, E,** medial view; **C, F,** oblique ventral view. Abbreviations: **c,** crus; **fp,** footplate; **h,** head; **mp,** muscular process.

Figs. 14B, 15A–B). As mentioned above, the diameter of the fenestra cochleae is larger than the one for the fenestra vestibuli. The cochlear aqueduct is present in CM 20975 and runs parallel to the vestibular aqueduct (see below) in posteromedial direction ("ca" in Fig. 14A). Additionally, its diameter is similar to that of the semicircular canals. In posterodorsal view, the cochlear aqueduct extends beyond the plane of the posterior semicircular canal ("psc" in Figs. 14E, 15B, D). In medial view, in front of the cochlear aqueduct, is a small canal connected to the basal region of the cochlea that might correspond to the cast of the vena aquaeductus cochleae ("vac" in Fig. 14A; Orliac and O´Leary 2016). The resolution of the µCT data does not allow us to trace this canal any farther.

Vestibule.— In medial view, the vestibular aqueduct bony channel is present and includes a bulge at its base ("va" in Figs. 14A, 15D). The root of the vestibular aqueduct is located anteroventral to the base of the common crus ("cc" in Fig. 14A, 15D). The course of the vestibular

TABLE 2. Measurements of 3D reconstructions from µCT data of the endocasts of the right bony labyrinth of *Thylacinus cynocephalus*, CM 20975 and compared taxa. Abbreviations: **ASC,** anterior semicircular canal; **H,** height; **L,** length; **LSC,** lateral semicircular canal; **PSC,** posterior semicircular canal; **R,** radius; **SBL,** secondary bony lamina; **W,** width.

Measurements	*Thylacinus cynocephalus* CM 20975	*Dasyurus hallucatus* AMNH 196840	*Mymecobius fasciatus* AMNH 155328	*Sminthopsis macroura* AMNH 108934	*Monodelphis* sp. DU BAA 0181	*Notoryctes caurinus* SAMA M3139	*Isoodon macrourus* AMNH 160364
Cochlea number of half turns	3	4	3	3	3	3	4
Cochlea added angle (°)	143.9	71.7	125.3	79.0	156.8	30.6	146.6
Cochlea total calculated angle (°)	683.9	791.7	665.3	619.0	696.8	570.6	866.6
Cochlea number of turns	1.90	2.20	1.85	1.72	1.94	1.59	2.41
Secondary lamina number of half turns	0	1	0	1	2	0	1
SBL added angle (°)	147	103.1	124.8	19.5	0	77.2	36.8
SBL total calculated angle (°)	147	283.1	124.8	199.5	360	77.2	216.8
Secondary bony lamina coil (%)	21.5	35.8	18.8	32.2	51.7	13.5	25.0
Angle ASC/LSC (°)	74.0	83.7	93.8	89.1	83.2	70.8	84.4
Angle ASC/PSC (°)	93.0	88.5	95.9	100.4	86.9	92.5	93.0
Angle LSC/PSC (°)	91.3	83.2	96.3	86.0	92.1	93.8	92.2
ASC Radius (mm)	2.51	1.48	1.96	0.89	1.03	0.82	1.65
PSC Radius (mm)	1.97	1.22	1.49	0.73	0.78	0.63	1.29
LSC Radius (mm)	1.65	1.05	1.27	0.59	0.66	0.45	1.06
ASC Height (mm)	4.93	2.94	4.08	1.76	1.96	1.80	3.35
ASC Width (mm)	5.11	2.99	3.76	1.80	2.14	1.49	3.23
PSC Height (mm)	4.03	2.35	2.88	1.39	1.47	1.26	2.56
PSC Width (mm)	3.84	2.52	3.06	1.52	1.63	1.24	2.60
LSC Height (mm)	3.03	1.74	2.29	1.01	1.24	0.93	1.86
LSC Width (mm)	3.55	2.44	2.77	1.36	1.41	0.87	2.38
ratio ASC H/W (mm)	0.96	0.98	1.09	0.98	0.92	1.21	1.04
ratio PSC H/W (mm)	1.05	0.93	0.94	0.91	0.90	1.02	0.98
ratio LSC H/W (mm)	0.85	0.71	0.83	0.74	0.88	1.07	0.78

aqueduct crosses the basal part of the common crus becoming narrower and is directed posteromedially (Fig. 14A). A groove is present on the surface of the common crus that coincides with the passage of the vestibular aqueduct (Fig. 14A). The apex part of the vestibular aqueduct becomes larger, similar in size to its basal region as it exits the petrosal (Fig. 14A). The canal leading to the foramen singulare is located on the anteroventral aspect of the posterior ampulla, which corresponds to the passageway of the nerve to the ampulla of the posterior semicircular canal ("fsg" in Fig. 14A, F; Wible 2008; Bertrand et al. 2020). The singulare canal has a similar diameter to the semicircular canals (Fig. 14A, F). The elliptical and spherical recesses correspond to the membranous utricle and saccule, respectively. Both recesses appear to be in distinct chambers separated by a groove when viewed posteromedially ("er" and sr" in Fig. 14F). The spherical recess is located ventral to the elliptical recess (Figs. 14A, F). The spherical recess forms a larger swelling in posteromedial view, while the elliptical recess is more expanded and forms a bulge in dorsal view (Figs. 14C, F). Both recesses exhibit small canals that exit from the bony labyrinth, which correspond to branches of

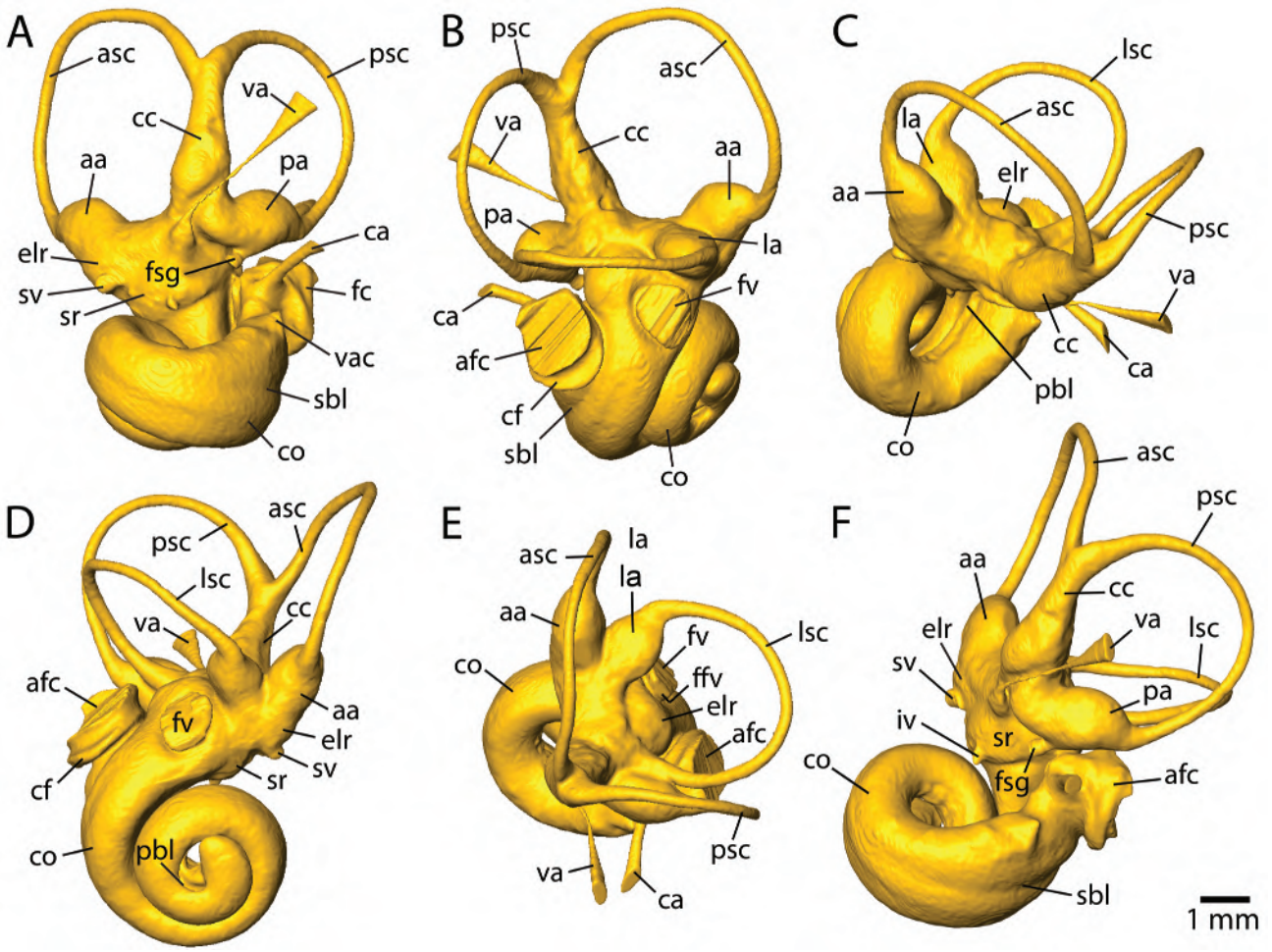

Fig. 14.—Virtual endocasts of the right bony labyrinth of *Thylacinus cynocephalus*, CM 20975. **A,** medial view; **B,** posterolateral view; **C,** dorsal view; **D,** anterolateral view; **E,** posterodorsal view; **F,** posteromedial view. Abbreviations: **aa,** anterior ampulla; **afc,** aperture for fenestra cochleae; **asc,** anterior semicircular canal; **ca,** cochlear aqueduct; **cc,** common crus; **cf,** cochlear fossula; **co,** cochlear canal; **elr,** elliptical recess; **ffv,** fossula of fenestra vestibuli; **fsg,** foramen singulare; **fv,** fenestra vestibuli; **iv,** inferior vestibular nerve; **la,** lateral ampulla; **lsc,** lateral semicircular canal; **pa,** posterior ampulla; **pbl,** primary bony lamina imprint; **psc,** posterior semicircular canal; **sbl,** secondary bony lamina imprint; **sr,** spherical recess; **sv,** superior vestibular nerve; **va,** vestibular aqueduct; **vac,** vena aquaeductus cochleae.

the superior and inferior vestibular nerve for the elliptical and spherical recesses, respectively ("iv" and "sv" in Figs. 14F, 15C–D).

Semicircular canals.— There is no secondary common crus in CM 20975 that forms the ventral portions of the posterior and lateral semicircular canals (Fig. 14C). In posterolateral view, when the lateral canal is positioned horizontally, the anterior semicircular canal extends considerably beyond the common crus, while the posterior semicircular canal is only slightly higher ("asc" in Figs. 14B, 15B). The crus commune has a diameter more than twice the size of the semicircular canals, and the basal and central regions of the common crus are even larger than the apex ("cc" in Fig. 14B). In the same view, the anterior ampulla is located dorsal to the lateral and posterior ampullae, which are both positioned on the same plane ("aa" and "pa" in Fig. 14B). All of the ampullae are relatively bulbous and have a much larger girth than the diameter of the semicircular canals (Fig. 14B). The roundest semicircular canal is the one that has the most similar combined width and height. In the case of CM 20975, it is the anterior semicircular canal (ratio of 0.96), but the posterior semicircular canal is also close to being round (ratio of 1.05; Table 2). The semicircular canal with the largest overall radius of curvature is the anterior semicircular canal (2.51; Table 2). In posterodorsal view, the lateral semicircular canal reaches beyond the posterior semicircular canal ("lsc" in Fig. 14E). The widest angle is between the anterior and the posterior semicircular canals with an angle of 93.0° (Table 2).

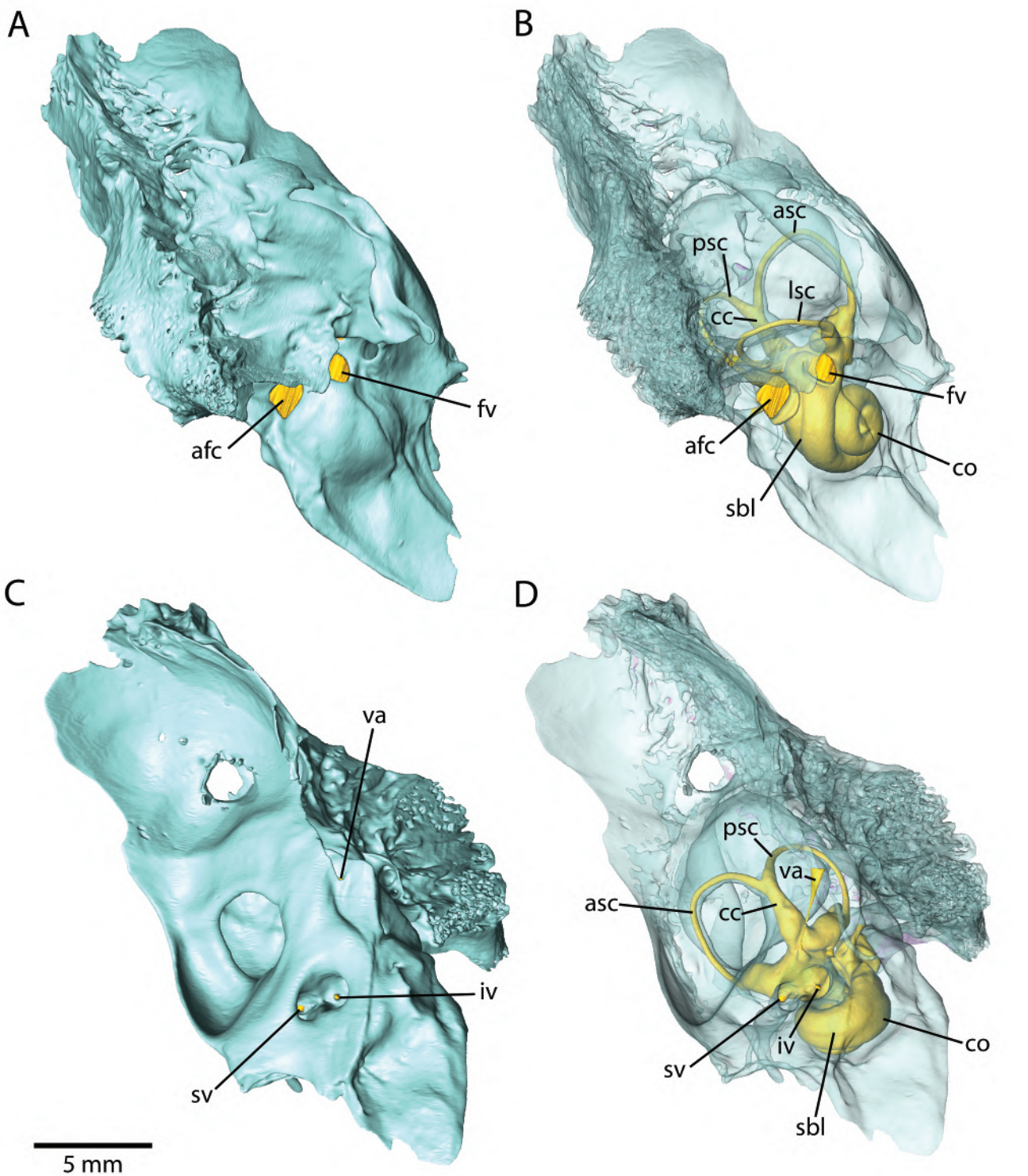

Fig. 15.—Virtual endocasts of the right bony labyrinth inside the petrosal bone of *Thylacinus cynocephalus*, CM 20975. **A,** and **B,** ventrolateral view; **C,** and **D,** medial view. Petrosal is transparent in B and D. Abbreviations: **afc,** aperture for fenestra cochleae; **asc,** anterior semicircular canal; **cc,** common crus; **co,** cochlear canal; **fv,** fenestra vestibuli; **iv,** inferior vestibular nerve; **psc,** posterior semicircular canal; **sbl,** secondary bony lamina imprint; **sv,** superior vestibular nerve; **va,** vestibular aqueduct.

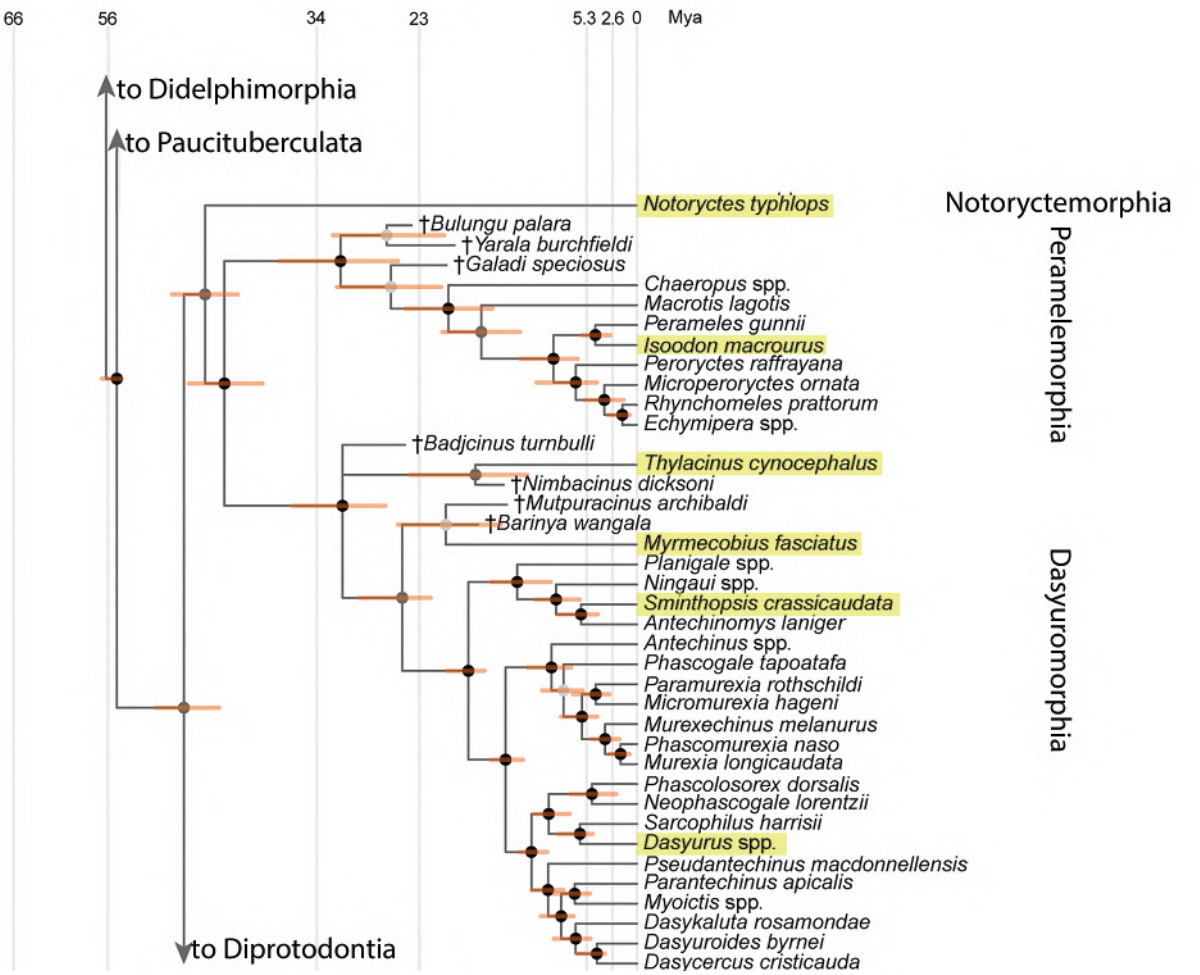

Fig. 16.—Segment of marsupial phylogenetic tree from Beck et al. (2022: fig. 33). Taxa highlighted in yellow have µCT datasets discussed in the current paper. This tree is the fifty-percent majority rule consensus of post-burn-in trees that resulted from dated Bayesian analysis (using combined tip-and-node dating and separate Independent Gamma Rates [IGR] clock models for the molecular and morphological partitions) of their total evidence dataset. Black dots at nodes indicate ≥0.95 Bayesian posterior probability ("strong support"); dark gray dots indicate 0.75–0.94 Bayesian posterior probability ("moderate support"). Nodes without dots were constrained a priori so that their ages could be calibrated. Orange bars represent 95% Highest Posterior Density (HPD) intervals on the ages of nodes. For clarity, 95% HPD intervals are not shown for the ages of fossil terminals.

In posterodorsal view, the anterior semicircular is slightly bent in the center, while the posterior and anterior canals are straight (Fig. 14E).

COMPARISONS

In choosing taxa for comparisons with *T. cynocephalus*, we utilized the recent total evidence phylogenetic analysis of marsupials in Beck et al. (2022). Figure 16 shows the relevant portion of Beck et al.'s (2022: fig. 33) fifty-percent majority rule consensus of post-burn-in trees that resulted from dated Bayesian analysis of their total evidence dataset. In that tree, *T. cynocephalus* is a dasyuromorphian outside the clade of the numbat *Myrmecobius fasciatus* and Dasyuridae, also recovered in the retrotransposon study of Feigin et al. (2018). The taxa highlighted in Figure 16 had µCT scan datasets that we accessed, with the addition of *Monodelphis*, which is not shown in this pruned marsupial tree. For the taxa in Figure 16, Beck et al. (2022) described and scored as characters some features that we discuss below. From the µCT datasets, we were able to isolate the petrosals, with the exception of *N. caurinus*, in which that bone is partially fused with its neighbors. The petrosal has been illustrated and described for *Notoryctes typhlops* Stirling, 1889, by Ladevèze et al. (2008: fig. 4).

Epitympanic wing and anterior septum.—All the specimens considered here have a well-developed epitympanic wing of the petrosal that is continuous with the rostral tympanic process ("ew" in Figs. 17A, 18A). The wing tapers anteriorly (Fig. 17), with the condition

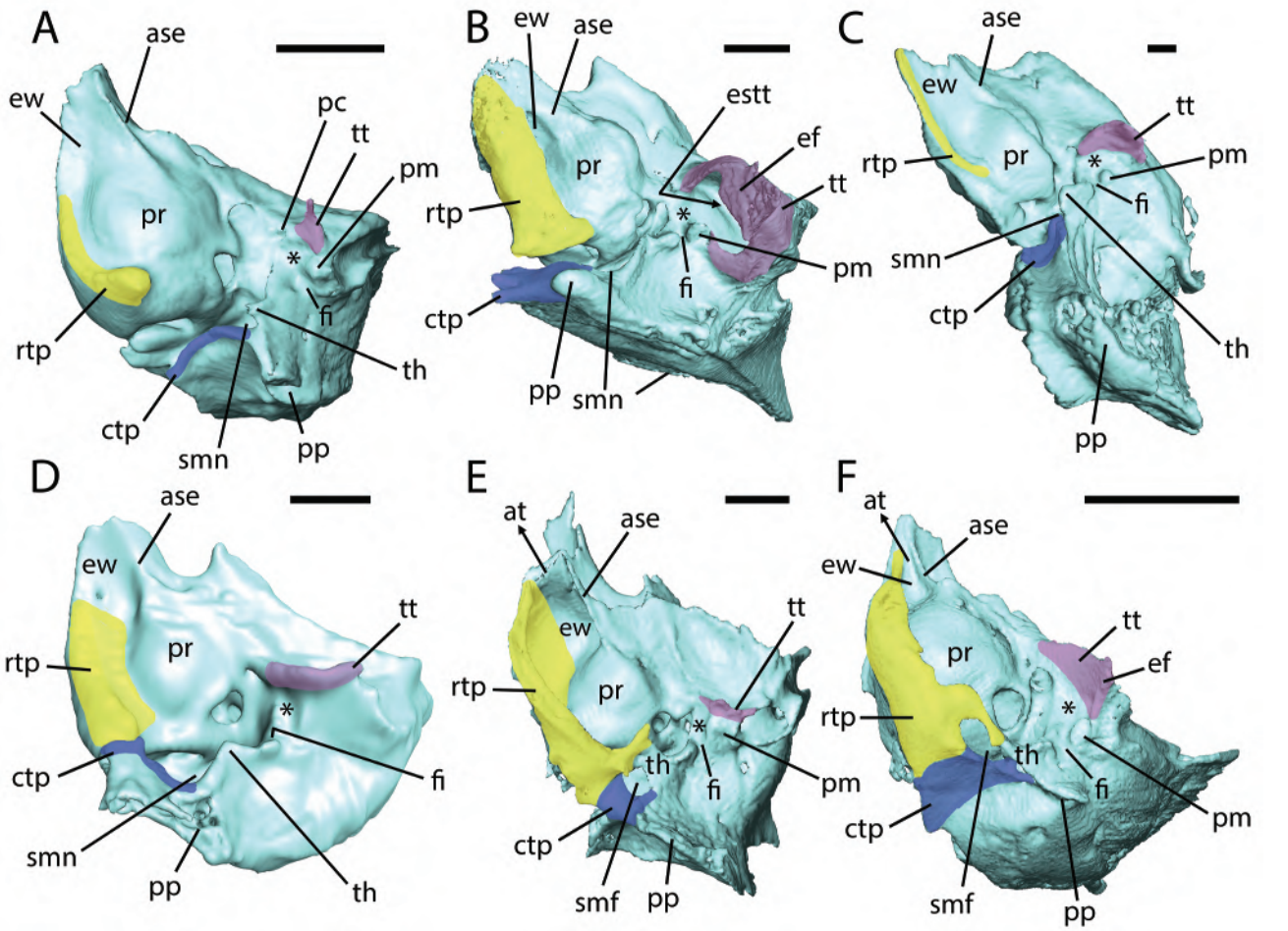

Fig. 17.—Isosurfaces of left petrosals derived from µCT scans in oblique ventral view. **A,** *Monodelphis domestica*, AMNH 261241; **B,** *Isoodon macrourus*, AMNH 160364 (reversed from right); **C,** *Thylacinus cynocephalus*, AMNH 35866 (reversed from right); **D,** *Myrmecobius fasciatus*, AMNH 155328; **E,** *Dasyurus hallucatus*, AMNH 196840; **F,** *Smithopsis macroura*, AMNH 108934. Anterior to top of page. Rostral tympanic process in yellow; anterior aspect of caudal tympanic process in blue; tegmen tympani in purple. Asterisk marks epitympanic recess. Scale is 2 mm. Abbreviations: **ase,** anterior septum; **at,** arrow indicates passage of auditory tube; **ctp,** caudal tympanic process; **ef,** ectotympanic facet; **estt**, epitympanic sinus of tegmen tympani; **ew,** epitympanic wing; **fi,** fossa incudis; **pc,** prootic canal; **pm,** postmeatal process; **pp,** paroccipital process; **pr,** promontorium; **rtp,** rostral tympanic process; **smf,** stylomastoid foramen; **smn,** stylomastoid notch; **th,** tympanohyal; **tt,** tegmen tympani.

in *N. caurinus* unknown due to fusion with neighboring bones (Fig. 18A). The petrosal of *N. typhlops*, illustrated in Ladevèze et al. (2008: fig. 4A) has a tapered wing. In the specimens studied here, the epitympanic wing invariably has an anterior septum extending from the promontorium ("ase" in Figs. 17A, 18A). The anterior septum is a narrow crest in all (Figs. 17A, C–F, 18A) except *I. macrourus*, where it is a thick ridge that is continuous at its anterior end with the rostral tympanic process (Fig. 17B). The tall anterior septum in *N. caurinus* is the posterior part of a crest that anteromedially contacts the entopterygoid process ("enp" in Fig. 18A); part of this crest contributes to the lateral wall of the carotid foramen ("cfo" in Fig. 18A) and is likely to be formed by the basisphenoid. In *Philander opossum* (Linnaeus, 1758) (Wible et al. 2021: fig. 2), *Mo. domestica*, *N. caurinus*, *I. macrourus*, *T. cynocephalus*, and *My. fasciatus*, most of the epitympanic wing and anterior septum are outside of the tympanic cavity and provide passage for the auditory tube (see arrow with "at" in Fig. 2B). In contrast, in *D. hallucatus* and *S. macroura*, the epitympanic wing and anterior septum are in the tympanic cavity, with only the anterior tip of the wing, anterior septum, and rostral tympanic process forming a U-shaped exit for the auditory tube ("at" in Figs. 17E–F). This exit is closed to form a foramen by the tympanic process of the alisphenoid. Wroe (1997) proposed this foramen for the auditory tube (his tubal foramen) as a dasyurid synapomorphy.

An epitympanic wing and thin anterior septum are present in metatherians outside crown Marsupialia, including

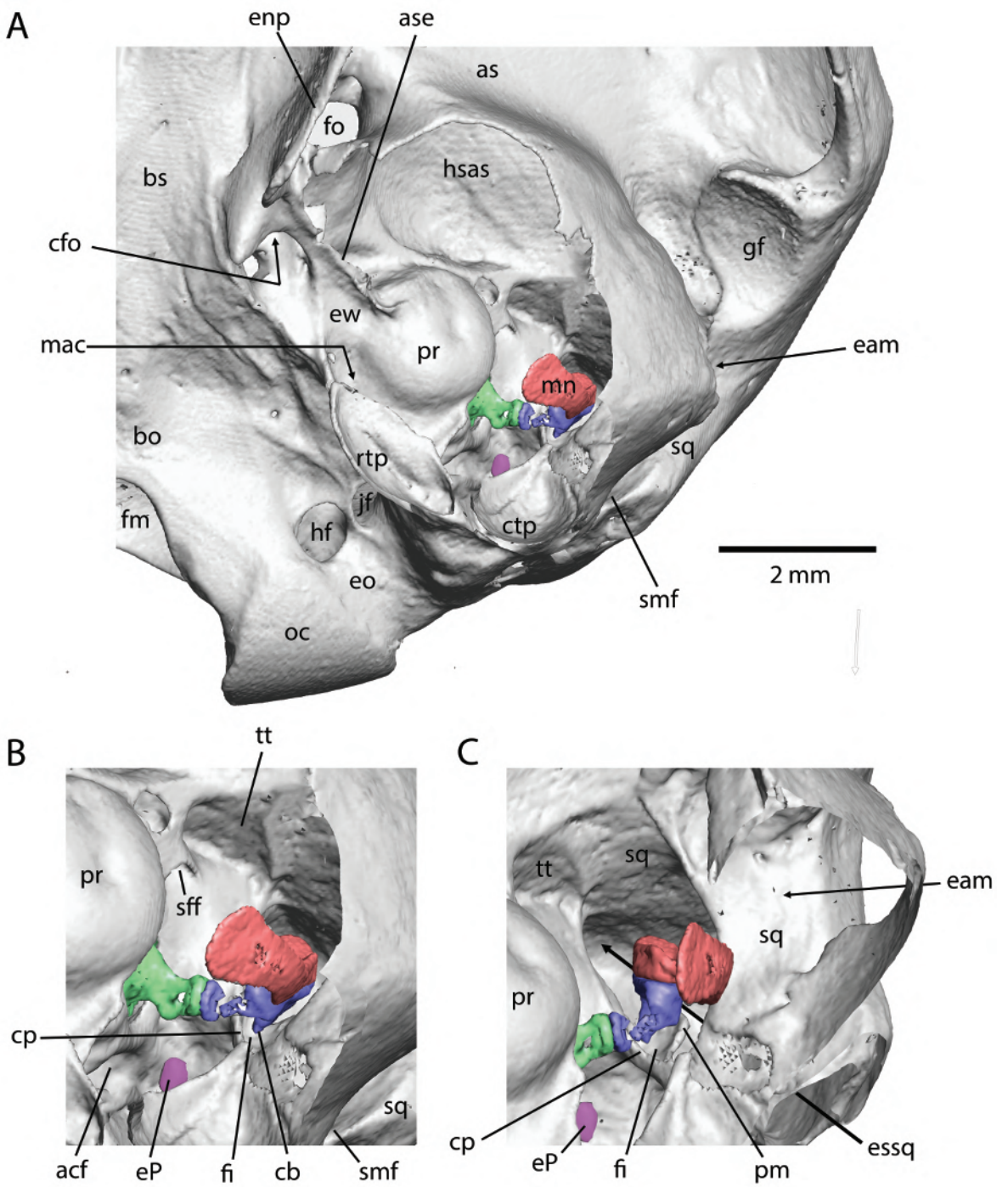

Fig. 18.—*Notoryctes caurinus*, SAM M3139. **A,** isosurface of left ear region (reversed from right) derived from μCT scans in oblique ventral view with bulla partially removed; **B,** close up of ear ossicles and environs taken from A; **C,** close up of ear ossicles and environs tilted dorsolaterally from A, squamosal is cut open to show the posterior extent of the posterior epitympanic sinus. Anterior to top of page. Malleus is red, incus blue, stapes green, and element of Paaw (see Wible et al. 2021) in purple. Most sutures delimiting bones are not preserved. Abbreviations: **acf,** aperture of cochlear fossula; **as,** alisphenoid; **ase,** anterior septum; **bo,** basioccipital; **bs,** basisphenoid; **cb,** crus breve of incus; **cfo,** carotid foramen; **cp,** crista parotica; **ctp,** caudal tympanic process of petrosal; **eam,** arrow through external acoustic meatus; **enp,** entopterygoid process; **eo,** exoccipital; **eP,** element of Paaw; **essq,** arrow through posterior epitympanic sinus of squamosal; **ew,** epitympanic wing of petrosal; **fi,** fossa incudis; **fm,** foramen magnum; **fo,** foramen ovale; **gf,** glenoid fossa; **hf,** hypoglossal foramen; **hsas,** hypotympanic sinus of alisphenoid; **jf,** jugular foramen; **mac,** medial accessory cavity; **mn,** manubrium of malleus; **oc,** occipital condyle; **pm,** postmeatal process; **pr,** promontorium; **rtp,** rostral tympanic process of petrosal; **sff,** secondary facial foramen; **smf,** stylomastoid foramen; **sq,** squamosal; **tt,** tegmen tympani.

Late Cretaceous *Deltatheridium pretrituberculare* Gregory and Simpson, 1926 (Rougier et al. 1998: fig. 3a) and early Paleocene *Andinodelphys cochabambensis* Marshall and Muizon, 1998 (Muizon and Ladevèze 2020: fig. 31). In the latter and related forms, the anterior septum has long been interpreted as forming the lateral border of a deep sulcus for the internal carotid artery (Muizon et al. 1997; Rougier et al. 1998; Muizon and Ladevèze 2020). Commenting on the many instances that this structure has been described in fossils is outside our scope here. However, we want to offer the possibility that this deep sulcus may in some cases serve a different purpose. In *Andinodelphys cochabambensis*, for example, the sulcus on the epitympanic wing appears to be much larger than the sulcus on the basisphenoid leading to the carotid foramen (Muizon and Ladevèze 2020: fig. 31). Given the relationship between the auditory tube and epitympanic wing in the marsupials studied here, we speculate that this sulcus on the epitympanic wing in *Andinodelphys cochabambensis* may have carried the auditory tube or perhaps both the auditory tube and internal carotid.

Rostral tympanic process.—We follow Beck et al. (2022) in recognizing prominences along the ventromedial aspect of the pars cochlearis as rostral tympanic processes of the petrosals ("rtp" highlighted in yellow in Figs. 17, 19). A rostral tympanic process is widely present in the taxa on the tree in Figure 16; the exception is the late Oligocene thylacinid *Badjcinus turnbulli* Muirhead and Wroe, 1998. The simplest form of the rostral tympanic process is expressed in *T. cynocephalus*, where it is a low ridge arising from the medial aspect of the promontorium near its midpoint and decreasing in height anteriorly along the medial edge of the epitympanic wing (Figs. 6, 17C). According to Muirhead and Wroe (1998:619), *Badjcinus turnbulli* lacks this ridge; "however, a small projection of bone is present that is likely to be a lesser developed equivalent." *Monodelphis domestica* is similar to *T. cynocephalus* except that the posterior end of the rostral tympanic process is considerably more prominent (Fig. 19A). In the remaining specimens (Figs. 17B, D–F, 18A), the main prominence of the rostral tympanic process is displaced medially from the promontorium, creating a shelf between the two. In *My. fasciatus* (Figs. 17D, 19D), the rostral process is thick and straight, but in *I. macrourus*, *D. hallucatus*, *S. macroura*, and *N. caurinus*, the rostral process is inflated, thin, and folded inward, partially flooring an accessory air space ("mac" in Figs. 18A, 19B, E–F). Archer (1976) employed the term periotic hypotympanic sinus for this space, but we find this problematic as the petrosal often contributes to the large hypotympanic sinus anterior to the main tympanic cavity. We follow MacPhee (1977, 1981) and use the term medial accessory cavity for this space. He reported on the ontogeny of the rostral tympanic process in some strepsirrhine primates, where pneumatic activity displaces the rostral process medially from its origin on the promontorium and creates the medial accessory cavity. The ontogeny of the rostral process in marsupials with a medial accessory cavity has not been studied, but it seems likely that a process similar to that in strepsirrhines is involved. We note that medial accessory cavity has been used by Ladevèze et al. (2008) for what we term the epitympanic sinus of the tegmen tympani in peramelids (see below).

The rostral process does not contact other bones in *T. cynocephalus*, as in some didelphids (e.g., *Philander opossum*; Wible et al. 2021). In *Mo. domestica*, the posterior crus of the ectotympanic has a small abutment on the most prominent part of the rostral process (Wible 2003). In *I. macrourus*, the rostral process is separated from the alisphenoid tympanic process and the posterior crus of the ectotympanic by narrow gaps in the μCT dataset. In *My. fasciatus*, the thick part of the rostral process opposite the promontorium contacts the inflated alisphenoid tympanic process and the rear of the rostral process abuts the caudal tympanic process (Fig. 17D). The rostral process in *N. caurinus* contributes to the formation of an inflated auditory bulla and is fused to the alisphenoid tympanic process, the caudal tympanic process (Fig. 18A), and the posterior crus of the ectotympanic. In *D. hallucatus* and *S. macroura*, most of the rostral process is in contact with other bullar elements. This includes the inflated alisphenoid tympanic process, the posterior crus of the ectotympanic, the caudal tympanic process and tympanohyal (see below; "th" in Figs. 17E–F).

Caudal tympanic process.—The caudal tympanic process of the petrosal is a simple ridge running medially from the stylomastoid notch in *Mo. domestica*, *I. macrourus*, and *T. cynocephalus* ("ctp" highlighted in blue in Figs. 17A–C). It is separated from the pars cochlearis and forms the posterior wall of the postpromontorial tympanic sinus. In contrast, in *My. fasciatus*, *N. caurinus*, *D. hallucatus*, and *S. macroura*, the caudal and rostral tympanic processes are in contact. In the first, a suture between the two processes is retained (Figs. 17D, 19D), but in the others the three are inflated and seamlessly fused (Figs. 17E F, 18A, 19E–F), forming a petrosal plate. In these four taxa, the contact between the rostral and caudal processes forms a wall separating the jugular fossa and foramen from the postpromontorial tympanic sinus. There is one or more small gaps in this wall allowing for the passage of nerves from the jugular foramen into the postpromontorial tympanic sinus, namely the tympanic nerve and the auricular branch of the vagus; therefore, these gaps represent the tympanic and mastoid canaliculi. The gap in *My. fasciatus* is in the suture between the rostral and caudal processes; this is likely the case in the others but that is masked by fusion of the two tympanic processes.

For *N. typhlops*, Ladevèze et al. (2008:691, figs. 4A, C–D) wrote "the facial nerve is enclosed in a canal that pierces the petrosal plate" and illustrated the stylomastoid foramen on the medial border of the petrosal in the vicinity of the jugular foramen. In *N. caurinus*, the stylomastoid foramen is on the posterior margin of the cranium

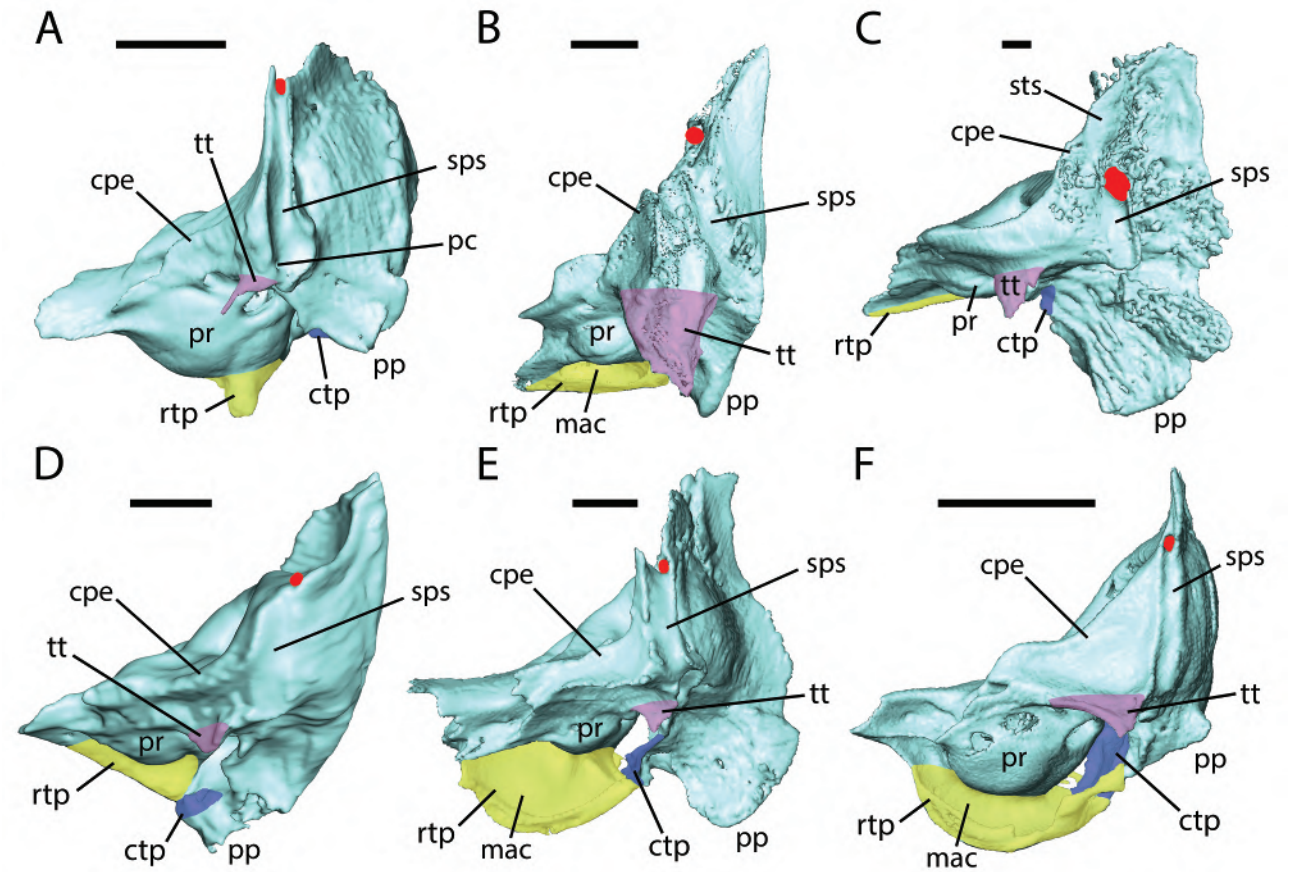

Fig. 19.—Isosurfaces of left petrosals derived from µCT scans in lateral view. **A,** *Monodelphis domestica*, AMNH 261241; **B,** *Isoodon macrourus*, AMNH 160364 (reversed from right); **C,** *Thylacinus cynocephalus*, AMNH 35866 (reversed from right); **D,** *Myrmecobius fasciatus*, AMNH 155328; **E,** *Dasyurus hallucatus*, AMNH 196840; **F,** *Smithopsis macroura*, AMNH 108934. Anterior to left. Rostral tympanic process in yellow; anterior aspect of caudal tympanic process in blue; tegmen tympani in purple; red marks position and size of sigmoid sinus. Scale is 2 mm. Abbreviations: **cpe,** crista petrosa; **ctp,** caudal tympanic process; **mac,** medial accessory cavity; **pc,** prootic canal; **pp,** paroccipital process; **pr,** promontorium; **rtp,** rostral tympanic process; **sps**, sulcus for prootic sinus; **sts,** sulcus for transverse sinus; **tt,** tegmen tympani.

between the squamosal and auditory bulla, far from the jugular foramen ("smf" in Fig. 18A). We believe Ladevèze et al. (2008) mistook the opening for the tympanic nerve off the glossopharyngeal nerve and the auricular branch of the vagus in *N. typhlops* as the stylomastoid foramen (see Tympanohyal below).

Prootic canal.—Of the specimens studied here, only *Mo. domestica* and *Monodelphis* sp. have a prootic canal (Wible 2003, 2022), which runs from the sulcus for the prootic sinus on the lateral surface ("pc" and "sps" in Fig. 19A) to the tympanic surface medial to the tegmen tympani ("pc" in Fig. 17A). As noted above, Sánchez-Villagra and Wible (2002) reported a prootic canal in one of nine specimens of *T. cynocephalus* (USNM 115365) and Beck (personal communication) found it in two specimens. Our observations of the absence of the prootic canal in the remaining taxa are congruent with those of Wroe et al. (2000), Sánchez-Villagra and Wible (2002), Ladevèze et al. (2008), and Beck et al. (2022).

Tegmen tympani—In describing the isolated petrosal of *Monodelphis* sp., Wible (2003) used the term tuberculum tympani for the small, anteroventrally-directed spinous process extending forward from the crista parotica ("tt" highlighted in purple in Figs. 17A, 19A), following Toeplitz's (1920) usage for the structure in pouch young *Didelphis marsupialis*. Wible (2003) noted the tuberculum tympani's homology with the tegmen tympani, and in his subsequent treatment of *Mo. domestica* (Wible 2022), he abandoned tuberculum tympani for tegmen tympani, which we follow here. The tegmen in *Mo. domestica* is positioned anterolateral to the epitympanic recess ("*" in Fig. 17A) and contacts the alisphenoid anteriorly (Wible 2022).

In *T. cynocephalus*, *My. fasciatus*, *D. hallucatus*, and *S. macroura*, the tegmen tympani resembles that in *Mo. domestica*, although it does not taper to a long spine and it is more vertical than anteroventrally directed (Figs. 17C–F, 19C–F). Their tegmen is a small triangular, flat process anterolateral to the epitympanic recess. The posterolateral edge of the tegmen tympani in *S. macroura* has a narrow contact with the anterior crus of the ectotympanic ("ef" in ig. 17F). These two elements approximate but do not touch in *My. fasciatus* and *D. hallucatus*, and we are uncertain of the condition in *T. cynocephalus* as ectotympanics are missing from the specimens studied.

In contrast to the small structure in these dasyuromorphians, the tegmen tympani in *I. macrourus* is massive, both in girth and height (Figs. 17B, 19B). It is built on the same pattern, that is, triangular, erect, and tapering to a point ventrally. Its ventromedial surface is flat, triangular, and has a broad contact with the anterior crus of the ectotympanic ("ef" in Fig. 17B). Dorsal to the ectotympanic facet, the medial base of the tegmen tympani has a large opening into a deep cavity that extends from the ventral tip of the tegmen nearly to the dorsal rim of the subarcuate fossa ("estt" in Fig. 17B). Kampen (1905:401) reported this cavity in his treatment of Peramelemorphia, but did not specify in what taxa it occurred. He was uncertain whether it was an accessory tympanic sinus or more likely in his opinion an enlarged fossa for the tensor tympani muscle (his fossa muscularis major). Klaauw (1931:81) made a similar observation for *Perameles*, which "shows that it may be impossible in the dry skull to distinguish an accessory sinus in the tegmen tympani of the periotic from an extraordinarily developed fossa muscularis major." To our knowledge, no mammal has a tensor tympani fossa within an inflated tegmen tympani that reaches the level of the dorsal rim of the subarcuate fossa. Additionally, Cords (1915: fig. 3) showed the tensor tympani muscle on the side of the cartilaginous cochlear capsule (future promontorium) in a pouch young of *Perameles* sp. and not near the tegmen tympani. We view the cavity in *I. macrourus* as resulting from pneumatization to form an accessory tympanic sinus that we term the epitympanic sinus of the tegmen tympani; it is continuous dorsomedially with the epitympanic recess. Other names have been applied to this space. Archer (1976) referred to it as the dorsal petrosal hypotympanic sinus, but it is more correctly an epitympanic sinus as it is derived from the epitympanic recess. Archer and Kirsch (1977) called it the dorsal periotic sinus, and Muirhead (1994) called it a mastoid epitympanic sinus. Finally, Ladevèze et al. (2008) called it the medial accessory cavity, but we reserve that term for the cavity in the rostral tympanic process (MacPhee 1977, 1981).

The lateral margin of the pars canalicularis is fused to the squamosal in *N. caurinus* (Fig. 18A). Nevertheless, we identify its tegmen tympani as small, vertical, and triangular, anterolateral to the secondary facial foramen (Fig. 18B). Ladevèze et al. (2008: fig. 4A) identified a different structure as the tegmen tympani in *N. typhlops*. Their tegmen is lateral to what they identified as the epitympanic recess, which we interpret as the fossa incudis. Anterior to this is a tongue-shaped process in *N. typhlops* that resembles what we identify as the tegmen tympani in *N. caurinus*.

Epitympanic recess and fossa incudis.—With the exception of *N. caurinus* (see below), the specimens studied here have a small epitympanic recess ("*" in Fig. 17) whose anterior border is formed by the ventrally- or anteroventrally-projecting tegmen tympani. In the posterior aspect of the epitympanic recess is a small depression, the fossa incudis ("fi" in Fig. 17), for the crus breve of the incus. Forming the medial wall of the fossa incudis is the anterior prolongation of the crista parotica. *Myrmecobius fasciatus* lacks a lateral wall to the fossa incudis and epitympanic recess (Fig. 17D), and immediately lateral to these structures is a deep posterior epitympanic sinus of the squamosal. Lateral to the fossa incudis in *Mo. domestica*, *I. macrourus*, *T. cynocephalus*, and *S. macroura* is a small postmeatal process ("pm" in Figs. 6B, 8A, 17A–C, F) that is covered by the squamosal; the postmeatal process is larger in *D. hallucatus*, also contributing to the lateral wall of the epitympanic recess (Fig. 17E).

Notoryctes caurinus does not have a bony roof over the malleoincudal articulation (Fig. 18C) and, therefore, it lacks a true epitympanic recess. Instead, the squamosal is deeply excavated to create a very large posterior epitympanic sinus of the squamosal that opens directly over the malleoincudal articulation ("essq" in Fig. 18C). At the rear of the opening into the sinus is a small shelf on the petrosal for the fossa incudis ("fi" in Figs. 18B–C). Both the medial and lateral edges of the fossa incudis are downturned; the former is the crista parotica and the latter the postmeatal process ("cp" and "pm" in Fig. 18C). The postmeatal process is at the lateral edge of the petrosal and is separated from the squamosal by the posterior epitympanic sinus. A similar arrangement may occur in *N. typhlops*; the structures labelled as the tegmen tympani and epitympanic recess by Ladevèze et al. (2008: fig. 4A) may be our postmeatal process and fossa incudis.

A postmeatal process was first identified by Wible (1990) in isolated metatherian petrosals from the Late Cretaceous Lance Formation and early Paleocene Bug Creek anthills of western USA. In these fossils, this process is more substantial than in the extant taxa here, but whether it is covered by squamosal is unknown. We are unclear how widely this process is distributed in marsupials as isolated petrosals are required to assay it. It is absent in isolated petrosals of *Didelphis virginiana* (Wible 1990: fig. 4) but present in *Philander opossum* (Wible et al. 2021: fig. 5A).

Tympanohyal and stylomastoid notch/foramen.—The tympanohyal is a small prominence on the crista parotica in *Mo. domestica*, *T. cynocephalus*, and *My. fasciatus* ("th" in Figs. 17A, C–D); it marks the anterior border of the stylomastoid notch for the exit of the facial nerve from the middle ear ("smn" in Figs. 17A, C–D). *Isoodon macrourus*

lacks an identifiable swelling on the crista parotica for the tympanohyal, but the stylomastoid notch (Fig. 17B) still can be located by the position of the facial sulcus; Kampen (1905) reported the tympanohyal absent in Peramelemorphia. In *D. hallucatus* and *S. macroura*, the tympanohyal is elongate and abuts an extension of the rostral tympanic process (Figs. 17E–F); the tympanohyal and rostral tympanic process remain separate in the former and are fused in the latter. In these dasyurids, the tympanohyal and rostral tympanic process contribute to the enclosure of a stylomastoid foramen ("smf" in Figs. 17E–F) along with the caudal tympanic process and overlying squamosal (not included in Fig. 17).

In *N. caurinus*, we followed the crista parotica ("cp" in Figs. 18B–C) from the fossa incudis posteriorly to where it abuts the bulla and did not encounter a prominence for the tympanohyal, but fusion with the bulla may mask it. The stylomastoid foramen is situated at the rear of the crista parotica between the bulla and squamosal ("smf" in Figs. 18A–B). In *N. typhlops*, Beck et al. (2022) characterized the stylomastoid foramen as between the squamosal, petrosal, and ectotympanic. Ladevèze et al. (2008: fig. 4A) illustrated a tiny tympanohyal in the appropriate place anterior to a stylomastoid notch on the rear of the isolated petrosal in *N. typhlops*. However, as noted above, these authors (Ladevèze et al. 2008: figs. 4A, C–D) reconstructed a separate stylomastoid foramen in the vicinity of the jugular foramen divorced from the stylomastoid notch. Both reconstructions cannot be valid. Their stylomastoid notch is in the same position as our stylomastoid foramen (Fig. 18B), whereas their stylomastoid foramen is in the position of the opening in the petrosal plate for the tympanic nerve and auricular branch of the vagus.

Paroccipital process.—The paroccipital process of the petrosal (mastoid process of Archer 1976) is typically the ventralmost projection on the pars canalicularis. It lies in the vicinity of the confluence between the caudal tympanic process and crista parotica and abuts the posttympanic process of the petrosal. The size and position of the paroccipital process varies across the sample here. A gracile paroccipital process occurs in *Mo. domestica* and *S. macroura* ("pp" in Figs. 17A, F, 19A, F); it does not extend ventral to the promontorium, is mediolaterally compressed, and projects posteroventrally. In the remaining specimens, except *N. caurinus* (see below), the paroccipital process is more robust, extending well ventral to the promontorium (Figs. 17B–E, 19B–E). It is mediolaterally compressed and more vertically oriented in *T. cynocephalus*, *My. fasciatus*, and *D. hallucatus* (Figs. 17C–E, 19C–E). In contrast, in *I. macrourus*, the paroccipital process is slightly anteroventrally directed and ends at a rounded knob (Figs. 17B, 19B). Because of the inflation to the caudal tympanic process and fusion between the petrosal and its neighbors, we are unsure of the limits of the paroccipital process in *N. caurinus* (Fig. 18A).

Crista petrosa.—The crista petrosa, the attachment point for the tentorium cerebelli, separating the middle and caudal cranial fossae, is a ridge primarily opposite the subarcuate fossa in the specimens studied here ("cpe" in Figs. 19), except *N. caurinus* (see below). Differences in the height of the ridge and the disposition of the bones anterior to it produce an exposure of the pars canalicularis in the rear of the middle cranial fossa of varying sizes ("*" in Fig. 20). The crista is low and the pars canalicularis exposure in the middle cranial fossa small in *My. fasciatus* (Figs. 19D, 20D), whereas the crista is tall and sharp and the middle cranial fossa exposure more substantial in the remaining specimens (Figs. 5, 19A–C, E–F, 20A–C, E–F).

In *N. caurinus*, the crista petrosa is absent opposite the subarcuate fossa but is a low, sharp ridge on the pars cochlearis opposite the internal acoustic meatus ("cpe" in Fig. 21A). Although the boundaries of the petrosal are not entirely clear, there appears to be exposure of both the pars cochlearis and pars canalicularis in the rear of the middle cranial fossa ("*" in Fig. 21A). Ladevèze et al. (2008: fig. 4B) illustrated similar morphologies in *N. typhlops*.

Internal acoustic meatus and subarcuate fossa.—These two openings on the endocranial surface of the petrosal vary in size relative to each other in the studied sample. In *Mo. domestica* and *S. macroura*, the internal acoustic meatus is wider than the subarcuate fossa and the two apertures are roughly equal in area ("1" and "2" in Figs. 20A, F). In *I. macrourus*, the two are subequal in width with the subarcuate fossa aperture slightly larger (Fig. 20B). *Notoryctes caurinus* also has the apertures subequal in width, but the subarcuate fossa aperture is much larger in area (Fig. 21A). In *My. fasciatus* and *D. hallucatus*, the subarcuate fossa aperture is slightly wider and larger in area (Figs. 20D–E); this is also the case in the subadult *T. cynocephalus*, CM 20975 (Fig. 5A). The most extreme difference is in the adult *T. cynocephalus*, AMNH 35866, with the internal acoustic meatus much narrower and smaller in area than the subarcuate fossa aperture (Fig. 20C). Given the distribution of these differences, it is likely that body size has an impact on the relative sizes of these openings, with the smaller taxa having wider internal acoustic meatuses relative to the subarcuate fossa than the larger taxa.

A feature common to the entire sample is the absence of a complete transverse crest dividing the internal acoustic meatus into superior and inferior openings.

Endocranial veins.—Although we intend in the future to pursue the endocranial venous pattern in thylacines and their relatives in more detail, we make some preliminary observations here regarding the veins associated with the petrosal.

Transverse sinus.—In *Didelphis virginiana*, the paired transverse sinuses begin at the midline confluens sinuum at the rear of the superior sagittal sinus (sinus sagittalis dorsalis of Dom et al. 1970); the transverse sinus then runs ventrolaterally in base of the tentorium cerebelli. As in

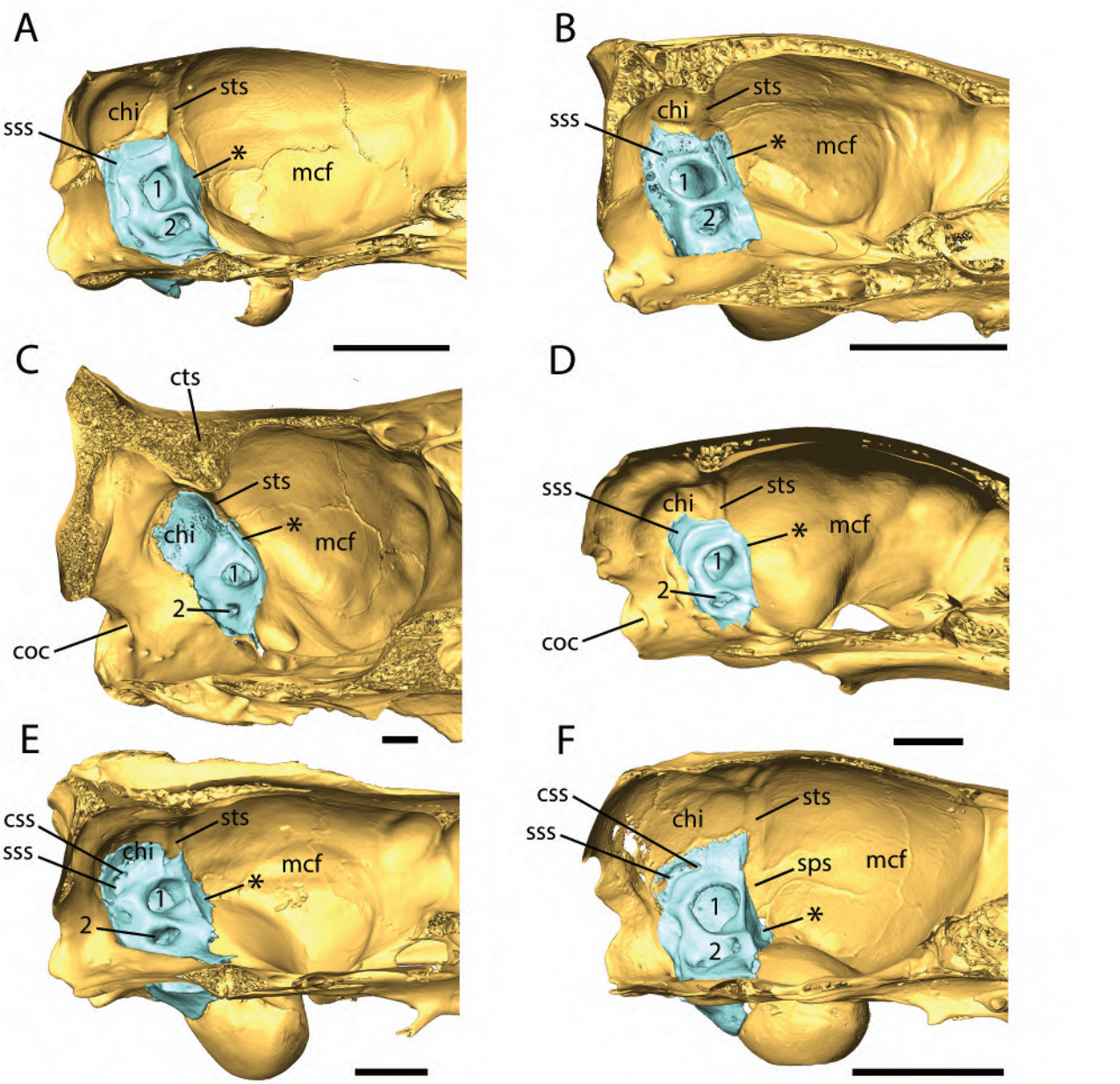

Fig. 20.—Isosurfaces of the left endocranium derived from µCT scans in medial view. **A,** *Monodelphis domestica*, AMNH 261241; **B,** *Isoodon macrourus*, AMNH 160364 (reversed from right); **C,** *Thylacinus cynocephalus*, AMNH 35866 (reversed from right); **D,** *Myrmecobius fasciatus*, AMNH 155328; **E,** *Dasyurus hallucatus*, AMNH 196840; **F,** *Smithopsis macroura*, AMNH 108934. Anterior to right; petrosal in light blue. * is on exposure of pars canalicularis in the middle cranial fossa; 1 is subarcuate fossa; 2 is internal acoustic meatus. Scale is 5 mm. Abbreviations: **chi,** cerebellar hemisphere impression; **coc,** condyloid canal; **css,** canal for sigmoid sinus; **cts,** canal for transverse sinus; **mcf,** middle cranial fossa; **sps,** sulcus for prootic sinus; **sss,** sulcus for sigmoid sinus; **sts,** sulcus for transverse sinus.

Didelphis virginiana, the transverse sinus in *Mo. domestica*, *N. caurinus*, *I. macrourus*, *My. fasciatus*, *D. hallucatus*, and *S. macroura* travels in an open sulcus on the parietal ("sts" in Figs. 20A–B, D–F, 21A) and terminates in its end branches dorsal to the petrosal (Figs. 21, 22A–B, D–F). In contrast, in *T. cynocephalus*, most of the course of the transverse sinus on the parietal is enclosed in a canal ("cts" in Fig. 5A) with only a short segment in a sulcus on the parietal ("sts" in Fig. 5A). Additionally, in *T. cynocephalus*, the transverse sinus does not terminate dorsal to the petrosal, but occupies a sulcus on the lateral surface of the petrosal before its termination ("sts" in Figs. 3, 8B, 10B, 19C; "ts" in Fig. 12B).

Prootic sinus/postglenoid vein.—In *Didelphis virginiana*, the prootic sinus (temporal sinus of Dom et al. 1970) is one of the end branches of the transverse sinus,

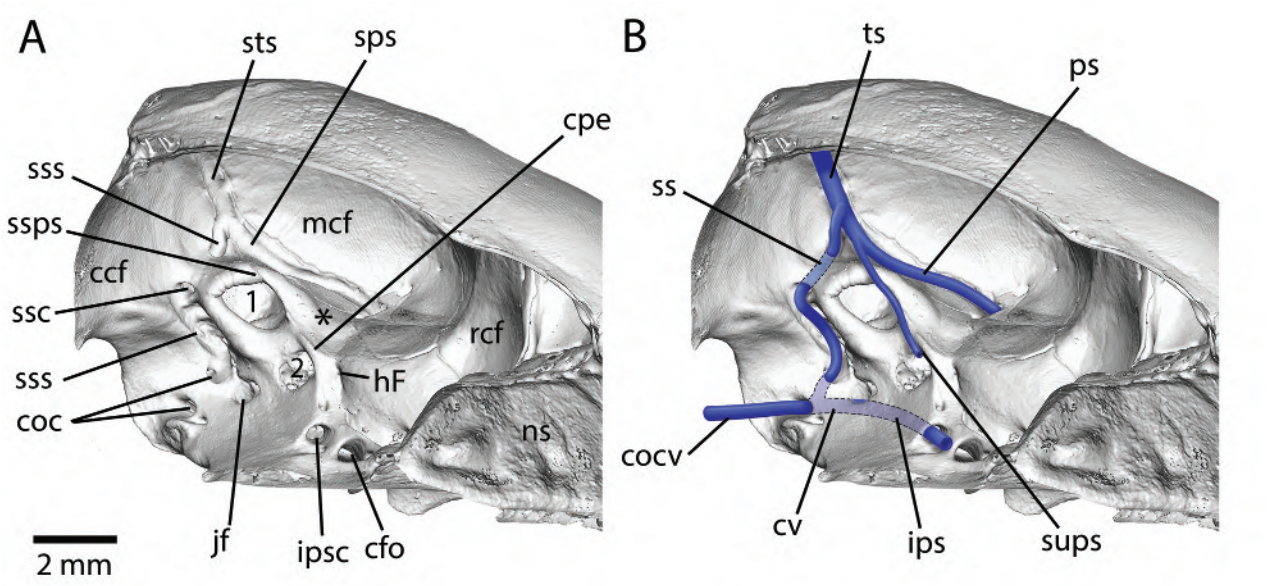

Fig. 21.—*Notoryctes caurinus*, SAM M3139. **A,** isosurface of left endocranium derived from μCT scans in oblique medial view; **B,** with major veins reconstructed based on sulci and canals. Anterior to right. In A,* is on exposure of pars canalicularis and pars cochlearis in the middle cranial fossa; 1 is subarcuate fossa; 2 is internal acoustic meatus. Abbreviations: **ccf,** caudal cranial fossa; **cfo,** carotid foramen; **coc,** condyloid canal; **cocv,** condyloid canal vein; **cpe,** crista petrosa; **cv,** connecting vein; **hF,** Hiatus Fallopii; **ips,** inferior petrosal sinus; **ipsc,** inferior petrosal sinus canal; **jf,** jugular foramen; **mcf,** middle cranial fossa; **ns,** nasal septum; **ps,** prootic sinus; **rcf,** rostral cranial fossa; **sps,** sulcus for prootic sinus; **ss,** sigmoid sinus; **ssc,** sigmoid sinus canal; **ssps,** sulcus for superior petrosal sinus; **sss,** sulcus for sigmoid sinus; **sts,** sulcus for transverse sinus; **sups,** superior petrosal sinus; **ts,** transverse

ultimately leaving the cranium as the postglenoid vein. With the exception of *N. caurinus* (see below), from its origin on the transverse sinus, the prootic sinus in the sample here runs in a sulcus on the lateral aspect of the petrosal ("sps" in Figs. 8B, 10B, 19) en route to its exit at the postglenoid foramen. This petrosal sulcus is enclosed in a canal by the squamosal in all except *S. macroura*, where the corresponding sulcus on the squamosal ("sps" in Fig. 20F) does not complete a canal. The endocranial course of the prootic sinus in *N. caurinus* is in an open sulcus that appears to be entirely on the squamosal (Fig. 21).

Sigmoid sinus.— In *Didelphis virginiana*, the sigmoid sinus is another end branch of the transverse sinus, ultimately leaving the cranium via the foramen magnum (Dom et al. 1970). The origin, course, and connections of the sigmoid sinus vary in the studied sample. In all but *T. cynocephalus* (see below), the sigmoid sinus arises from the transverse sinus dorsolateral to the subarcuate fossa (Figs. 19A–B, D–F, 21B, 22A–B, D–F). It runs posteriorly dorsal to the subarcuate fossa in an open sulcus in *Mo. domestica*, *I. macrourus*, and *My. fasciatus* ("sss" in Figs. 20A–B, D) and partly in a canal in *N. caurinus*, *D. hallucatus*, and *S. macroura* ("css" in Figs. 20E–F, 21A). Wible (2003) reported a canal in *Monodelphis* sp., CM 5024 and 5061. Posterior to the subarcuate fossa, the sigmoid sinus turns ventrally in a sulcus that is on the occipital in *My. fasciatus* (Fig. 20D), but is primarily on the petrosal in the remainder (Figs. 20A–B, E–F, 21A). The sulcus for the sigmoid sinus is directed toward the jugular foramen in *Mo. domestica*, *I. macrourus*, *D. hallucatus*, and *S. macroura* (Figs. 22A–B, E–F), toward both the jugular foramen and condyloid canal in *My. fasciatus* (Fig. 22D), and toward only the condyloid canal in *N. caurinus* (Fig. 21). A condyloid canal does not occur in *M. domestica*, *I. macrourus*, *D. hallucatus*, and *S. macroura* (Figs. 20A–B, E–F).

The most extreme deviation from the above pattern occurs in *T. cynocephalus*. In light of the size of its sulcus and canal, the sigmoid sinus is a more substantial vessel than in the other taxa (Figs. 19, 22), and its course is entirely within canals. Its origin is not dorsolateral to the subarcuate fossa in the endocranial cavity, but is more ventrally placed in an intramural space on the lateral aspect of the petrosal (Figs. 12B, 19C). It passes to the medial side of the petrosal in a canal well posterior to the subarcuate fossa (Fig. 12A). Once through the sigmoid canal in the petrosal, the sigmoid sinus joins the parieto-occipital diploic vein (Figs. 12A, 22C; see below) and runs ventromedially in a canal in the exoccipital. It joins a communicating vein from the inferior petrosal sinus and ultimately exits the condyloid canal in the rim of the foramen magnum.

Superior petrosal sinus.—In *Didelphis virginiana*, Dom et al. (1970) reported the superior petrosal sinus (their sinus petrosus dorsalis) as the third end branch of the transverse sinus. It runs along the anterior lip of the subarcuate fossa, posterior to the crista petrosa. Four specimens in our sample have sulci in the appropriate place, and we

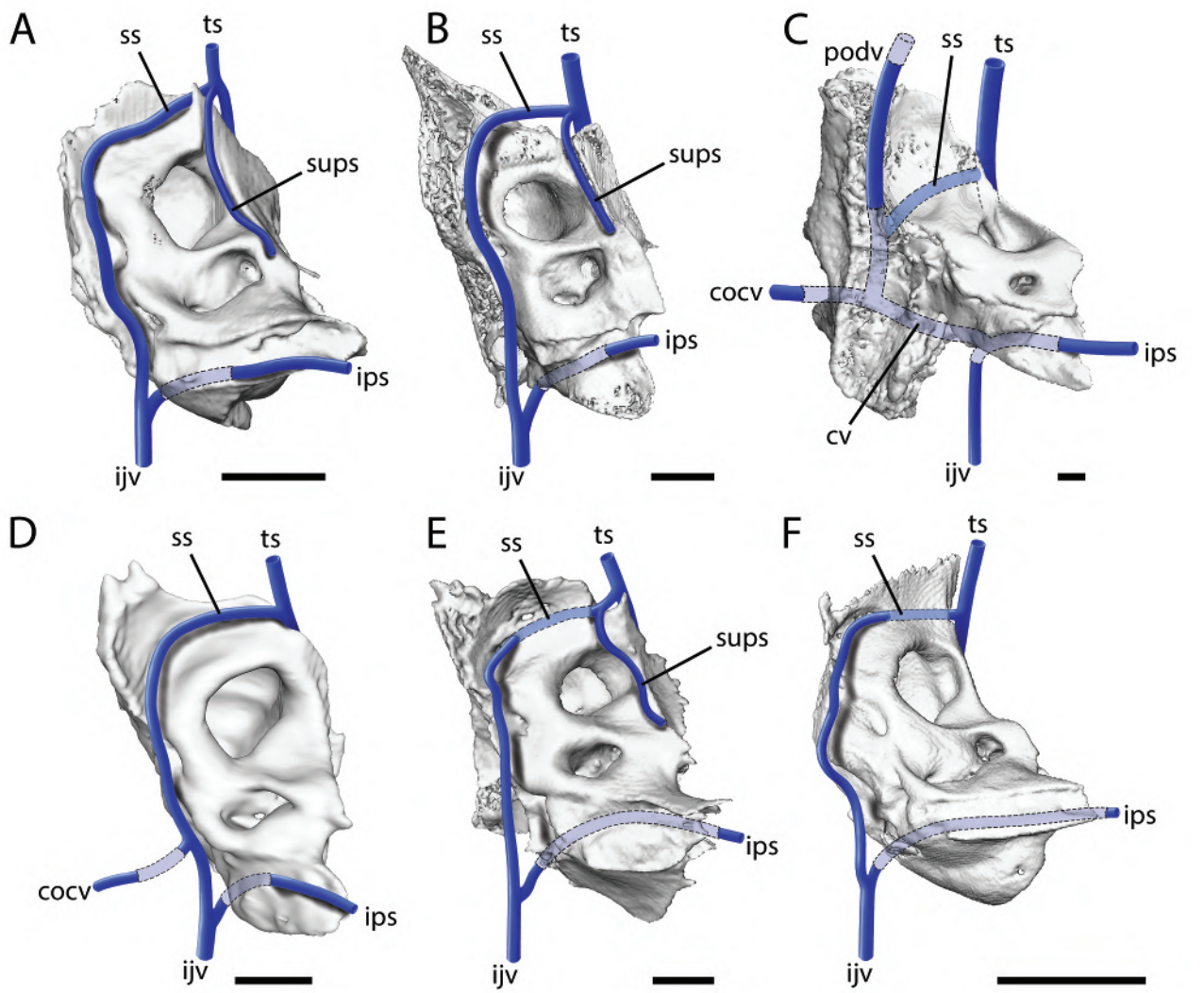

Fig. 22.—Isosurfaces of left petrosals derived from µCT scans in lateral view with veins reconstructed based on preserved sulci, canals, and foramina. **A,** *Monodelphis domestica*, AMNH 261241; **B,** *Isoodon macrourus*, AMNH 160364 (reversed from right); **C,** *Thylacinus cynocephalus*, AMNH 35866 (reversed from right); **D,** *Myrmecobius fasciatus*, AMNH 155328; **E,** *Dasyurus hallucatus*, AMNH 196840; **F,** *Smithopsis macroura*, AMNH 108934. Veins that are not enclosed in canals are in dark blue; gray veins with dashed outer lines are in canals between bones; blue vein with dashed outer lines is in canal in petrosal. Anterior to left. Scale is 2 mm. Abbreviations: **cocv,** condyloid canal vein; **cv,** connecting vein; **ijv,** internal jugular vein; **ips,** inferior petrosal sinus; **podv,** parieto-occipital diploic vein; **ss,** sigmoid sinus; **sups,** superior petrosal sinus; **ts,** transverse sinus.

reconstruct the superior petrosal sinus for them: *Mo. domestica*, *I. macrourus*, *D. hallucatus*, and *N. caurinus* (Figs. 21B, 22A–B, D). Archer (1976:312) noted "Sulci or crests associated with the dorsal petrosal sinus are variably present in didelphids, thylacinids (intra-specific variation), and dasyurids. They are absent in myrmecobiids but present in notoryctids."

Inferior petrosal sinus.—In *Didelphis virginiana*, the inferior petrosal sinus (sinus petrosus ventralis of Dom et al. 1970) runs posteriorly from the cavernous sinus around the hypophysis; the bulk of its exit is via the foramen magnum but it sends a small vessel out of the jugular foramen as the internal jugular vein. In the studied sample, the inferior petrosal sinus travels near the contact between the petrosal and basioccipital, with the extent of enclosure in canals and the point of exit varying (see also Wroe 1999). In *Mo. domestica* (Fig. 22A) and *My. fasciatus* (Fig. 22D), the inferior petrosal sinus is open anteriorly within the endocranium on the petrosal in the former and the basioccipital in the latter, and posteriorly is in a short canal

between the basioccipital and petrosal. The vessel exits the cranial cavity via a separate foramen for the inferior petrosal sinus, which is distinct from the jugular foramen in *Mo. domestica*, but opens into the jugular fossa in *My. fasciatus*. In *I. macrourus* (Fig. 22B), there is a short endocranial course for the inferior petrosal sinus in a sulcus on the petrosal and basioccipital, and then a canal between the two leading to a separate foramen for the inferior petrosal sinus. Both *D. hallucatus* (Fig. 22E) and *S. macroura* (Fig. 22F) have a canal for the inferior petrosal sinus that runs the length of the pars cochlearis, opening posteriorly at a foramen well anterior to the jugular foramen. The canal is entirely in the basioccipital anteriorly in *S. macroura* and then between the petrosal and basioccipital posteriorly, but between the two bones the entire length in *D. hallucatus*. As in the dasyurids, the inferior petrosal sinus canal runs the length of the pars cochlearis in *T. cynocephalus* (Fig. 22C); it is in the basioccipital anteriorly and then in between the petrosal and exoccipital anteriorly. A separate foramen for the inferior petrosal sinus occurs anterior to the jugular foramen between the exoccipital and petrosal. However, not all the blood in the inferior petrosal sinus exits here; there is a connecting vein ("cv" in Figs. 12A, 22C) that continues posteriorly through a canal in the exoccipital and joins the sigmoid sinus. *Notoryctes caurinus* (Fig. 21) has a canal running the length of the pars cochlearis that appears to begin anteriorly entirely in the basioccipital; it ends at a separate inferior petrosal sinus foramen in the jugular fossa. As in *T. cynocephalus*, *N. caurinus* has a connecting vein that runs through a short canal in the exoccipital; it empties into the condyloid canal vein as did the sigmoid sinus.

Parieto-occipital diploic vein.—Diploic veins only occur where cancellous or spongy bone unites the two tables of the cranium. In the dog (Evans and Christensen 1979), there are diploic veins in the frontal, parietal, and occipital, all of which are in the middle cranial fossa adjacent to the cerebrum; the first two arise from the superior sagittal sinus and the last from the transverse sinus. In contrast, the parieto-occipital diploic vein reported here for *T. cynocephalus* (Figs. 12A, 22C) is in the caudal cranial fossa adjacent to the cerebellum. It is a large venous channel arising from the transverse sinus and running posteriorly in a canal through the parietal, interparietal, and supraoccipital, and lastly in a canal between the petrosal and exoccipital that is unique to *T. cynocephalus* (Figs. 12A, 22C) in the studied sample. Additionally, to our knowledge, this vessel is unique to the thylacine among mammals. CM 20975 and AMNH 35866 differ in two regards: in the former, the vein is bilateral and the canal between the petrosal and exoccipital is closed, while in the latter the vein is only on the right side and part of the canal is open in the caudal cranial fossa (Fig. 22C).

Recently, Gaillard et al. (2024: fig. 11C) showed a digital reconstruction of a canal in the early Miocene sparassodont *Sipalocyon externus* Ameghino, 1902, that resembles the proximal (dorsal) part of the parieto-occipital diploic vein of the thylacine. Their interparietal diploic vein occurs only on the left side, runs posteriorly from the transverse sinus, and then perhaps medially towards the occiput, with a gap between the posteriorly- and medially-directed parts. Wible (2022) interpreted a similar canal arising from the transverse sinus and ending in the interparietal in *Mo. domestica* as for an interparietal diploic vein. Muizon et al. (2018) and Muizon and Ladevèze (2020) reported foramina within the sulcus for the transverse sinus in various fossil metatherians (e.g., early Paleocene *Allqokirus australis* Marshall and Muizon, 1988; *Andinodelphys cochabambensis*) that they identified as for parietal diploic veins. Muizon et al. (2018:400) also stated these foramina are in "*Didelphis, Dromiciops, Thylacinus, Dasyurus*, among others, and are apparently present in all therians." While this is an intriguing proposal, we only speak to the situation in the thylacines studied here. Unlike the fossils described by Muizon et al. (2018) and Muizon and Ladevèze (2020), the medial portion of the thylacine transverse sinus is entirely enclosed in bone, whereas the fossils have an open sulcus. Both thylacines studied here have paired foramina in the tentorial process of the parietals that open directly into the canal for the transverse sinus ("vf" in Fig. 5A) and are likely the openings that Muizon et al. (2018) identified as parietal diploic foramina. As the vein in that foramen does not run through the diploë, it is not a diploic vein, but is more likely a cerebellar vein. The parietal openings in the thylacine and the fossil metatherians reported by Muizon et al. (2018) are not homologous.

Another feature of the parieto-occipital channel in *T. cynocephalus* is that it communicates with a foramen in the supraoccipital off the midline just below the nuchal crest ("vf" in Fig. 4B). Gaillard et al. (2024) reported similarly-situated openings as emissary foramina in *Sipalocyon externus* and diploic foramen in *Sipalocyon gracilis* Ameghino, 1887.

Posttemporal foramen.—A posttemporal foramen on the occiput between the petrosal and squamosal is variably present in didelphids, but is rarely found in other marsupials (Sánchez-Villagra and Wible 2002). This foramen is absent in the sample studied here. Recently, MacPhee et al. (2023: figs. 29B–C) labelled a posttemporal foramen in *T. cynocephalus*, AMNH 144316; on the left side, the foramen appears to be between the medial border of the petrosal and the exoccipital, whereas on the right side, it is within the petrosal at the dorsal limit of that bone's exposure on the occiput near the supraoccipital. Neither of these is likely a posttemporal foramen, which typically lies on the lateral border of the petrosal at around mid-height and transmits an arteria diploëtica magna and accompanying vein that run in a groove on the lateral aspect of the pars canalicularis (Wible 1987, 1990). These openings in AMNH 144316 are more likely outlets for the parieto-occipital diploic vein. Of the two thylacine specimens studied here, only the right side of AMNH 35866 has a tiny foramen in a position like the right side of AMNH 144316.

It is a nutrient foramen and only leads into the substance of the petrosal.

Cerebellar hemisphere impression.—Most of the specimens studied here have an impression for the cerebellar hemisphere in the caudal cranial fossa; the main exception is *N. caurinus*, where such an impression is not delimited (Fig. 21A). The impression is faint in *S. macroura* ("chi" in Fig. 20F), but it is well marked in the remainder (Figs. 5, 20A–E). In all the specimens with the impression, the petrosal has an exposure within it (Fig. 20). However, the extent of the petrosal exposure varies in the sample, with the largest contribution by far in *T. cynocephalus* (Figs. 5, 20C), followed by *D. hallucatus* (Fig. 20E). As the petrosal is fused to the occipital in the caudal cranial fossa in *N. caurinus* (Fig. 21A), the extent of petrosal exposure dorsal to the subarcuate fossa in unknown. Ladevèze et al. (2008: fig. 4B) illustrated what appears to be a small petrosal exposure dorsal to the subarcuate fossa in *N. typhlops*.

The transparent petrosals in Figures 15 and 23 that include the inner ear show the size relationship between these two structures. In *Monodelphis* sp. (Figs. 23B, D) and *S. macroura* (Figs. 23R, T), the inner ear occupies a significant portion of the petrosal; in *I. macrourus* (Figs. 23F, H), *My. fasciatus* (Figs. 23J, L), and *D. hallucatus* (Figs. 23N, P), the proportion of inner ear to petrosal is reduced; and lastly, in *T. cynocephalus* (Figs. 15B, D), there appears to be more petrosal without the inner ear than with it. The "extra" bone in the last is posterior and posterodorsal to the inner ear, in the impression for the cerebellar hemisphere and in the paroccipital process base. The differences across this sample may result from body size with the smallest having a close fit between petrosal and inner ear and the largest a great disparity, as reported by multiple authors for various mammals (e.g., Jones and Spells 1997; Spoor et al. 2007; Costeur et al. 2019).

Stapes.— Stapes are not preserved in most of the studied sample and were segmented from the µCT scans for only *T. cynocephalus*, CM 20975, and *N. caurinus*, SAM M3139 (Fig. 13). Both are columelliform with a footplate that is concave on the surface facing the fenestra vestibuli. Primary differences concern the height of the stapes (short and squat in *N. caurinus*) and the size of the muscular process (large in *N. caurinus*). Beck et al. (2022: characters 65–66) scored two characters about the stapes in their morphological phylogenetic analysis. In the first, columelliform versus triangular shape with an obturator foramen present, all the genera in our studied sample have columelliform stapes except *Mo. domestica* (Sánchez-Villagra et al. 2002: fig. 10A). The second is whether the footplate is concave, flat, or convex. *Monodelphis domestica* and *N. typhlops* were scored flat, *T. cynocephalus* and *Dasyurus* were unknown, and *I. macroura*, *My. fasciatus*, and *Sminthopsis* were concave. Schmelzle et al. (2005) also scored the contour of the footplate, with the concave state in four dasyurids (*Dasycercus byrnei*, *Dasyurus viverrinus*, *Antechinus agilis*, and *Phascogale tapoatafa*) and flat in two peramelids (*Perameles nasuta* and *Echymipera* sp.). The stapedial footplate of *T. cynocephalus*, CM 20975, is concave as is that of *N. caurinus*, SAM M3139 (Figs. 13C, F). Although *N. typhlops* has a different state than *N. caurinus* and *Perameles nasuta* a different state than *I. macroura*, a concave footplate may be a synapomorphy of the notoryctemorph(peramelemorph+dasyuromorph) clade in Figure 16, the Agreodontia of Beck et al. (2014).

Inner ear.— Among the compared specimens, *Monodelphis* sp., *I. macrourus*, and *D. hallucatus* have a higher cochlear turn and rotation than *T. cynocephalus,* CM 20975 (Table 2). In contrast, *N. caurinus*, *My. fasciatus*, and *S. macroura* have lower values for the cochlea compared to *T. cynocephalus* (Table 2). As in *T. cynocephalus*, both laminae are visible, and the secondary bony lamina starts dorsolateral to the fenestra cochleae in all compared specimens ("sbl" in Figs. 14B, 24A, G, M, 25A, G, M). The secondary bony lamina extends beyond the basal turn and for a longer part of the cochlear canal in *Monodelphis* sp., *I. macrourus*, and *D. hallucatus* than in *T. cynocephalus*, which has a shorter secondary bony lamina (Table 2). The remaining specimens, *N. caurinus*, *My. fasciatus*, and *S. macroura*, have a shorter secondary lamina that does not extend beyond the basal turn in contrast to *T. cynocephalus* (Table 2). The cochlear fossula is less marked and does not have a visible bulge in *D. hallucatus* and *S. macroura* compared to *Monodelphis* sp., *N. caurinus, I. macrourus,* and *T. cynocephalus* ("cf" in Figs. 14B, D, 24D, J, P, 25J, P). The bulge is present but very subtle in *My. fasciatus* (Fig. 25D). As in *T. cynocephalus*, there is a fossula leading to the fenestra vestibuli in *Monodelphis* sp., *I. macrourus*, *D. hallucatus*, and *S. macroura* ("ffv" in Figs. 14E, 24D, P, 25J, P). This contrasts with *My. fasciatus* and *N. caurinus*, which do not have a fossula on the fenestra vestibuli (Figs. 24H, 25B). Using the 3D model of the cranium, we observe that as in *T. cynocephalus*, the fenestra cochleae is oriented posterolaterally in *N. caurinus.* In all other specimens, the fenestra cochleae is postero-ventrolaterally oriented. Additionally, the fenestra vestibuli is oriented laterally in *N. caurinus*, *I. macrourus*, *My. fasciatus*, and *T. cynocephalus*, whereas in the remaining specimens, *Monodelphis* sp., *D. hallucatus,* and *S. macroura,* it is more ventrolaterally oriented. Finally, in contrast to *T. cynocephalus* in which the fenestra cochleae is larger than the fenestra vestibuli, the opposite is true for *I. macrourus*, *My. fasciatus*, and *D. hallucatus.* Both fenestrae have approximately the same size in *Monodelphis* sp., *N. caurinus*, and *S. macroura*. The cochlear aqueduct runs parallel to the vestibular aqueduct with a posteromedial direction in *Monodelphis* sp., *N. caurinus*, and *D. hallucatus* as in *T. cynocephalus* ("va" and "ca" in Figs. 14B, E, 24A, G, 25G). In *I. macrourus* and *S. macroura*, the course of the cochlear aqueduct is also posteromedially oriented but is divergent from the one of the vestibular aqueduct (Figs. 24M, 25M). The cochlear

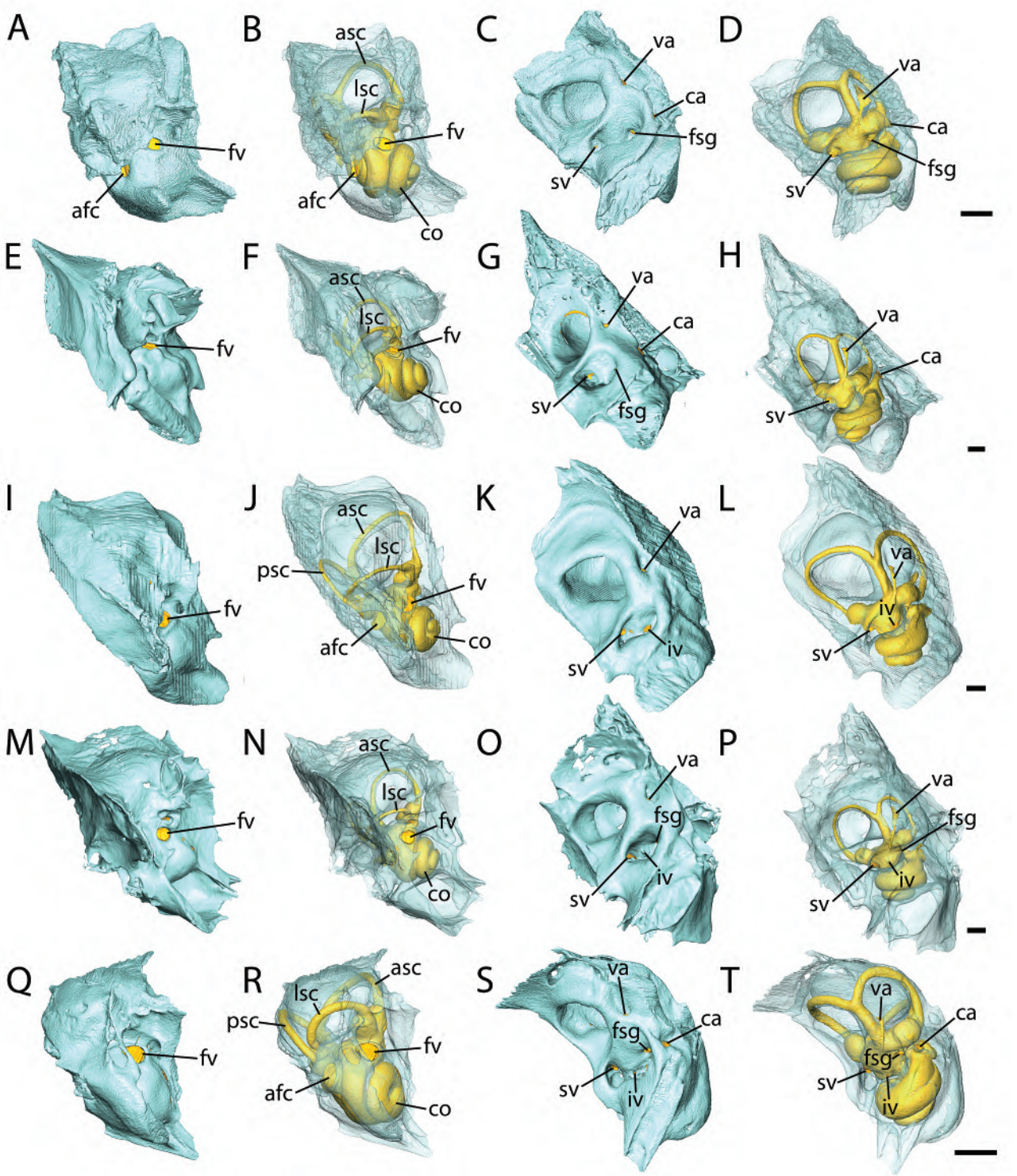

Fig. 23.—Virtual endocasts of the right bony labyrinth inside the petrosal bone. **A–D,** *Monodelphis* sp., DU BAA 0181 (left mirrored); **E–H,** *Isoodon macrourus*, AMNH 160364; **I–L,** *Mymecobius fasciatus*, AMNH 155328; **M–P,** *Dasyurus hallucatus*, AMNH 196840 (left mirrored); **R–U,** *Sminthopsis macroura,* AMNH 108934 (left mirrored). **A, E, I, M, Q,** and **B, F, J, N, R,** ventrolateral view; **C, G, K, O, S,** and **D, H, L, P, T,** medial view. Scale is 1 mm. Abbreviations: **afc,** aperture for fenestra cochleae; **asc,** anterior semicircular canal; **ca,** cochlear aqueduct; **co,** cochlear canal; **fsg,** foramen singulare; **fv,** fenestra vestibuli; **iv,** inferior vestibular nerve; **lsc,** lateral semicircular canal; **psc,** posterior semicircular canal; **sv,** superior vestibular nerve; **va,** vestibular aqueduct.

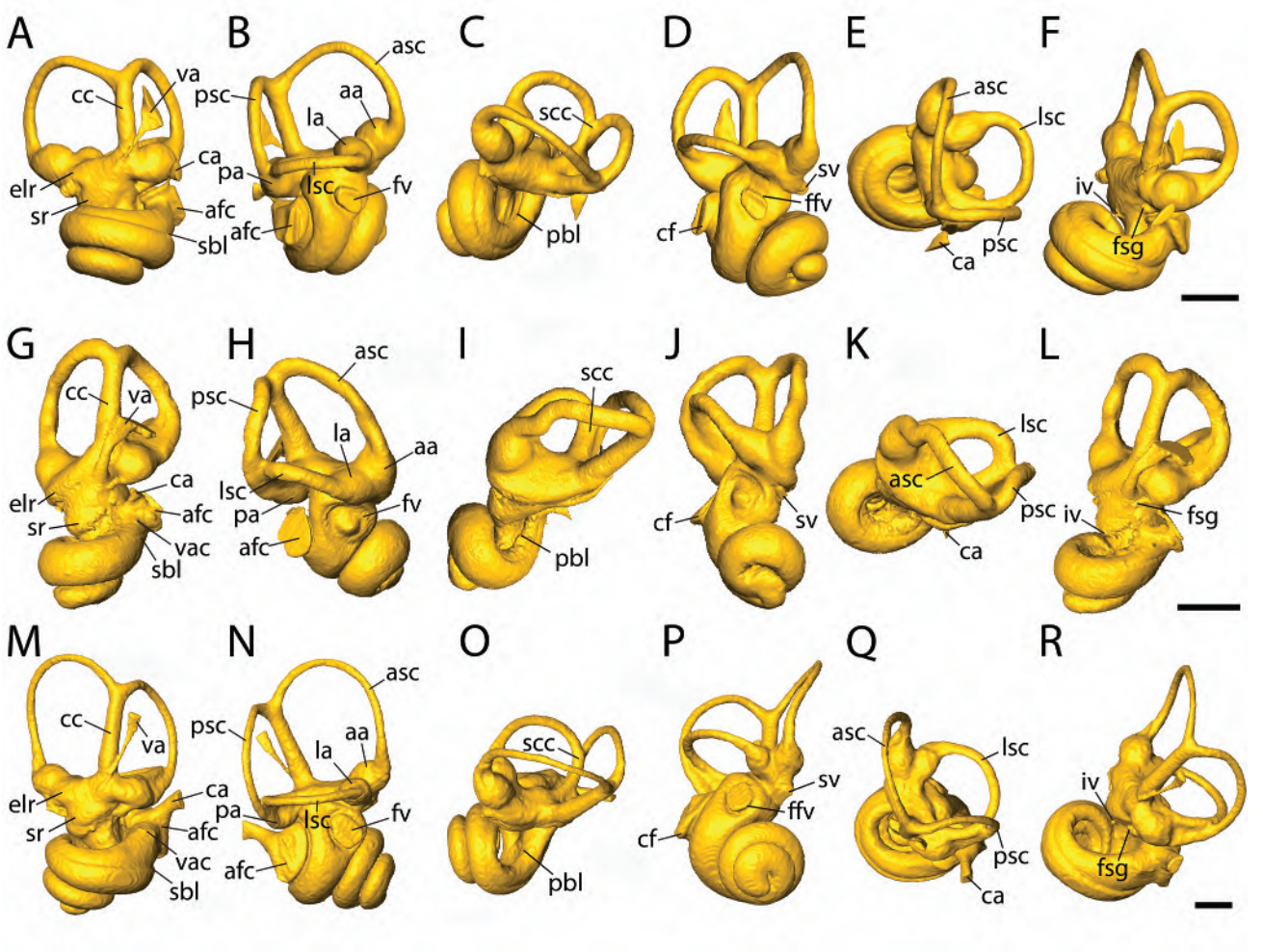

Fig. 24.—Virtual endocasts of right bony labyrinths. **A–F,** *Monodelphis* sp., DU BAA 0181 (left mirrored); **G–L,** *Notoryctes caurinus*, SAMA M3139; **M–R,** *Isoodon macrourus*, AMNH 160364). **A, G, M,** medial view; **B, H, N,** posterolateral view; **C, I, O,** dorsal view; **D, J, P,** anterolateral view; **E, K, Q,** posterodorsal view; **F, L, R,** posteromedial view. Scale is 1 mm. Abbreviations: **aa,** anterior ampulla; **afc,** aperture of fenestra cochleae; **asc,** anterior semicircular canal; **ca,** cochlear aqueduct; **cc,** common crus; **cf,** cochlear fossula; **co,** cochlear canal; **elr,** elliptical recess; **ffv,** fossula of fenestra vestibuli; **fsg,** foramen singulare; **fv,** fenestra vestibuli; **iv,** inferior vestibular nerve; **la,** lateral ampulla; **lsc,** lateral semicircular canal; **pa,** posterior ampulla; **pbl,** primary bony lamina imprint; **psc,** posterior semicircular canal; **sbl,** secondary bony lamina imprint; **scc,** secondary crus commune; **sr,** spherical recess; **sv,** superior vestibular nerve; **va,** vestibular aqueduct; **vac,** vena aquaeductus cochleae.

aqueduct is absent in *My. fasciatus* (Fig. 25A), but we note that a higher resolution µCT scan could reveal this structure. The shape of the cochlear aqueduct at its proximal end is circular in *I. macrourus* and *S. macroura* as in *T. cynocephalus* (Figs. 14C, 24M, 25M), while it is flattened in *Monodelphis* sp., *N. caurinus*, and *D. hallucatus* (Figs. 24A, 24G, 25G). In posterodorsal view, the cochlear aqueduct extends beyond the posterior semicircular canal in all compared specimens as in *T. cynocephalus* (Figs. 14E, 24E, K, Q, 25K, Q). The cast of the vena aquaeductus cochleae is visible in *N. caurinus* and *I. macrourus*, but could not be reconstructed in other specimens ("vac" in Figs. 14A, 24G, M). A higher resolution would likely reveal this structure in other specimens.

The vestibular aqueduct bony channel of *My. fasciatus* is the only one showing a bulge at its base as in *T. cynocephalus* ("va" in Figs. 14A, 25A). The root of the vestibular aqueduct is located anteroventral to the base of the common crus in all specimens as in *T. cynocephalus* (Figs. 14, 24–25). The vestibular aqueduct follows the same course crossing the basal part of the common crus in *Monodelphis* sp., *N. caurinus*, *I. macrourus*, and *S. macroura* as in *T. cynocephalus* (Figs. 14A, 24A, G, M, 25M). In contrast, in *My. fasciatus* and *D. hallucatus*, the vestibular aqueduct crosses ventral to the common crus ("cc" in Figs. 25A, G). Using the µCT data, the vestibular aqueduct is directed posteromedially in *Monodelphis* sp., *N. caurinus*, *I. macroura*, and *D. hallucatus* as in *T. cynocephalus* (Figs. 14A,

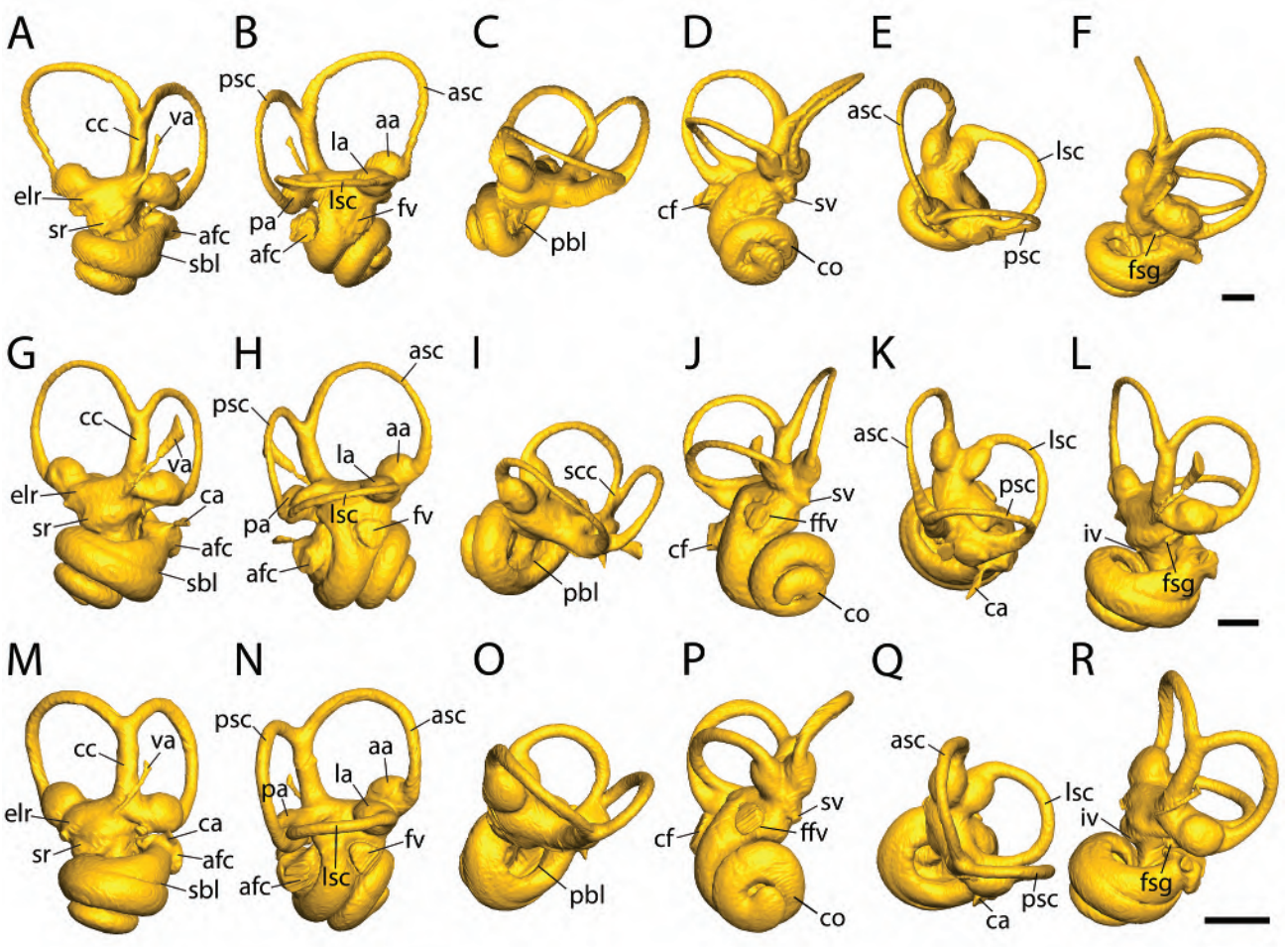

Fig. 25.—Virtual endocasts of right bony labyrinths. **A–F,** *Mymecobius fasciatus*, AMNH 155328; **G–L,** *Dasyurus hallucatus*, AMNH 196840 (left mirrored); **M–R,** *Sminthopsis macroura,* AMNH 108934 (left mirrored). **A, G, M,** medial view; **B, K, N,** posterolateral view; **C, I, O,** dorsal view; **D, J, P,** anterolateral view; **E, K, Q,** posterodorsal view; **F, I, R,** posteromedial view. Scale is 1 mm. Abbreviations: **aa,** anterior ampulla; **asc,** anterior semicircular canal; **ca,** cochlear aqueduct; **cc,** common crus; **cf,** cochlear fossula; **co,** cochlear canal; **elr,** elliptical recess; **ffv,** fossula of fenestra vestibuli; **fsg,** foramen singulare; **fv,** fenestra vestibuli; **iv,** inferior vestibular nerve; **la,** lateral ampulla; **lsc,** lateral semicircular canal; **pa,** posterior ampulla; **pbl,** primary bony lamina imprint; **psc,** posterior semicircular canal; **sbl,** secondary bony lamina imprint; **sr,** spherical recess; **sv,** superior vestibular nerve; **va,** vestibular aqueduct.

25A). In contrast, in *My. fasciatus* and *S. macroura,* it is directed dorso-posteromedially. The central part is narrower than the base of the vestibular aqueduct in *My. fasciatus* as in *T. cynocephalus* (Figs. 14A, 25A). In other specimens, *N. caurinus*, *I. macrourus*, *D. hallucatus,* and *S. macroura*, the center and base are similar in size, while in *Monodelphis* sp., the center is wider than the base of the vestibular aqueduct (Figs. 24A,G, M, 25G, M). The vestibular aqueduct apex is similar to the base in *My. fasciatus* as in *T. cynocephalus* (Figs. 14A, 25A). In all other compared specimens, the apex of the vestibular aqueduct is wider than the base (Figs. 24A, G, M, 25G, M). There is no groove on the common crus for the passage of the vestibular aqueduct in any of the compared specimens, a feature that is present in *T. cynocephalus* (Fig. 14A). The foramen singulare is positioned on the anteroventral aspect of the posterior ampulla in all compared specimens as in *T. cynocephalus* ("fsg" in Figs. 14A, F, 24F, L, R, 25F, L, R). The singular foramen is similar in size compared to the semicircular canals in *I. macrourus* as in *T. cynocephalus* (Figs. 14F, 24R). This structure is narrower in *N. caurinus*, *My. fasciatus, D. hallucatus,* and *S. macroura*, but wider than the semicircular canals in *Monodelphis* sp. (Figs. 24F, L, 25F, L, R). The elliptical and spherical recesses are in distinct chambers, and there is a visible groove that separates the chambers for both recesses in all compared specimens, as is the case for *T. cynocephalus* ("elr" and "sr" in Figs. 14F, 24A, G, M, 25A, G, M). In posteromedial view, the

spherical recess is more expanded in all specimens as in *T. cynocephalus*, except in *D. hallucatus* in which the two chambers are similar in size (Figs. 14F, 24F, I, R, 25 F, I, R). In dorsal view, the elliptical recess displays a large bulge in *Monodelphis* sp., *I. macrourus*, *D. hallucatus,* and *S. macroura* as in *T. cynocephalus*; this bulge is flatter in *My. fasciatus* and almost not visible in *N. caurinus* (Figs. 14C, 24C, I, O, 25C, I, O). The branches of the superior and inferior vestibular nerves could be reconstructed in all specimens as in *T. cynocephalus* except in *My. fasciatus* in which only the superior vestibular nerve could be reconstructed; however, a higher resolution µCT scan would likely reveal this feature ("sv" and "iv" in Figs. 14F, 24D, F, J, L, P, R, 25D, J, L, P, R).

The secondary common crus is absent in *My. fasciatus* and *S. macroura* as in *T. cynocephalus*. In contrast, the secondary common crus is present and relatively short in *Monodelphis* sp., *I. macrourus*, and *D. hallucatus*, while it is relatively longer in *N. caurinus* in relation to the semicircular canal size ("scc" in Figs. 24–25). Other dasyurids have been reported to display a secondary common crus including *Antechinus stuarti* Macleay, 1841 (Pfaff et al. 2017: fig. 1), *Pseudantechinus macdonnellensis* (Spencer, 1896) and *Antechinus minimus* (É. Geoffroy, 1803) (Alloing-Séguier et al. 2013). The presence/absence of this feature appears to be relatively variable in marsupials (Alloing-Séguier et al. 2013). The anterior semicircular canal expands much more than the posterior semicircular canal beyond the common crus in *Monodelphis* sp. and *S. macroura*, as in *T. cynocephalus* ("asc" and "psc" in Figs. 14B, 24B, 25N). The same is true for *My. fasciatus* and *D. hallucatus*; however, the posterior semicircular canal expands more, but not as much as the anterior semicircular canal (Figs. 25B, H). In *N. caurinus* and *I. macrourus*, only the anterior semicircular canal goes beyond the common crus (24H, N). In all compared specimens, the common crus has the same diameter throughout its length, which contrasts with *T. cynocephalus* in which the diameter decreases in size from the base to the apex (Figs. 14A, 24 A, G, M, 25A, G, M). The common crus is twice the size of the semicircular canal diameter in *I. macrourus*, *My. fasciatus*, and *D. hallucatus*, as in *T. cynocephalus* (Figs. 14A, 24M, 25A, G). The common crus is more than half, but less than twice, the size of the canals in *Monodelphis* sp. and *S. macroura* (Figs. 24A, 25M). In *N. caurinus*, the common crus and the semicircular canals have similar diameters (Fig. 24G). The anterior ampulla is positioned dorsal to the posterior and lateral ampullae in all compared specimens, as in *T. cynocephalus* ("aa," "pa," and "la" in Figs. 14B, 24B, H, N, 25B, H, N). In posterolateral view, the posterior and lateral ampullae are on the same plane in *N. caurinus*, *D. hallucatus*, and *S. macroura*, as in *T. cynocephalus* (Figs. 14B, 24H, 25H, N). In comparison, the lateral ampulla is positioned more dorsally than the posterior ampulla in *Monodelphis* sp., *I. macrourus*, and *My. fasciatus* (Figs. 24B, N, 25B). The ampullae are bulbous and larger than the semicircular canals in all compared taxa, as in *T. cynocephalus* (Figs. 14B, 24B, H, N, 25B, H, N). In posterodorsal view, the lateral semicircular canal reaches farther than the posterior semicircular canal in all compared specimens, as in *T. cynocephalus*, except for *N. caurinus* in which both canals are at the same level (Figs. 14E, 24E, K, Q, 25E, K, Q). The lateral semicircular canal goes the farthest in *T. cynocephalus* compared to all other specimens showing the same configuration (Figs. 14E, 24E, K, Q, 25E, K, Q). *Notoryctes caurinus* has a bend on its anterior semicircular canal, but it is closer to the anterior ampulla than the slight bend in *T. cynocephalus* (Figs. 14E, 24K). In all compared specimens, the anterior semicircular canal has the largest radius of curvature as in *T. cynocephalus* (Table 2). The roundest canal is the anterior semicircular canal, followed by the posterior semicircular canal in *Monodelphis* sp., *D. hallucatus*, and *S. macroura*, which is similar to *T. cynocephalus*. In *I. macrourus* and *My. fasciatus*, the roundest canal is the posterior, followed by the anterior semicircular canal. Finally, the posterior and then the lateral canals are the roundest in *N. caurinus* (Table 2). The widest angle is between the anterior and the posterior semicircular canals in *I. macrourus*, *D. hallucatus,* and *S. macroura* as in *T. cynocephalus*. In contrast, the widest angle is between the lateral and posterior semicircular canals in *Monodelphis* sp., *N. caurinus*, and *My. fasciatus* (Table 2). The lowest angle is between the anterior and the lateral semicircular canals in all taxa (Table 2). The inner ear of the adult *T. cynocephalus* does not show notable morphological differences from the subadult specimen.

CONCLUSIONS

Although the basicranium of the thylacine, *T. cynocephalus*, has been treated previously based on osteological specimens by Archer (1976) and others, the µCT scans employed here provide an extra level of detail that cannot be gleaned from intact crania. A variety of features have been uncovered via this study. In particular of interest are those hidden within or between bones of the basicranium, including the first published description of the bony labyrinth. Regarding the bony labyrinth, those of *T. cynocephalus* and the other compared species of marsupials are very similar. However, we note three features that distinguish *T. cynocephalus*: 1) a groove on the common crus for the passage of the vestibular aqueduct; 2) the apex is narrower than the more basal aspect of the common crus; and 3) the lateral semicircular canal reaches well beyond the posterior semicircular canal in posterodorsal view. One notable feature is the absence of a secondary common crus in *T. cynocephalus*, *My. fasciatus*, and *S. macroura*, but it is present in *D. hallucatus* and three other published dasyurids. The high variability present in this rather small sample makes it challenging to assess the ancestral condition for the group.

Some osteological features are unexpected as they have not hitherto been reported in any mammal. These relate to

the unusual pattern of the dural sinuses and endocranial veins. Specifically, included are the enclosure of the sigmoid sinus entirely in a canal through the substance of the petrosal; a course for the transverse sinus through a canal between the petrosal and squamosal; a novel venous channel (the parieto-occipital diploic vein) and canal system through the parietal, interparietal, supraoccipital, exoccipital, and petrosal; and a canal through the exoccipital carrying a vein connecting the inferior petrosal sinus and sigmoid sinus with the vein of the condyloid canal. Of these venous features, only the last was found in one representative of our comparative sample, the northern marsupial mole, *N. caurinus*. We also encountered an unexpected difference in the parieto-occipital diploic vein in our two thylacine specimens: bilaterally present vs. present only on the right side. Through future study of a broader sample of thylacines and other marsupials, we hope to understand these variations and why the thylacine endocranial venous system is so unique.

In addition to highlighting the power of the study of μCT scans, a goal here is to show that this recently extinct animal still has much to offer for morphologists interested in the evolutionary history of mammals. There is a treasure trove of osteological specimens of thylacines in museums across the globe (Sleightholme and Ayliffe, 2013), and we have only touched on two here. No doubt many mysteries will remain unsolved, given the absence of live animals to study or many soft tissues to sample. Yet, science should do the maximum to honor the legacy of the thylacine.

ACKNOWLEDGMENTS

We are grateful to the organizers of MorphoSource.org for creating online repositories for CT scanned data. Without access to these data, our study would not have been possible. We thank Paul Bowden, Section of Mammals, Carnegie Museum of Natural History for his artwork in Figures 7, 9, 11–12, 21B, and 22. At the Center for Quantitative Imaging at Pennsylvania State University, we thank Odette Mina, Whitney Yetter, and especially Tim Stecko for their assistance with the μCT scanning of *T. cynocephalus*, CM 20975. For their helpful reviews, we thank Robin Beck and Charlene Gaillard. Funding for this project is from National Science Foundation Grant DEB 1654949, the Carnegie Museum of Natural History, and the R.K. Mellon North American Mammal Research Institute. This work was also supported by the Beatriu de Pinós Programme funded by the Direcció General de Recerca de la Generalitat de Catalunya (General Directorate for Research in the Government of Catalonia) and managed by AGAUR, expedient number: 2021 BP 00042 to OCB; Research was also supported by the Generalitat de Catalunya/CERCA Programme, the Agència de Gestió d'Ajust Universitaris i de Recerca of the Generalitat de Catalunya (2021 SGR 00620) to David M. Alba (Institute Catala De Paleontologia).

LITERATURE CITED

ALLOING-SÉGUIER, L., M.R. SÁNCHEZ-VILLAGRA, M.S.Y. LEE, AND R. LEBRUN. 2013. The bony labyrinth in diprotodontian marsupial mammals: diversity in extant and extinct forms and relationships with size and phylogeny. Journal of Mammalian Evolution, 20:191–198.

AMEGHINO, F. 1887. Enumeración sistemática de las especies de mamíferos fósiles coleccionados por Carlos Ameghino en los terrenos eocenos de la Patagonia austral y depositados en el Museo La Plata. Boletin del Museo de La Plata, 1:1–26.

———. 1902. Première contribution à la connaissance de la fauna mammalogique des 520 couches à *Colpodon*. Boletin de la Academia Nacional de Ciencias de Córdoba, 17:71–141.

APLIN, K.P. 1990. Basicranial regions of diprotodontian marsupials: anatomy, ontogeny and phylogeny. Unpublished Ph.D. dissertation, University of New South Wales, Sydney.

ARCHER, M. 1976. The basicranial region of marsupicarnivores (Marsupialia), relationships of carnivorous marsupials, and affinities of the insectivorous marsupial peramelids. Zoological Journal of the Linnean Society, 59:217–322.

ARCHER, M., AND J.A.W. KIRSCH. 1977. The case for Thylacomyidae and Myrmecobiidae, or why are marsupial families so extended? Proceedings of the Linnean Society of New South Wales, 102:18–25.

BECK, R.M.D., K. TRAVOUILLON, K.P. APLIN, H. GODTHELP, AND M. ARCHER. 2014. The osteology and systematics of the enigmatic Australian Oligo-Miocene metatherian *Yalkaparidon* (Yalkaparidontidae; Yalkaparidontia; ?Australidelphia; Marsupialia). Journal of Mammalian Evolution, 21(2):127–172.

BECK, R.M.D., R.S. VOSS, AND S.A. JANSA. 2022. Craniodental morphology and phylogeny of marsupials. Bulletin of the American Museum of Natural History, 457:1–350.

BERTRAND, O.C., S.L. SHELLEY, J.R. WIBLE, T.E. WILLIAMSON, L.T. HOLBROOK, S.G.B. CHESTER, I.B. BUTLER, AND S.L. BRUSATTE. 2020. Virtual endocranial and inner ear endocasts of the Paleocene 'condylarth' *Chriacus*: new insight into the neurosensory system and evolution of early placental mammals. Journal of Anatomy, 236(1):21–49.

CHURCHILL, T.J., M. ARCHER, AND S.J. HAND. 2024. Three new thylacinids (Marsupialia, Thylacinidae) from late Oligocene deposits of the Riversleigh World Heritage Area, northwestern Queensland. Journal of Vertebrate Paleontology, 44(1). https://doi.org/10.1080/02724634.2024.2384595

COPE, E.D. 1880. On the foramina perforating the posterior part of the squamosal bone of the Mammalia. Proceedings of the American Philosophical Society, 18:452–461.

CORDS, E. 1915. Uber das Primordialcraniums von *Perameles* spec.? unter Berücksicthigung der Deckknochen. Anatomische Hefte, 52:1–84.

COSTEUR, L., B. MENNECART, B. MÜLLER, G. SCHULZ, B. MÜLLER, AND G. WANG. 2019. Observations on the scaling relationship between bony labyrinth, skull size and body mass in ruminants. *In* Developments in X-Ray Tomography XII (B. Müller and G. Wang, eds.). Proceedings of SPIE, 11113:1111313.

COUES, E. 1872. On the osteology and myology of *Didelphys virginiana*. Memoirs of the Boston Society of Natural History, 2:41–149.

CZERNY, S. 2015. Funktionsmorphologische und phylogenetische Untersuchungen der Mittel- und Innenohrregion ausgewählter "Ameridelphia" und Australidelphia (Metatheria, Mammalia). Unpublished M.Sc. thesis, University of Vienna, Vienna.

DICKSON, B.V. 2012. Using endopetrosal anatomy to investigate the phylogeny and palaeoecology of dasyuromorphian marsupials. Unpublished Honours thesis, University of New South Wales, Sydney.

DOM, R., B.L. FISHER, AND G.F. MARTIN. 1970. The venous system of the head and neck of the opossum (*Didelphis virginiana*). Journal of Morphology, 132:487–496.

DORAN, A.H.G. 1878. Morphology of mammalian ossicula auditûs. Transactions of the Linnean Society of London, second series, Zoology, 1:391–497.

EKDALE, E.G. 2009. Variation within the bony labyrinth of mammals. Ph.D. Dissertation, The University of Texas, Austin.

———. 2013. Comparative anatomy of the bony labyrinth (inner ear) of placental mammals. PLoS One, 8(6):e66624.

———. 2016. Form and function of the mammalian inner ear. Journal of Anatomy, 228(2):324–337.

EVANS, H.E., AND G.C. CHRISTENSEN. 1979. Miller's Anatomy of the

Dog. W.B. Saunders Company, Philadelphia. 1181 pp.
FEIGIN, C.Y., A.H. NEWTON, L. DORONINA, J. SCHMITZ, C.A. HIPSLEY, K.J. MITCHELL, G. GOWER, B. LLAMAS, J. SOUBRIER, T.N. HEIDER, B.R. MENZIES, A. COOPER, R.J. O'NEILL, AND A.J. PASK. 2018. Genome of the Tasmanian tiger provides insights into the evolution and demography of an extinct marsupial carnivore. Nature Ecology & Evolution, 2(1):182–192.
GAILLARD, C., A.M. FORASIEPI, S.D. TARQUINI, R.D.E. MACPHEE, AND S. LADEVÈZE. 2024. Cranium of *Sipalocyon externus* (Metatheria, Sparassodonta) with remarks on the paleoneurology of hathliacynids and insights into the early Miocene sparassodonts of Patagonia, Argentina. Swiss Journal of Palaeontology, 143:20.
GEISLER, J.H., AND Z. LUO. 1996. The petrosal and inner ear of *Herpetocetus* sp. (Mammalia: Cetacea) and their implications for the phylogeny and hearing of archaic mysticetes. Journal of Paleontology, 70(6):1045–1066.
GELDEREN, C. VAN. 1924. Die Morphologie der Sinus durae matris. Zweiter Teil. Die vergleichenden Ontogenie der neurokraniellen Venen der Vogel und Säugetiere. Zeitschrift für Anatomie und Entwicklungsgeschichte, 74:432–508.
GEOFFROY, É. 1803. Note sur les espèces du genre dasyure. Bulletin de l'Association française pour l'avancement des sciences, 3:158–159.
GOULD, J. 1842. Characters of a new species of *Perameles*, and new species of *Dasyurus*. Proceedings of the Zoological Society of London, 1842(part X):41–42.
———. 1845. Descriptions of five new species of mammals. Proceedings of the Zoological Society of London, 1845:77–79.
GREGORY, W.K., AND G.G. SIMPSON. 1926. Cretaceous mammal skulls from Mongolia. American Museum Novitates, 225:1–20.
HARRIS, G.P. 1808. Description of two new species of *Didelphis* from Van Diemen's Land. Transactions of the Linnean Society of London, 9:174–178.
HIIEMAE, K., AND F.A. JENKINS, JR. 1969. The anatomy and internal architecture of the muscles of mastication in *Didelphis marsupialis*. Postilla, 140:1–49.
JONES, G.M., AND K.E. SPELLS. 1997. A theoretical and comparative study of the functional dependence of the semicircular canal upon its physical dimensions. Proceedings of the Royal Society of London, Series B. Biological Sciences, 157(968):403–419.
KAMPEN, P.N. VAN. 1905. Die Tympanalgegend des Säugetierschädels. Gegenbaurs Morphologisches Jahrbuch, 34:321–722.
KEALY, S., AND R.M.D. BECK 2017. Total evidence phylogeny and evolutionary timescale for Australian faunivorous marsupials (Dasyuromorphia). BMC Evolutionary Biology, 17(1):240.
KERR, R. 1792. The Animal Kingdom, or Zoological System, of the Celebrated Sir Charles Linnaeus. Class I. Mammalia. London. 651 pp.
KLAAUW, C.J. VAN DER. 1931. The auditory bulla in some fossil mammals with a general introduction to this region of the skull. Bulletin of the American Museum of Natural History, 62:1–352.
KLINTWORTH, G.K. 1968. The comparative anatomy and phylogeny of the tentorium cerebelli. The Anatomical Record, 160:635–642.
LADEVÈZE, S. 2004. Metatherian petrosals from the late Paleocene of Itaboraí (Brazil), and their phylogenetic implications. Journal of Vertebrate Paleontology, 24:202–213.
———. 2005. La région auditive des métathériens (Mammalia, Metatheria) du Tertiaire inférieur d'Amérique du Sud. Incidence sur l'origine phylogénétique et la systématique des Notometatheria (métathériens d'Australie et d'Amérique du Sud. Unpublished Ph.D. dissertation, Muséum National d'Histoire Naturelle, Paris.
———. 2007. Petrosal bones of metatherian mammals from the late Palaeocene of Itaboraí (Brazil), and a cladistic analysis of petrosal features in metatherians. Zoological Journal of the Linnean Society, 15(1):113–121.
LADEVÈZE, S., R.J. ASHER, AND M.R. SÁNCHEZ-VILLAGRA. 2008. Petrosal anatomy in the fossil mammal *Necrolestes*: evidence for metatherian affinities and comparisons with the extant marsupial mole. Journal of Anatomy, 213:686–697.
LADEVÈZE, S., AND C. DE MUIZON. 2007. The auditory region of early Paleocene Pucadelphydae (Mammalia, Metatheria) from Tiupampa, Bolivia, with phylogenetic implications. Palaeontology, 50:1123–1154.
LINNAEUS, C. 1758. Systema Naturae per regna tria naturae, secundum classis, ordines, genera, species cum characteribus, differentiis, synonymis, locis. Tenth ed., Vol. 1. Laurentii Salvii, Stockholm. 824 pp.
LINNARD, G., AND S.R. SLEIGHTHOLME. 2023. An exploration of the evidence surrounding the identity of the last captive thylacine. Australian Zoologist, 43(2):287–338.
MACLEAY, W.S. 1841. Notice of a new genus of Mammalia discovered by J. Stuart, Esq., in New South Wales. Annals and Magazine of Natural History, 8:241–243.
MACPHEE, R.D.E. 1977. Ontogeny of the ectotympanic-petrosal plate relationship in strepsirhine prosimians. Folia primatologica, 27:245–283.
———. 1981. Auditory regions of primates and eutherian insectivores: morphology, ontogeny, and character analysis. Contributions to Primatology, 18:1–282.
MACPHEE, R.D.E., C. GAILLARD, A.M. FORASIEPI, AND R.B. SULSER. 2023. Transverse canal foramen and pericarotid venous network in Metatheria and other mammals. Bulletin of the American Museum of Natural History, 462:1–122.
MAGA, A.M. 2008. Systematic paleontological investigation of the metatherian fauna from the Paleogene Uzunçarşıdere Formation, Central Turkey. Unpublished Ph.D. dissertation, The University of Texas, Austin.
MARSHALL, L.G., AND C. DE MUIZON. 1988. The dawn of the age of mammals in South America. National Geographic Research, 4(1):23–55.
MENG, J., AND R.C. FOX. 1995. Osseous inner ear structures and hearing in early marsupials and placentals. Zoological Journal of the Linnean Society, 115(1):47–71.
MUIRHEAD, J. 1994. Systematics, evolution and palaeobiology of recent and fossil bandicoots (Marsupialia: Peramelemorphia). Unpublished Ph.D. dissertation, University of New South Wales, Sydney.
MUIRHEAD, J., AND S. WROE. 1998. A new genus and species, *Badjcinus turnbulli* (Thylacinidae: Marsupialia), from the late Oligocene of Riversleigh, northern Australia, and an investigation of thylacinid phylogeny. Journal of Vertebrate Paleontology, 18: 612–626.
MUIZON, C. DE., R.L. CIFELLI, AND R. CÉSPEDES PAZ. 1997. The origin of the dog-like borhyaenoid marsupials of South America. Nature, 389:486–489.
MUIZON, C. DE, AND S. LADEVÈZE. 2020. Cranial anatomy of *Andinodelphys cochabambensis*, a stem metatherian from the early Palaeocene of Bolivia. Geodiversitas, 42(30): 597–739.
MUIZON, C. DE, S. LADEVÈZE, C. SELVA, R. VIGNAUD, AND F. GOUSSARD. 2018. *Allqokirus australis* (Sparassodonta, Metatheria) from the early Palaeocene of Tiupampa (Bolivia) and the rise of the metatherian carnivorous radiation in South America. Geodiversitas, 40(3):363–459.
MURRAY, P.F., AND D. MEGIRIAN. 2006. Cranial morphology of the Miocene thylacinid *Mutpuracinus archibaldi* (Thylacinidae, Marsupialia) and relationships within the Dasyuromorphia. Alcheringa Special Issue, 1:229–276.
NEWTON, A.H., F. SPOUTIL, J. PROCHAZKA, J.R. BLACK, K. MEDLOCK, R.N. PADDLE, M. KNITLOVA, C.A. HIPSLEY, AND A.J. PASK. 2018. Letting the 'cat' out of the bag: pouch young development of the extinct Tasmanian tiger revealed by X-ray computed tomography. Royal Society Open Science, *5*(2):171914.
NOMINA ANATOMICA VETERINARIA, SIXTH EDITION. 2017. Editorial Committee Hanover (Germany), Ghent (Belgium), Columbia, MO (U.S.A.), Rio de Janeiro (Brazil).
ORLIAC, M.J., AND M.A. O'LEARY. 2016. The inner ear of *Protungulatum* (Pan-Euungulata, Mammalia). Journal of Mammalian Evolution, 23(4):337–352.
PFAFF, C., S. CZERNY, D. NAGEL, AND J. KRIWET. 2017. Functional morphological adaptations of the bony labyrinth in marsupials (Mammalia, Theria). Journal of Morphology, 278(6):742–749.
REINHARD, K.R., M.E. MILLER, AND H.E. EVANS. 1962. The craniover-

tebral veins and sinuses of the dog. American Journal of Anatomy, 111:67–87.

ROUGIER, G.W., J.R. WIBLE, AND M.J. NOVACEK. 1998. Implications of *Deltatheridium* specimens for early marsupial history. Nature, 396:459–463.

ROVINSKY, D.S., A.R. EVANS, AND J.W. ADAMS. 2019. The pre-Pleistocene fossil thylacinids (Dasyuromorphia: Thylacinidae) and the evolutionary context of the modern thylacine. PeerJ, 7:e7457.

SÁNCHEZ-VILLAGRA, M.R., AND T. SCHMELZLE. 2007. Anatomy and development of the bony inner ear in the woolly opossum, *Caluromys philander* (Didelphimorphia, Marsupialia). Mastozoología Neotropical, 14(1):53–60.

SÁNCHEZ-VILLAGRA, M.R., AND J.R. WIBLE. 2002. Patterns of evolutionary transformation in the petrosal bone and some basicranial features in marsupial mammals, with special reference to didelphids. Journal of Zoological Systematics and Evolutionary Research, 40:26–45.

SCHMELZLE, T., S. NUMMELA, AND M.R. SÁNCHEZ-VILLAGRA. 2005. Phylogenetic transformations of the ear ossicles in marsupial mammals, with special reference to diprotodontians: a character analysis. Annals of Carnegie Museum, 74(3):189–200.

SCHMELZLE, T., M.R. SÁNCHEZ-VILLAGRA, AND W. MAIER. 2007. Vestibular labyrinth diversity in diprotodontian marsupial mammals. Mammal Study, 32(2) (2007):83–97.

SEGALL. W. 1970. Morphological parallelisms of the bulla and auditory ossicles in some insectivores and marsupials. Fieldiana, Zoology, 51:169–205.

SLEIGHTHOLME, S., AND N. AYLIFFE. 2013. International Thylacine Specimen Database, 5th Revision. Zoological Society, London.

SPENCER, B. 1896. Preliminary description of certain new marsupials from central Australia. Proceedings of the Royal Society of Victoria, 8:5–13.

SPOOR, F., T. GARLAND, G. KROVITZ, T.M. RYAN, M.T. SILCOX, AND A. WALKER. 2007. The primate semicircular canal system and locomotion. Prceedings of the National Academy of Sciences USA, 104(26):10808–10812.

SPOOR, F., AND F. ZONNEVELD. 1998. Comparative review of the human bony labyrinth. American Journal of Physical Anthropology, 107(S27):211–251.

STIRLING, E.C. 1889. Abstracts of Proceedings of the Royal Society of South Australia for 1888–1889. Transactions of the Royal Society of South Australia, 12:158.

THOMAS, O. 1920. *Notoryctes* in north-west Australia. Annals and Magazine of Natural History, 6(31):111–113.

TOEPLITZ, C. 1920. Bau und Entwicklung des Knorpelschädels von *Didelphys marsupialis*. Zoologica, Stuttgart, 27:1–84.

TURNBULL, W.D. 1970. Mammalian masticatory apparatus. Fieldiana, Geology, 18:149–356.

WAGNER, A. 1842. Diagnosen neuer Arten brasilischer Säugthiere. Archiv für Naturgeschichte, 8(1):356–362.

WARBURTON, N.M., K.J. TRAVOUILLON, AND A.B. CAMENS. 2019. Skeletal atlas of the thylacine (*Thylacinus cynocephalus*). Palaeontologia Electronica, 22.2.29A 1–56. https://doi.org/10.26879/947

WATERHOUSE, G.R. 1836. Description of a new genus (*Myrmecobius*) of mammiferous animals from New Holland, probably belonging to the marsupial type. Proceedings of the Zoological Society of London, 1836(part IV):69–70.

WIBLE, J.R. 1987. The eutherian stapedial artery: character analysis and implications for superordinal relationships. Zoological Journal of Linnean Society, 91:107–135.

———. 1990. Petrosals of Late Cretaceous marsupials from North America, and a cladistic analysis of the petrosal in therian mammals. Journal of Vertebrate Paleontology, 10(2):183–205.

———. 2003. On the cranial osteology of the short-tailed opossum *Monodelphis brevicaudata* (Didelphidae, Marsupialia). Annals of Carnegie Museum, 72(3):137–202.

———. 2008. On the cranial osteology of the Hispaniolan solenodon, *Solenodon paradoxus* Brandt, 1833 (Mammalia, Lipotyphla, Solenodontidae). Annals of Carnegie Museum, 77(3):321–402.

———. 2022. CT study of the cranial osteology of the short-tailed opossum *Monodelphis domestica* (Wagner, 1842) (Marsupialia, Didelphidae) and comments on the internal nasal skeleton floor. Annals of Carnegie Museum 87(4):249–289.

WIBLE, J.R., AND O.C. BERTRAND. 2024. Basicranial anatomy of *Leptictis haydeni* Leidy, 1868 (Mammalia, Eutheria, Leptictidae). Annals of Carnegie Museum, 90(1):1–36.

WIBLE, J.R., M.J. NOVACEK, AND G.W. ROUGIER. 2004. New data on the skull and dentition in the Mongolian Cretaceous eutherian mammal *Zalambdalestes*. Bulletin of the American Museum of Natural History, 281:1–144.

WIBLE, J.R., S.L. SHELLEY, AND C. BELZ. 2021. The element of Paaw in marsupials and the middle ear of *Philander opossum* (Linnaeus, 1758) (Didelphimorphia, Didelphidae). Annals of Carnegie Museum, 87(1):1–35.

WROE, S. 1997. A reexamination of proposed morphology-based synapomorphies for the families of Dasyuromorphia (Marsupialia). I. Dasyuridae. Journal of Mammalian Evolution, 4(1):19–52.

———. 1999. The geologically oldest dasyurid (Marsupialia), from the Miocene Riversleigh, northwestern Queensland. Palaeontology, 42:501–527.

WROE, S., J. BRAMMALL, AND B.N. COOKE. 1998. The skull of *Ekaltadeta ima* (Marsupialia, Hypsiprymnodontidae?): an analysis of some cranial features within Marsupialia and a re-investigation of propleopine phylogeny; with notes on the inference of carnivory among mammals. Journal of Paleontology, 72(4):738–751.

WROE, S., M. EBACH, S. AHYONG, C. DE MUIZON, AND J. MUIRHEAD. 2000. Cladistic analysis of dasyuromorphian (Marsupialia) phylogeny using cranial and dental characters. Journal of Mammalogy, 81(4): 1008–1024.